Natural Resources Canada | Ressources naturelles Canada

GEOLOGICAL SURVEY OF CANADA
OPEN FILE 7718

Environmental and Economic Significance of Gossans

M.-C. Williamson (Editor)

2015

Canada

GEOLOGICAL SURVEY OF CANADA
OPEN FILE 7718

Environmental and Economic Significance of Gossans

M.-C. Williamson (Editor)

Geological Survey of Canada, 601 Booth Street, Ottawa, Ontario

2015

doi:10.4095/296571

This publication is available for free download through GEOSCAN (http://geoscan.nrcan.gc.ca/).

Recommended citation
Williamson, M.-C. (ed.), 2015. Environmental and Economic Significance of Gossans; Geological Survey of Canada, Open File 7718, 100 p. doi:10.4095/296571

Publications in this series have not been edited; they are released as submitted by the author.

ENVIRONMENTAL AND ECONOMIC SIGNIFICANCE OF GOSSANS

ENVIRONMENTAL AND ECONOMIC SIGNIFICANCE OF GOSSANS

Guest Editors:

Dr. Helen R. Smyth
Regional Geoscientist - Neftex
Halliburton
97 Jubilee Avenue
Abingdon, Oxfordshire, OX14 4RW
United Kingdom
Email: helen.smyth@halliburton.com

Dr. Benoit-Michel Saumur
Chercheur Postdoctoral du CRSNG – NSERC Postdoctoral Research Fellow
Natural Resources Canada – Ressources naturelles Canada
Commission géologique du Canada – Geological Survey of Canada
601 Booth, Ottawa, Ontario, K1A 0E8
Canada
Email: Benoit-Michel.Saumur@nrcan.gc.ca

Recommended citation for individual papers within this volume:

Wilton, D.H.C., Thompson, G.M., and Evans-Lamswood, D.M., 2015. MLA-SEM examination of sulphide mineral breakdown in till, Voisey's Bay Ni-Cu-Co deposit, Labrador: The distribution and quantitative mineralogy of weathered sulphide phases in a transect from massive sulphide through gossanous regolith to till cover, *in* Environmental and Economic Significance of Gossans, (ed.) M.-C. Williamson; Geological Survey of Canada, Open File 7718, p. 29-39.

INTRODUCTION TO OPEN FILE 7718, "ENVIRONMENTAL AND ECONOMIC SIGNIFICANCE OF GOSSANS"

Marie-Claude Williamson
Geological Survey of Canada, 601 Booth Street, Ottawa, Ontario, K1A 0E8
(email: Marie-Claude.Williamson@nrcan.gc.ca)

This publication is a conference report that highlights recent research on gossans as natural laboratories used in environmental geosciences and metallogeny. Gossans preserve anomalous concentrations of metals that are routinely investigated in the search for new ore bodies. Under certain conditions, gossans also constitute analogues of mine waste deposits. On a regional scale, the streams, lakes and permafrost that are affected by the specific mineralogy of gossans provide indicators of environmental impact. What is often overlooked in field investigations of gossans is the stratigraphic, mineralogical and geochemical complexity of these surficial deposits.

The 2014 Annual Meeting of the Geological Association of Canada (GAC) Special Session: *SY4. Environmental and Economic Significance of Gossans Associated with Mineralization in Rifts and Large Igneous Provinces* was intended as a forum for geologists from government, industry and academia who have mapped and investigated gossans and wish to become part of a new GAC community of interest. SY4 was convened by M.-C. Williamson, J.R. Harris and C.G. Kingsbury; and held on May 23, 2014, at the University of New Brunswick, Fredericton. The day-long program consisted of eleven oral presentations on the remote predictive mapping of gossans in Canada's North; the structural controls and indicator minerals present at the Voisey's Bay Ni-Cu-Co deposit, Labrador; the mineralogy and classification of arctic gossans and regolith; and the environmental impact of arctic gossans on local stream waters and sediments. The idea of an Open File dedicated to gossans was met with enthusiasm by the presenters. This report includes short papers based on nine oral presentations as well as one invited paper by D.H.C. Wilton et al. presented in S*Y6. Applied aspects of mineralogy: A tribute to John Leslie Jambor*.

The first two papers describe recent progress in the detection of gossans by remote sensing methods. J.R. Harris et al. demonstrate how the High Lake Gossan, Northwest Territories, can be detected using satellite imagery, emphasizing the advantage of using hyperspectral sensors. The paper by C.G. Kingsbury specifically examines the detection of gossans in volcanic terrain of the High Arctic Large Igneous Province (HALIP) exposed in western Axel Heiberg Island, Nunavut. Two papers focus on the Voisey's Bay Deposit, Labrador. The paper by P.C. Lightfoot and D.M. Evans-Lamswood is an overview of structural models applied to orthomagmatic deposits associated with Large Igneous Provinces on a global scale. The authors discuss the implications of these models for the genesis of fertile, shallow deposits. The second paper, by D.H.C. Wilton et al., is a mineralogical study of the gossanous soils and glacial deposits exposed along the north wall of the Mini-Ovoid open pit mine. The paper contributed by H.G. Dill describes the wide range of deposits associated with supergene mineralization worldwide. The next three papers present the results of field investigations of gossans located in the Northwest Territories and Nunavut, Canadian Arctic Islands. The paper by M.M. Battler et al. describes the complex mineralogy of the Golden Deposit, Northwest Territories. The next paper, contributed by E.C. Turner, is a field report on gossanous and non-gossanous Pb-Zn showings mapped in the Cornwallis District of Nunavut. Finally, J.B. Percival et al. propose a first order classification scheme for gossans based on field work on Victoria Island, NT, and Axel Heiberg Island, Nunavut. The last two papers, contributed by M.-C. Williamson et al. and R.J.

McNeil et al., are complementary. These papers report new findings on the effects of gossans on the permafrost and on the geochemistry of stream waters and sediments with implications for base metal prospectivity.

ACKNOWLEDGEMENTS

The conveners wish to thank David Lentz and Jim Walker for their support of Symposium no. 4, the first on this topic to be endorsed by the Geological Association of Canada (GAC). Sponsors included the GAC's Environmental Earth Sciences (EESD) and Mineral Deposits (MDD) Divisions, Vale (Copper Cliff), SRK Consulting and Agnico Eagle. The short papers were expertly reviewed by Guest Editors Helen Smyth and Benoit Saumur. Special thanks to Roger Paulen for reviewing the entire open file, and to Victoria Tschirhart for technical advice.

In closing, I wish to express my gratitude to the Arctic Gossans research team, 2011-2014, for their support. Their contributions to this volume are the result of their involvement in two Earth Sciences Sector (ESS) Programs: *Environmental Geoscience* and *Geo-mapping for Energy and Minerals* (GEM-1); in collaboration with faculty and students at Queen's University (Kingston) and Carleton University (Ottawa). They are in order of appearance:

Ron Peterson, Rob Rainbird, Jeff Harris, Jean Bédard, Pouran Behnia, Jackson Froome, Lindsay Fenwick, Jeanne Percival, Étienne Girard, Cole Kingsbury, Richard Ernst, Rick McNeil, Stephen Day, Christopher Harrison, Martin McCurdy, Eric Grunsky, Jacques Pinard, Beth Hillary, Guy Buller, Odette Nehza, Jeffrey Shepherd and Meaghan Pinard.

The Arctic Gossans Activity was approved in April 2011 by Bernard Vigneault, Program Manager for *Environmental Geoscience*, and led by Sharon Smith, project leader for *Environmental Assessments in the North*.

John Percival, Program Manager for GEM-1, is thanked for enabling the successful completion of the first environmental and economic study of gossans in the Canadian Arctic Archipelago. Such a vision benefits northern communities by promoting greater accountability at each stage of the mining cycle in Canada's North.

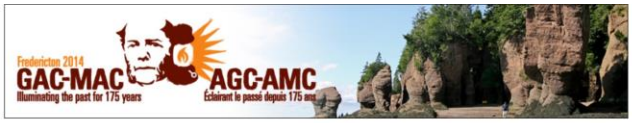

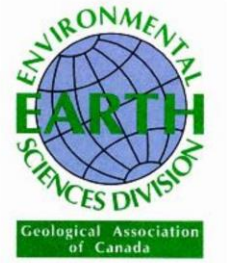

DETECTING AND MAPPING GOSSANS USING REMOTELY-SENSED DATA

Jeff R. Harris, Marie-Claude Williamson, Jeanne B. Percival, Pouran Behnia, Roger F. Macleod
Geological Survey of Canada, 601 Booth Street, Ottawa, Ontario, K1A 0E8
(email: Jeff.Harris@nrcan.gc.ca)

INTRODUCTION

Gossans are surficial deposits that form in host rocks by the oxidation of sulphides by acidic and oxidizing fluids. In a classic gossan profile, primary sulphides are replaced by iron-bearing pseudomorphs such as ferrihydrite, goethite and jarosite (Percival et al. – this volume). Gossans are important vectors to buried ore deposits and many mineral deposits have been found by mapping gossans (Lightfoot et al., this volume). Reactive gossans impact the polar environment because the resulting acid solution transfers transition metals into the permafrost and local catchment basin (McNeil et al. and Williamson et al., this volume).

Remote sensing can be used not only to detect and map gossans but, with the advent of hyperspectral imaging, to uniquely identify iron-bearing minerals. This paper reviews image processing techniques developed for the detection and identification of gossan mineralogy using a variety of moderate resolution spectral and spatial sensors as well as more advanced high resolution instruments. The High Lake Gossan, Nunavut, (N 67º 23' 10", W 110º 50' 55"; Figure 1), were selected as a case study for detecting and mapping gossans in a northern environment. The field and laboratory spectra of a range of iron-bearing minerals found at High Lake (Petch, 2005; West et al., 2009) are compared to the signatures derived from the remotely sensed data.

DETECTION OF GOSSANS WITH OPTICAL SATELLITE DATA

Surficial deposits or soils that form by the oxidation of sulphides in host rocks accumulate as an oxide cap (gossan) that has a distinct ochre colour ranging from red to orange to yellow due to increasing ferric iron content. In some cases, the oxide cap is black due to the presence and subsequent weathering of manganese oxides. The distinctive colours of the oxide cap allow for the identification and mapping of gossans using multispectral and hyperspectral optical remotely sensed imagery especially in the visible-near-infrared (VNIR) portion of the electromagnetic (EM) spectrum. Gossans are more difficult to detect on a traditional black and white air photograph due to their monochromatic nature. Figure 2 shows how gossans develop above sulphide-enriched bedrock and/or surficial deposits.

Remote Predictive Mapping (RPM) involves the compilation and interpretation of all geoscience data sources to produce predictive maps. These datasets guide geologists and serve as first order geological information in preparation for mapping, which is particularly important for fieldwork in remote areas such as Canada's North (Harris, 2008; Harris et al., 2012). The detection and mapping of gossans by RPM techniques is an important aspect of bedrock mapping (Behnia et al., 2012). The small size of most gossans (15 m to less than 1 or 2 km in length) requires access to higher spatial resolution images that will enable the detection of smaller gossans in poorly-vegetated regions such as Canada's North. There are many satellite-borne optical multispectral sensors (e.g. Quickbird, WorldView, Spot 6, RapidEye) that offer extremely high spatial resolution (1 m or less) and are, therefore, ideal for the detection and mapping of gossans. Spatial resolution obviously dictates the scale of mapping. Moderate resolution sensors such as LANDSAT allow mapping at 1:50,000 scale whereas the higher-resolution sensors mentioned above allow mapping at scales greater than 1:5,000. Not all these sensors collect information in the blue wavelengths due to intense atmospheric scattering.

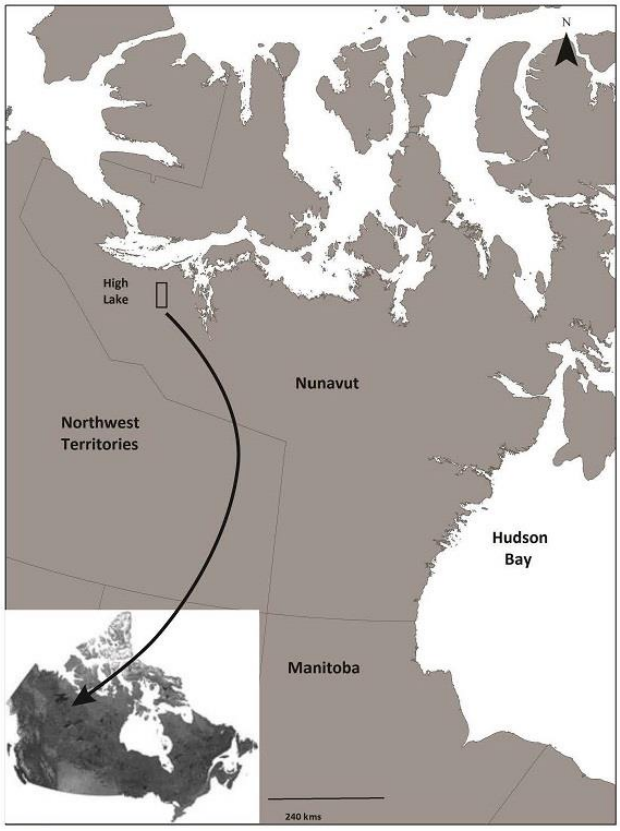

Figure 1. Location of the High Lake Gossans study area in the Northwest Territories.

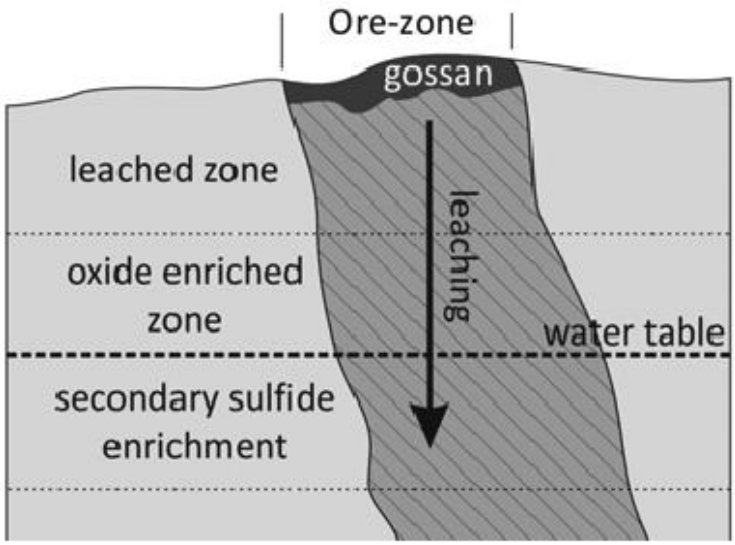

Figure 2. Simplified illustration showing the enrichment of primary iron sulphide rock below a gossan (modified from Taylor, 2011).

As a result, there are limits to the type of image processing techniques that can be utilized. High spectral resolution (i.e., hyperspectral) allows for not only the detection of gossans but also the identification and mapping of specific iron minerals based on their unique spectral characteristics. Figure 3 shows the unique spectral signatures of a range of iron oxides in the VNIR portion of the EM spectrum. Remarkably, jarosite, hematite and goethite can be uniquely identified by their spectral reflectance characteristics which comprise absorptions and reflectance peaks at specific wavelengths. The specific absorption bands and reflection peaks and their wavelength positions in the VNIR are caused by electronic transitions and charge transfer processes (changes in energy states of electrons bound to atoms of molecules) associated with transitions elements, particularly Fe. High energy levels, and therefore short wavelengths (i.e., VNIR), are required for such electronic processes to occur. This results in broad absorption bands and reflection peaks (Figure 3).

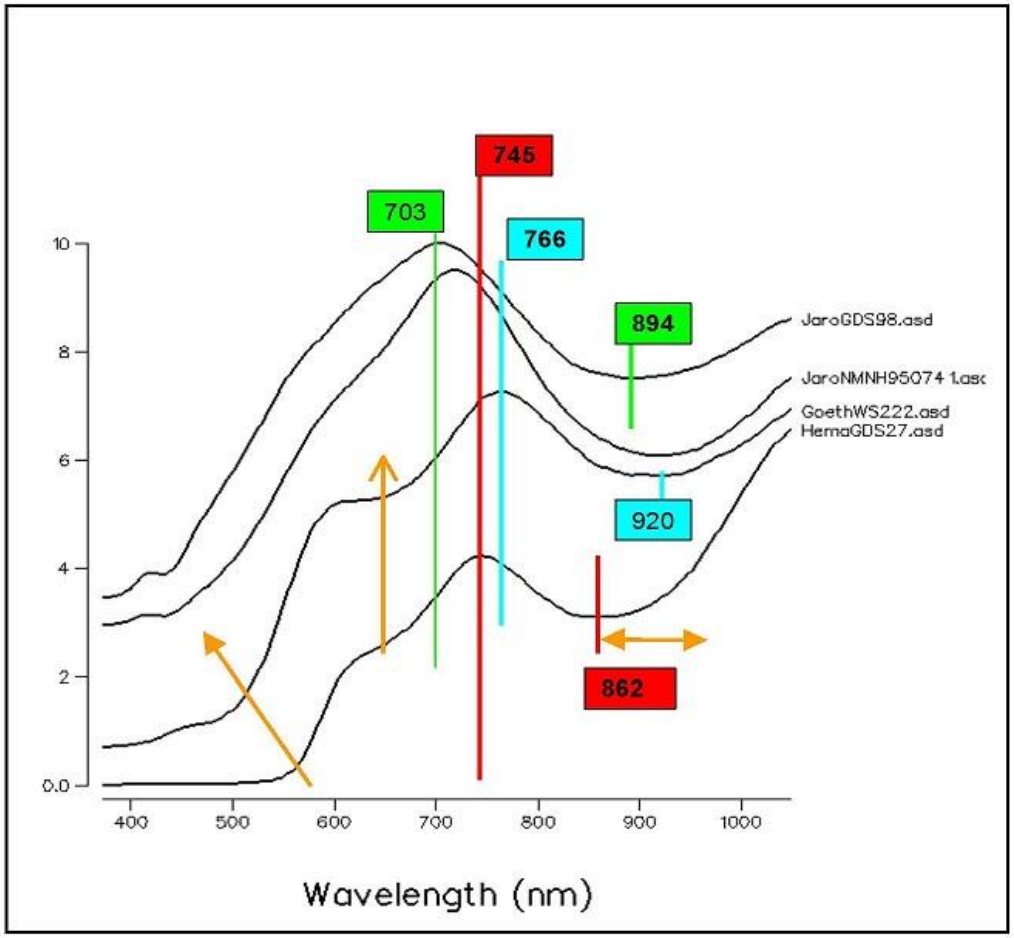

Figure 3. Spectral plot of various iron oxides (jarosite, goethite, hematite). Spectra were obtained from the United States Geological Survey (http://speclab.cr.usgs.gov/spectral-lib.html). Numbers represent absorption bands and peaks in nanometers. The orange arrows represent absorption bands, and the y-axis measures reflectance.

DATA PROCESSING AND ENHANCEMENT TECHNIQUES

The detection of gossans for RPM can be carried out on remotely sensed optical imagery using techniques ranging from (a) the generation of simple natural colour composites whereby each wavelength is matched to the additive display color (red-green-blue) producing a colour image in which colours are presented as seen by the human eye to (b) more complicated machine-learning techniques such as supervised classification. Table 1 presents a brief summary of some of the image processing techniques that can be used to detect and map gossans on multispectral and hyperspectral optical remotely sensed imagery.

Gossans can be recognized by their distinct colour on natural colour composites derived from various optical sensors. Figures 4a and 4b show natural colour composites of the High Lake Gossan (Nunavut) derived from LANDSAT-7 and airborne hyperspectral data, respectively. Ratioing, which involves dividing one remotely sensed band (wavelength) by another, highlights spectral differences (strong reflection vs. strong absorption) as a function of different wavelengths and is a common image processing technique in vegetation studies as well as for mapping alteration minerals and detecting gossans. Ratioing has the additional advantage of reducing topographic effects on remotely sensed imagery. A red/blue wave-length ratio (i.e., ferric iron ratio) can be applied to multispectral or hyperspectral data (Figures 5a and 5b) and is commonly used to identify gossans.

Table 1. Summary of techniques for enhancing satellite imagery.

Technique	Description
Natural Colour composite	Blue, green and red wavelengths are matched to the RGB display colours – image can be enhanced by contrast stretching
Ratioing	Red/blue band ratio is often used to enhance gossans by leveraging high reflectance of red energy and absorbtion of blue energy – for LANDSAT – 7 this involves dividing band 3 (red) by band 1(blue) and then enhance through contrast stretching and extract potential gossans by isolating high ratio values
Principal Component Analysis – Crosta technique	Apply a principal component transform to a multispectral or hyperspectral dataset-examine the component loadings (i.e. eigenvectors) and choose the component with positive weighting for band 3 (red) and negative weight for band 1 (blue) – contrast stretch and/or extract potential gossans by isolating high values in the component image
Supervised classification (maximum likelihood, SVM, neural Networks, Random Forests)	Identify gossans on the image and collect spectral characteristics f rom the imagery (e.g., training areas) – use the extracted gossan signatures in concert with a classification algorithm to produce a map showing areas with similar signatures that may represent gossans

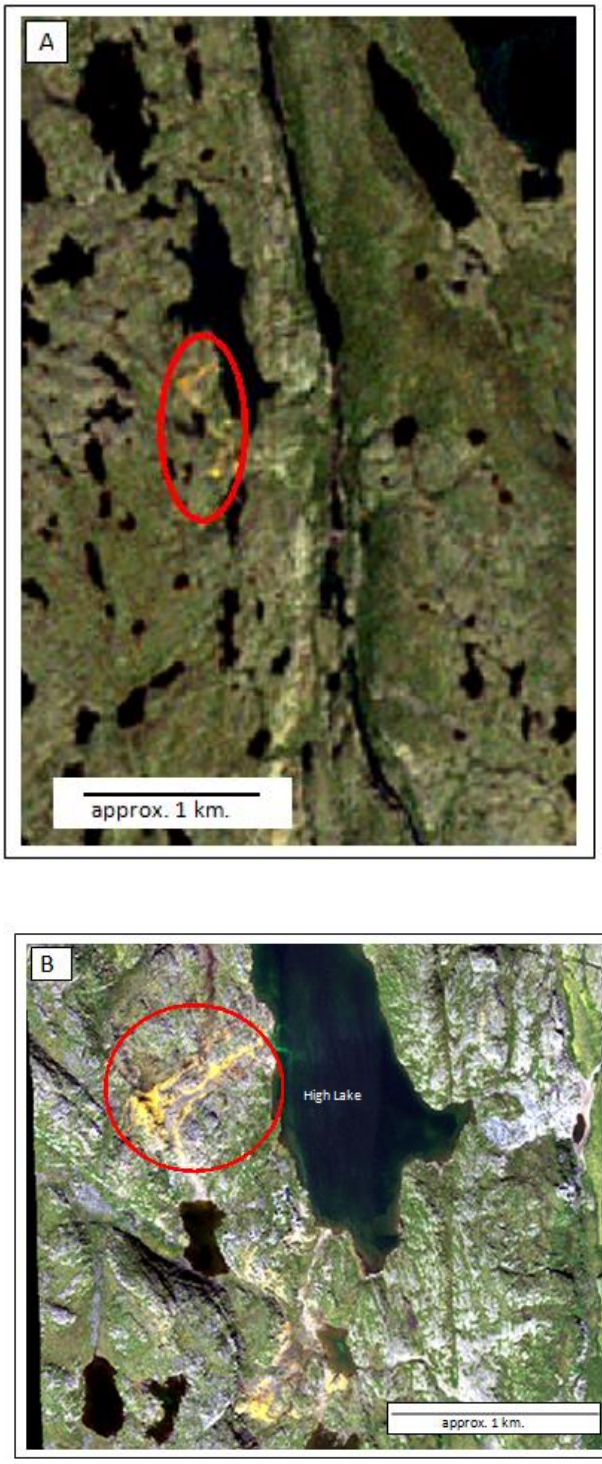

Figure 4. (A) LANDSAT-7 natural colour composite image of High Lake Gossan (at only 30 metres spatial resolution), and low spectral resolution at 4 bands in VNIR. High Lake Gossan appears yellowish-red in colour. (B) Airborne hyperspectral natural colour composite image of High Lake Gossan (SPEC-TIR, with high spatial resolution at 1 meter and good spectral resolution at 306 bands). High Lake Gossan appears orange-yellow in colour.

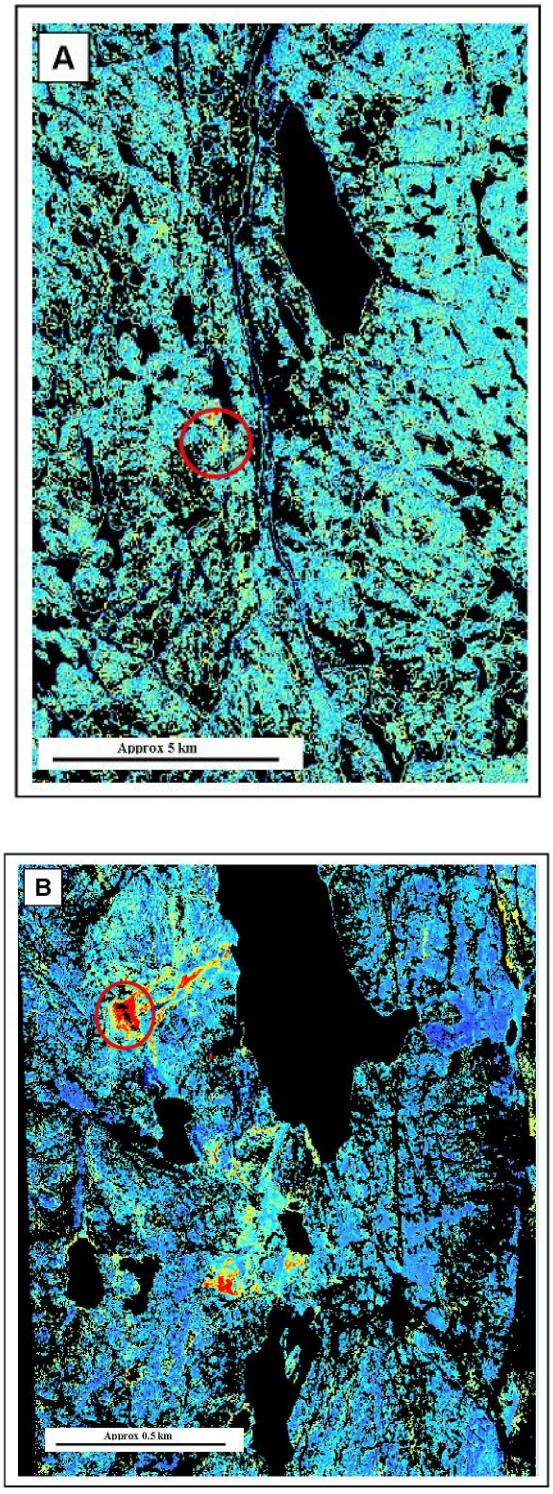

Figure 5. (A) Red/Blue (LANDSAT-7 bands 3/1) ratio highlights the High Lake Gossan. This ratio leverages high reflection of red energy – the reason why gossans appear in shades of red, orange and yellow – and strong absorption of blue energy. High Lake Gossan is circled, but another 10 potential smaller gossans located to the South can also be detected. (B) Red/blue ratio derived from airborne hyperspectral data. High Lake Gossan and other associated gossans are shown in red.

Principal Component analysis (PCA; Crosta and Moore, 1989) is also a proven technique for detecting potential gossans. This involves applying a PCA transform to the remotely sensed data and selecting the component image that has a negative loading (e.g. eigenvector – see Table 2) for the blue band and a high positive weighting for the red band (Figure 6).

Table 2. Eigenvalues derived from a PC transform of the LANDSAT data (Figure 4A).

Eigenvector	Band 1	Band 2	Band 3	Band 4	Band 5	Band 6
Band 1	-0.114726	-0.154303	-0.171018	-0.597711	-0.742153	-0.160413
Band 2	0.222077	0.183090	0.246289	-0.780377	0.497428	0.008867
Band 3	-0.115265	-0.126616	-0.168484	-0.121907	-0.026925	0.962657
Band 4	-0.419797	-0.456020	-0.592140	-0.130189	0.448091	-0.217834
Band 5	-0.764718	-0.099052	0.635790	-0.030085	0.015814	0.003316
Band 6	0.403993	-0.841945	0.356159	0.032227	0.003676	0.004152

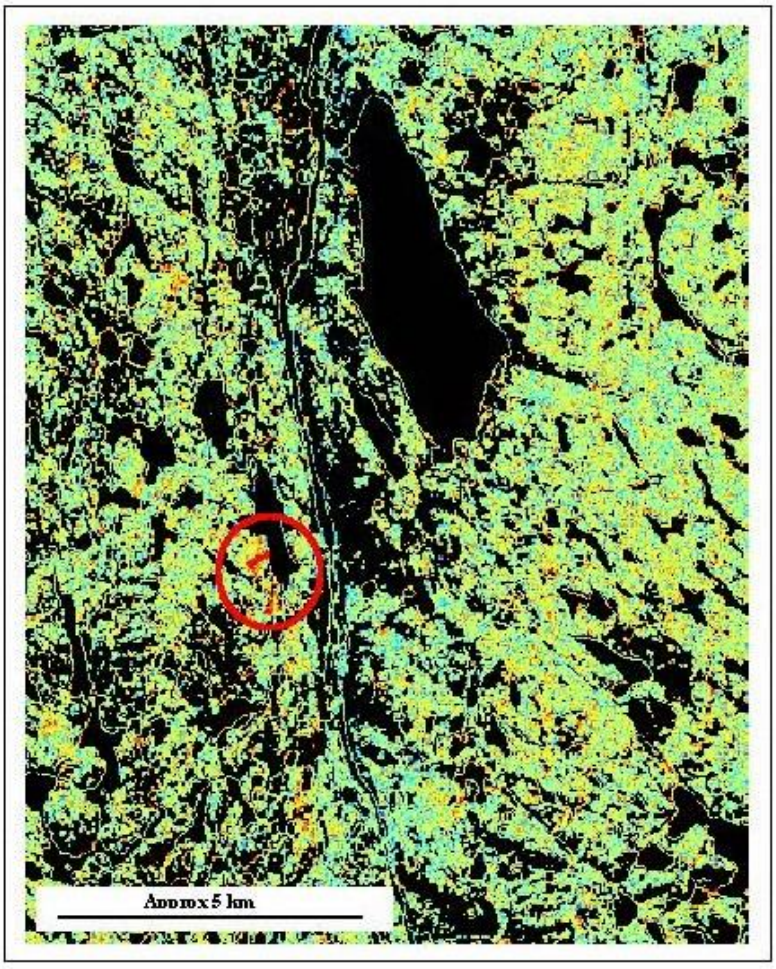

Figure 6. PCA 5 component image based on a principal component transform of LANDSAT – 7 data. The PCA 5 component image was selected due to the high positive loading of the red band (band 3) and high negative loading of the blue band (band 1). See **Table 2** for a list of eigenvectors.

Supervised classification can also be used to map potential gossans. Supervised classification techniques require representative statistics (reflectance spectra) of known gossans (e.g. Behnia et al., 2012). These training areas can be derived from a spectral library of various iron oxide minerals or, alternatively, from the imagery under analysis itself. A classification algorithm then uses these training statistics to find areas with similar signatures that may represent gossan exposures.

It should be noted that in all these image-processing techniques, particularly with supervised classification, other targets with a similar spectral response to gossans can be misidentified as the latter. Uniquely relying on colour contrasts revealed by multispectral sensors implies that red to yellow geological units (shale, sandstone), surficial deposits (eolian, glaciofluvial and littoral glaciomarine sediments) and/or vegetation (bogs) can be confused with gossans. These false targets must be screened out using more detailed spectral and pattern analysis.

MINERAL MAPPING USING HYPERSPECTRAL REMOTE SENSING

As mentioned above, recognition of individual iron oxides is possible if the sensor has sufficient spectral resolution. This is the advantage offered by hyperspectral optical sensors for mapping the mineralogy of gossans. As shown in Figure 3, various iron oxides have unique spectral characteristics. To illustrate this point, Figure 7 compares a gossan spectra extracted from LANDSAT-7 data over the High Lake Gossan with spectra extracted from hyperspectral data over the same gossans. The differences in the spectra are obvious. The LANDSAT-7 spectra only show high reflection in the red band and absorption in the blue band, making detection of the gossan feasible but not that of the individual iron oxide mineral(s) contained within the gossan. In contrast, the spectra extracted from the hyperspectral data show far more detail, and best matches the goethite spectra obtained through spectral reflectance analysis of iron oxide minerals (Figure 8). In fact, from an airborne hyper-spectral mapping perspective, the majority of the spectra extracted from the High Lake Gossan represent pure goethite, some hematite and mixtures of these two oxides. There is only one hyperspectral satellite (HYPERION) orbiting the globe at present and it is geared to research and development. Furthermore, data quality is constrained by a poor signal to noise ratio. However, a number of high-resolution, spectrally-rich sensors (WorldView-2 and -3) are already showing promise to detect and map gossans (Froome et al., 2012; Williamson et al., 2014) and hyperspectral satellite-borne sensors are planned for launch in the next few years (e.g. Enmap). These will offer excellent sources of data that will allow both the mapping of gossans with respect to their surroundings, and the mapping of iron oxides within individual gossans.

CONCLUSIONS

Gossans have been detected and mapped on colour air photographs for over 50 years and on satellite-borne optical multispectral imagery since 1972 with the launch of the first LANDSAT satellite (ERTS-1). The distinct red-orange-yellow ochre colour of gossans not only allows their easy identification in the field, but also on optical multispectral satellite data. However, gossans can be confused with other surficial units or vegetation with a high content in ferric iron, resulting in similar spectral signatures derived from optical sensors characterized by low to moderate spectral resolution. These false positives can be screened out if hyperspectral data are available. The spatial and spectral resolution of optical sensors are key aspects to consider in the detection and mapping of gossans. Higher spatial resolution combined with moderate spectral resolution, typical of many optical sensors now orbiting the Earth, allow for the detection of smaller gossans (~ 2 m or greater in spatial extent). Moderate spatial resolution sensors (e.g., LANDSAT) allow for the detection of larger gossans (~ 30 m in spatial extent). With the advent of widely accessible hyperspectral optical remote sensing data, it should be possible to map the mineralogy of individual gossans, which can be extremely useful for both mineral exploration and environmental studies.

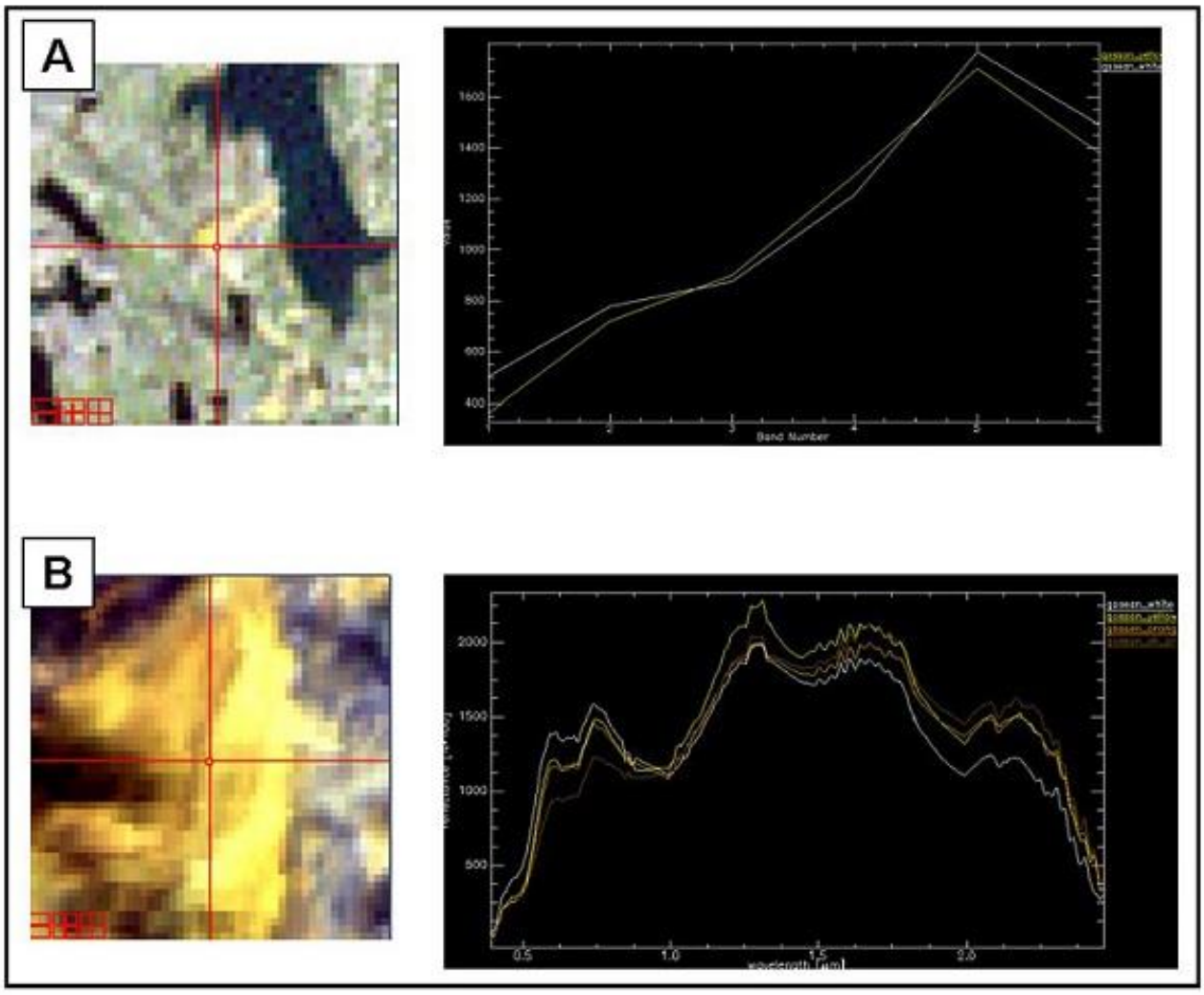

Figure 7. Spectra of the High Lake Gossan extracted from (A) LANDSAT – 7 data and (B) airborne hyperspectral data. Image (A) is based on LANDSAT data. The spectral signature is based on only 6 bands. This low spectral resolution does not allow identification of individual iron oxides. Image (B) is based on hyperspectral data from 306 bands. The high spectral resolution allows identification of individual iron oxides. With hyperspectral data, we can move from detecting gossans to identification of the predominant minerals in the oxide cap.

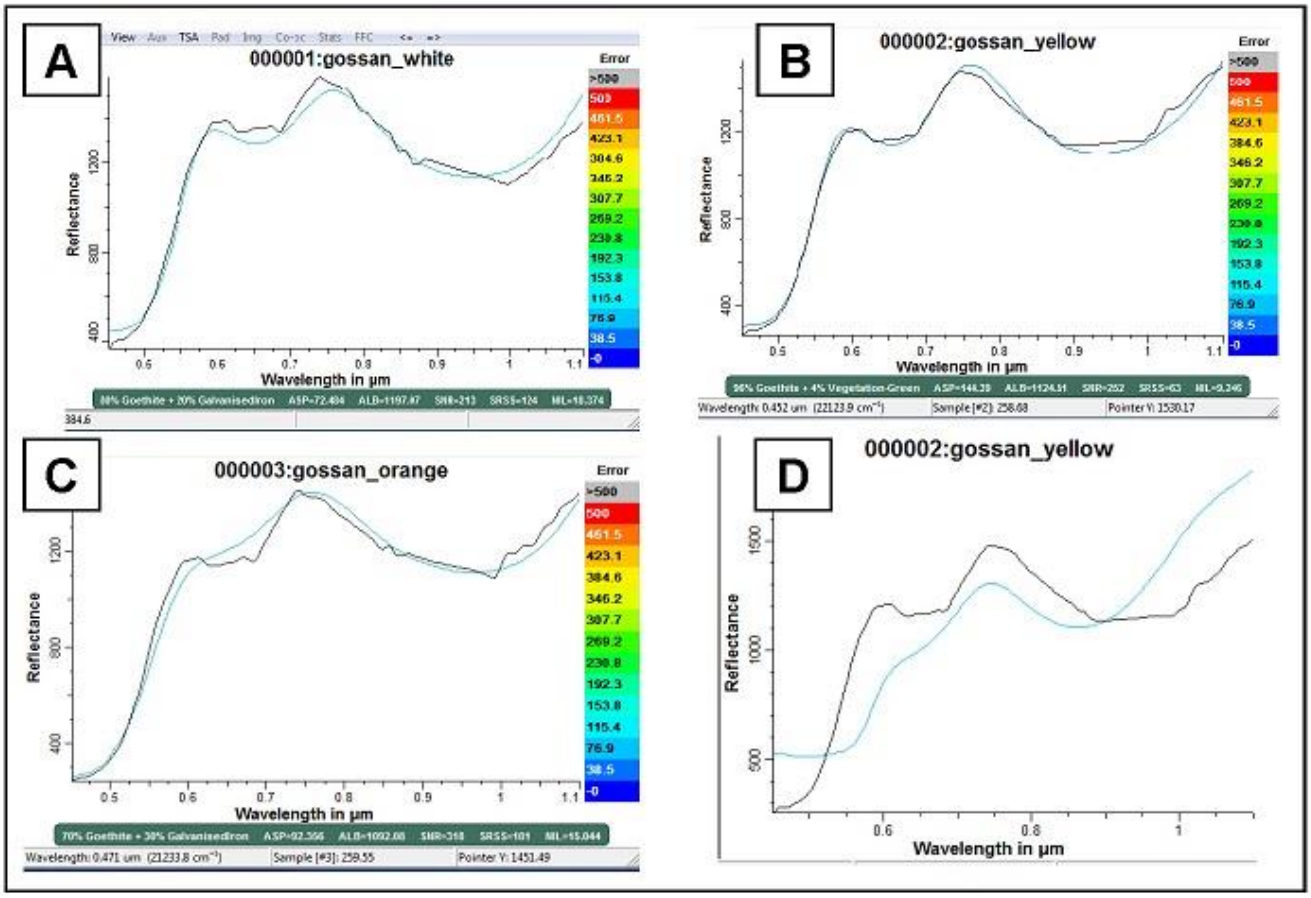

Figure 8. (A, B, C) Spectra extracted from different regions within the High Lake Gossan (shown in black) as well as best spectral match from the United States Geological Survey library (USGS; http://speclab.cr.usgs.gov/spectral-lib.html). The best match for all three extracted spectra based on laboratory spectra is goethite shown in blue. (D) This figure shows the difference between the extracted spectra (goethite - black) and lab spectra of hematite (blue).

ACKNOWLEDGEMENTS

The acquisition of hyperspectral data at High Lake, Nunavut, was carried out by SpecTIR Hyperspectral Imaging and Geospatial Solutions for the Geological Survey of Canada (D. James) with funding from the Strategic Investments Northern Economic Development Fund (SINED[1]). We thank Beth Hillary for help with the figures presented in this paper. Guest Editors Helen Smyth and Benoit Saumur provided comments that improved the manuscript. ESS Contribution number 20130434.

[1] http://actionplan.gc.ca/en/initiative/strategic-investments-northern-economic

REFERENCES

Behnia, P., Harris, J.R., Rainbird, R.H., Williamson, M.-C., and Sheshpari, M., 2012. Remote predictive mapping of bedrock geology using image classification of LANDSAT and SPOT data, western Minto Inlier, Victoria Island, Northwest Territories, Canada; International Journal of Remote Sensing, v.33 (21), p. 6876-6903. doi: 10.1080/01431161.2012.693219

Crosta, A. and Moore, J.M., 1989. Enhancement of LANDSAT thematic mapper imagery for residual soil mapping in SW Minas Gerais State, Brazil, a prospecting case history in greenstone belt terrain *In* Proceedings of the ERIM 7th Thematic Conference: Remote Sensing for Exploration Geology, p. 1173- 1187.

Froome, J., Williamson, M.-C., and Peterson, R.C., 2012. Applied reflectance spectroscopy and mineralogical studies of Gossan Hill, Victoria

Island, Northwest Territories, Canada; Geological Association of Canada-Mineralogical Association of Canada, Program with Abstracts, v. 35, p. 46.

Harris, J.R. (ed.), 2008. Remote predictive mapping: An aid for northern mapping; Geological Survey of Canada, Open File 5643, DVD.

Harris, J.R., Schetselaar, E., and Behnia, P., 2012. Remote Predictive Mapping: An approach for the geological mapping of Canada's Arctic; Dr. Imran Ahmad Dar, ed., Earth Sciences, InTech, p. 495-524.

Lightfoot, P.C. and Evans-Lamwood, D.M., 2015. Near surface manifestations of the controls on Ni-Cu-PGE sulphide mineralisation in the structural roots of large igneous provinces, *in* Environmental and Economic Significance of Gossans, (ed.) M.-C. Williamson; Geological Survey of Canada, Open File 7718, p. 25-30.

McNeil, R.J., Day, S.J.A., and Williamson, M.-C., 2015. Stream sediment and water geochemical study, Axel Heiberg Island, Nunavut, Canada, *in* Environmental and Economic Significance of Gossans, (ed.) M.-C. Williamson; Geological Survey of Canada, Open File 7718, p. 85-96.

Percival, J.B., Williamson, M.-C., McNeil, R.J., and Harris, J.R., 2015. Morphology of gossans in the Canadian Arctic Islands, *in* Environmental and Economic Significance of Gossans, (ed.) M.-C. Williamson; Geological Survey of Canada, Open File 7718, p. 58-73.

Petch, C.A., 2005. The geology and mineralization of the High Lake volcanic-hosted massive sulphide deposits, Nunavut; Exploration and Mining Geology, v. 13, p. 37-47.

Taylor, R., 2011. Gossans and Leached Cappings, Field Assessment, Springer-Verlag, Berlin, 146 pp.

West, L., McGown, D.J., Onstott, T.C., Morris, R.V., Suchecki, P., and Pratt, L.M, 2009. High Lake gossan deposit: An Arctic analogue for ancient Martian surficial processes? Planetary and Space Science, v. 57, p. 1302–1311.

Williamson, M.-C., Percival, J.B., Harris, J., Peterson, R.C., Froome, J., Bédard, J., McNeil, R.J., Day, S.J., Kingsbury, C.G., Grunsky, E., McCurdy, M., Shepherd, J., Hillary, B., and Buller, G., 2014. Environmental and economic impact of oxide-sulphide gossans, Northwest Territories and Nunavut, Geological Survey of Canada, Open File 7486, 10 p. + poster. doi:10.4095/293922

Williamson, M.-C, McNeil, R.J., Day, S.J.A., McCurdy, M.M., Rainbird, R.H., and Grunsky, E.C., 2015. Environmental impact of gossans revealed by orientation surveys for base metals in the Canadian Arctic Islands, *in* Environmental and Economic Significance of Gossans, (ed.) M.-C. Williamson; Geological Survey of Canada, Open File 7718, p. 74-84.

REMOTE PREDICTIVE MAPPING OF BASE METAL GOSSANS ASSOCIATED WITH EVAPORITE DIAPIRS AND MAFIC INTRUSIONS IN THE SOUTH FIORD AREA, AXEL HEIBERG ISLAND, NUNAVUT

Cole G. Kingsbury
Department of Earth Sciences, Ottawa-Carleton Geoscience Centre, Carleton University,
1125 Colonel By Drive, Ottawa, Ontario, K1S 5B6
(email: cole_kingsbury@carleton.ca)

INTRODUCTION

The author was an invited participant in the 2013 Isachsen field expedition to Axel Heiberg Island organized by the Geological Survey of Canada (Kingsbury et al., 2014a; Figure 1). The goals of this expedition were: (1) to sample and characterize base metal gossans as natural analogues to potential interactions between mine waste and continuous permafrost, (e.g. Williamson et al., 2014); (2) to conduct stream sediment geochemical and heavy metal concentrate studies; and, (3) to map and sample mafic dykes, sills and lava flows in the field area in order to understand intrusive styles (dyke vs. sill) and to geochemically fingerprint them for magmatic and Ni-Cu-PGE metallogenic processes.

Geologic expeditions in remote areas such as Axel Heiberg Island by nature are resource and time intensive. In terms of scientific preparation, field work planning included remote predictive mapping (RPM) of the study area using Landsat-7 Thematic Mapper (TM) in concert with Advanced Spaceborne Thermal Emissions Radiometer (ASTER) sensors to delimit regions where gossans may be concentrated, and to elucidate first-order hypotheses as to the style of mafic intrusions of the study area (Figure 1). The results of these analyses are the focus of this study.

GEOLOGY

The geology of the study area consists of sandstones, siltstones and shales with subordinate basaltic lava flows of lower Cretaceous age that, together, previous workers have mapped as the Isachsen Formation of the Sverdrup Basin (Thorsteinsson & Tozer, 1971). Mafic dykes, and sills of early Cretaceous age intrude the Isachsen formation and are local constituents of the High Arctic Large Igneous Province (HALIP), a widespread episode of magmatism that affected the Arctic margins in Canada, Svalbard (Norway) and Franz Josef Land (Russia) (Drachev and Saunders, 2006). Two major evaporite diapirs (the South Fiord and East Fiord diapirs), consisting predominantly of anhydrite and gypsum from the Carboniferous Otto Fiord Formation, intrude the Isachsen formation and HALIP tabular intrusive structures and impose a major structural control on the Cretaceous rocks exposed in the detailed field area (Jackson & Harrison, 2006) (Figure 1).

METHODS

Landsat-7 TM, with a spatial resolution of 30 m, consists of six bands of the electromagnetic spectrum: three in the visible, one in the thermal infrared and two in the shortwave infrared. Different earth materials reflect in different parts of the electromagnetic spectrum (Figure 2) (Wilford & Creasey, 2002). In order to understand where base metal gossans may be concentrated, imagery derived from Landsat-7 TM was used in the construction of a predictive map by way of composite band ratios (Figure 3) using ESRI® ArcGIS v10.1. A prerequisite for undertaking geologic RPM is first delimiting, and then masking out pixels that represent vegetation. Green vegetation is highly reflective in the near infrared (band 4) but reflects close to nil in visible red (band 3) (Figure 2). Therefore, a vegetation index (VI) ratio of [4] / [3] was applied to the imagery.

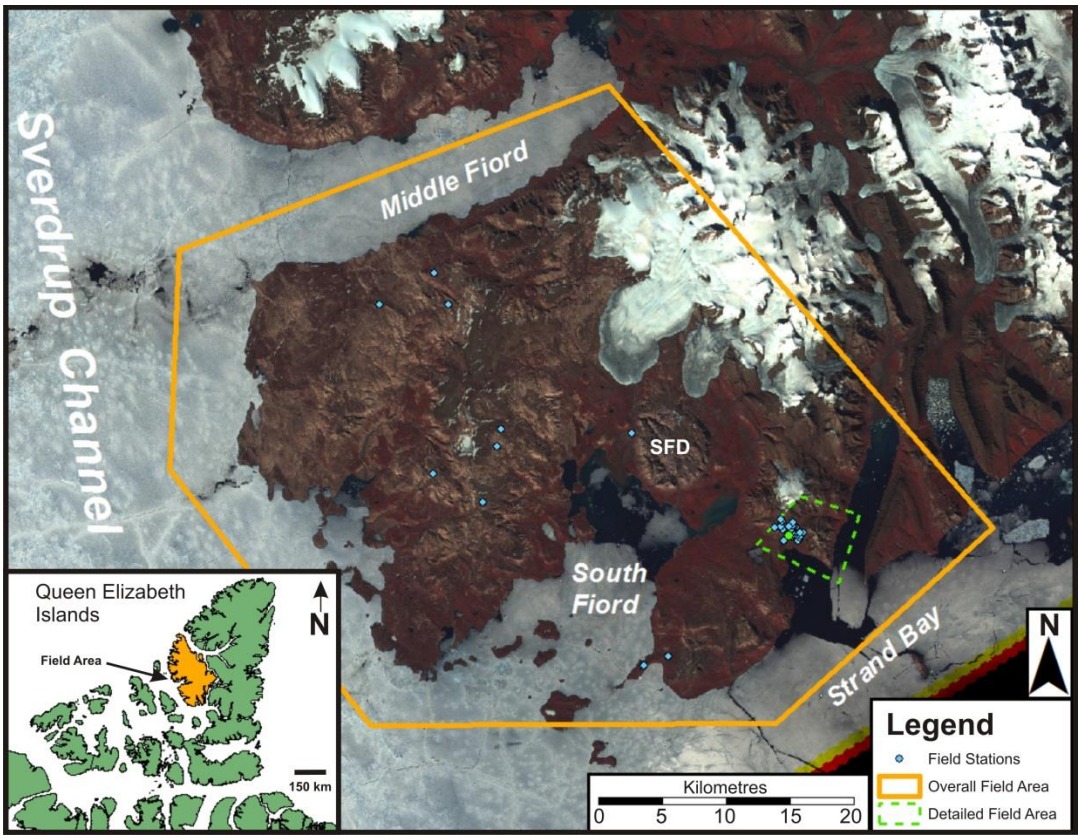

Figure 1. False-colour Landsat-7 TM imagery (R[4]; G[3]; B[2]) of the 2013 study area on western Axel Heiberg Island centered around South Fiord. Areas in red denote vegetation; orange and buff colours denote sedimentary rocks and evaporite diapirs; dark brown represent igneous rocks. SFD = South Fiord Diapir. The inset map in the lower-left shows the location of Axel Heiberg Island (orange) within the Queen Elizabeth Islands in northernmost Nunavut.

This serves as a reasonable first-order determination of vegetation cover on a pixel-by-pixel basis. VI values range from 0 to ~2 with higher values denoting increasing vegetation. In order to mask pixels that represent vegetation, pixels with a VI > 1 were classified as vegetation (Figure 3A) after manually testing different cutoff values against the red pixels in the false-colour imagery such as that shown in Figure 1. Assigning higher cutoff values would have negatively impacted the efficacy of masking. This classified VI mask then was added into the GIS program as a layer (Figure 3B). In order to delimit regions of the South Fiord studat area that may be prospective for gossans, a composite band ratio map (Figure 4) was made consisting of entering band ratios [5] / [7] into the red channel, [3] / [2] into the green channel and [4] / [5] into the blue channel (Figure 3A). This composite ratio map, called the Abrams ratio map (Abrams et al., 1983; Kudamnya et al., 2014; Mia & Fujimitsu, 2012) highlights in bright red regions that contain elevated clay content in alteration zones which is a major constituent of gossan deposits in Canada's Arctic Islands (Williamson, et al., 2011; Williamson et al., 2014). One objective of the 2013 field campaign was to understand the style of igneous intrusion in the field area (Figure 5). In order to achieve this and also to plan the field season, satellite imagery from the 15 m-resolution ASTER sensor was acquired (J. Shepherd, written communication, 2013) (Figure 6). By entering ASTER bands 1, 2, and 3 into the red, green and blue channels, respectively, a near-true colour satellite image is generated. Sedimentary rocks and evaporite diapirs are off-white in colour, while mafic intrusions and lava flows appears dark grey to dark red.

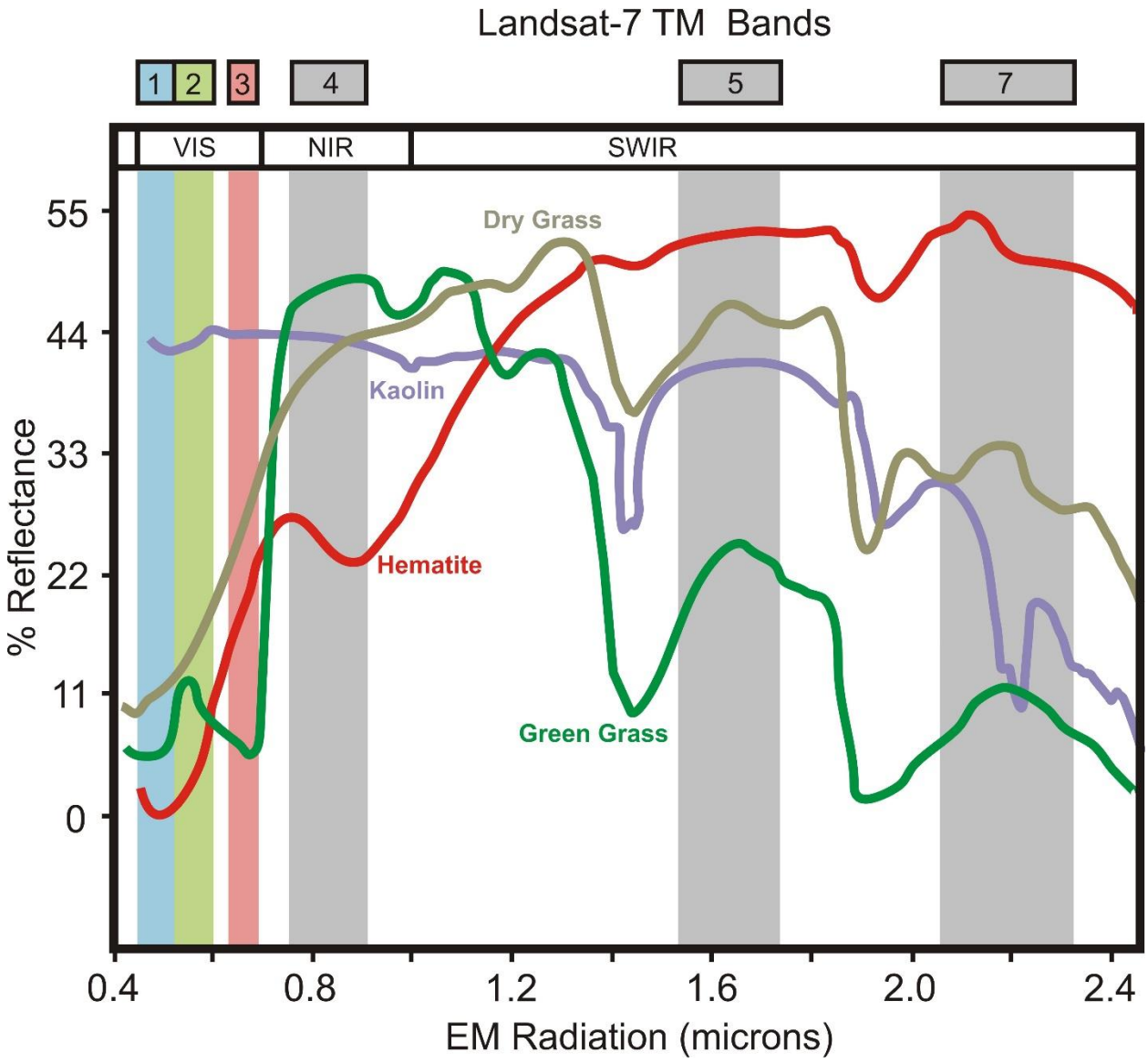

Figure 2. Reflectance values of selected earth materials in the context of the Landsat-7 TM Satellite bands. Bands 1, 2 and 3 denote blue, green and red visible (VIS) bands. Band 4 is in the near-infrared (NIR) and bands 5 and 7 are in the shortwave infrared (SWIR) part of the electromagnetic (EM) spectrum. Note that green grass is highly reflective in the NIR while almost completely absorbent in the red visible wavelengths. Modified from (Wilford and Creasey, 2002).

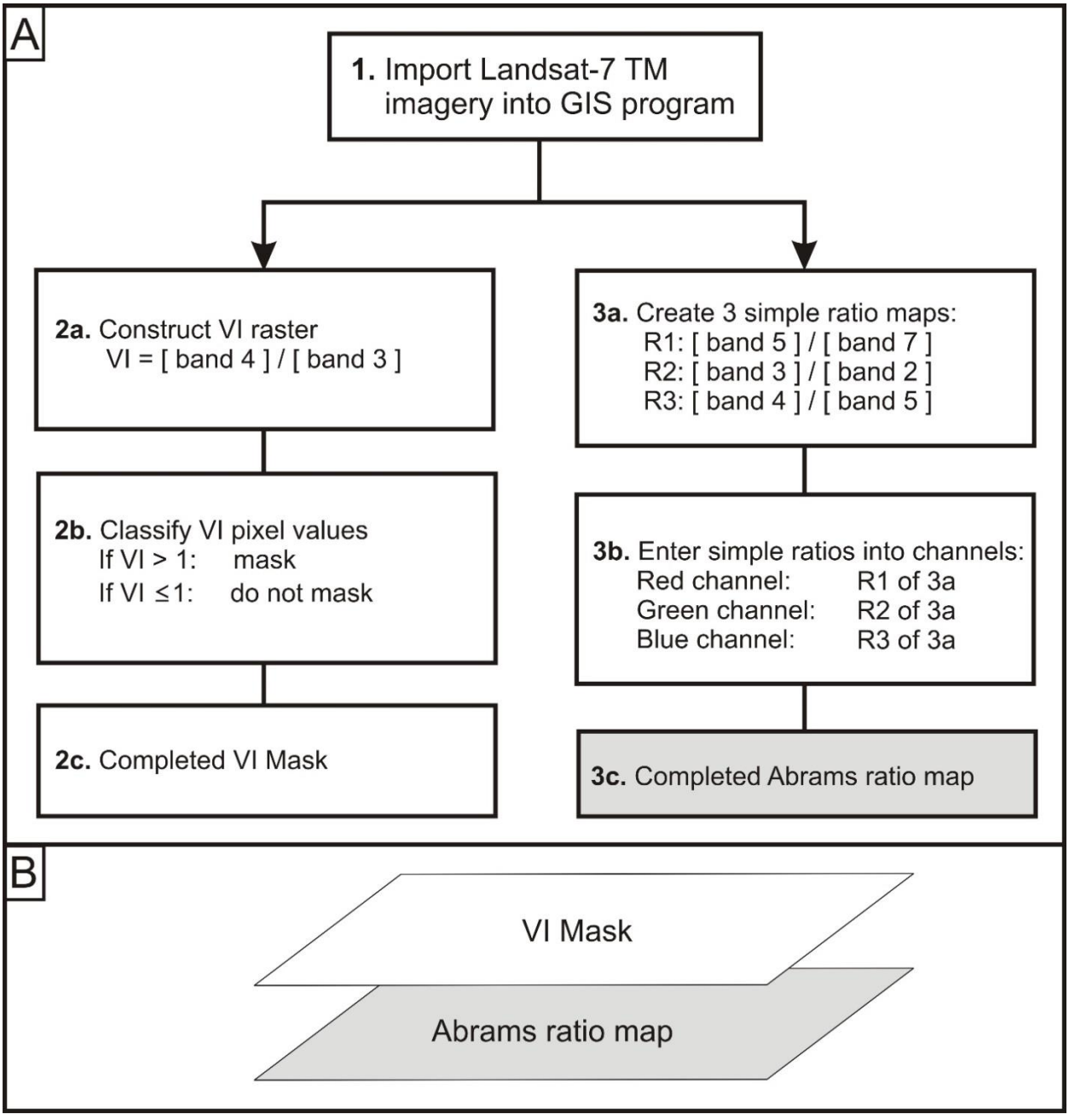

Figure 3. (A) Flow chart of the process in constructing the Abrams composite ratio map using GIS software. (B) Schematic diagram showing the VI mask as a layer above the Abrams remote predictive map.

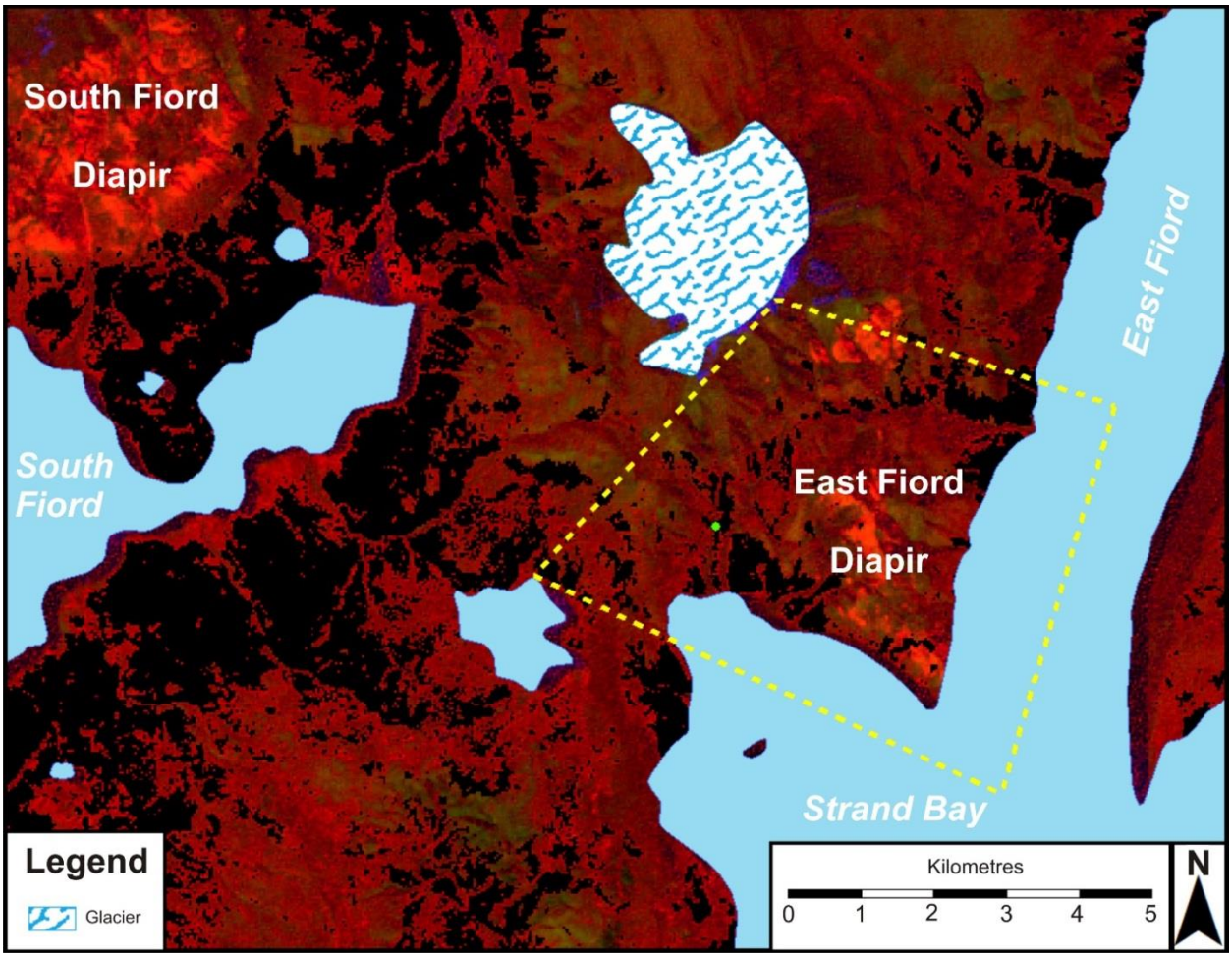

Figure 4. Abrams composite ratio map (R[5]/[7]; G[3]/[2]; B[4]/[5]) of a portion of the 2013 field area emphasizing the detailed study area (yellow-dashed outline). Blackened pixels represent areas that the VI identified as vegetation and have thus been masked out. Note the bright red in the vicinity of the evaporite diapirs indicating an elevated clay content relative to ambient conditions. Diffuse green areas denote slightly elevated iron oxide content.

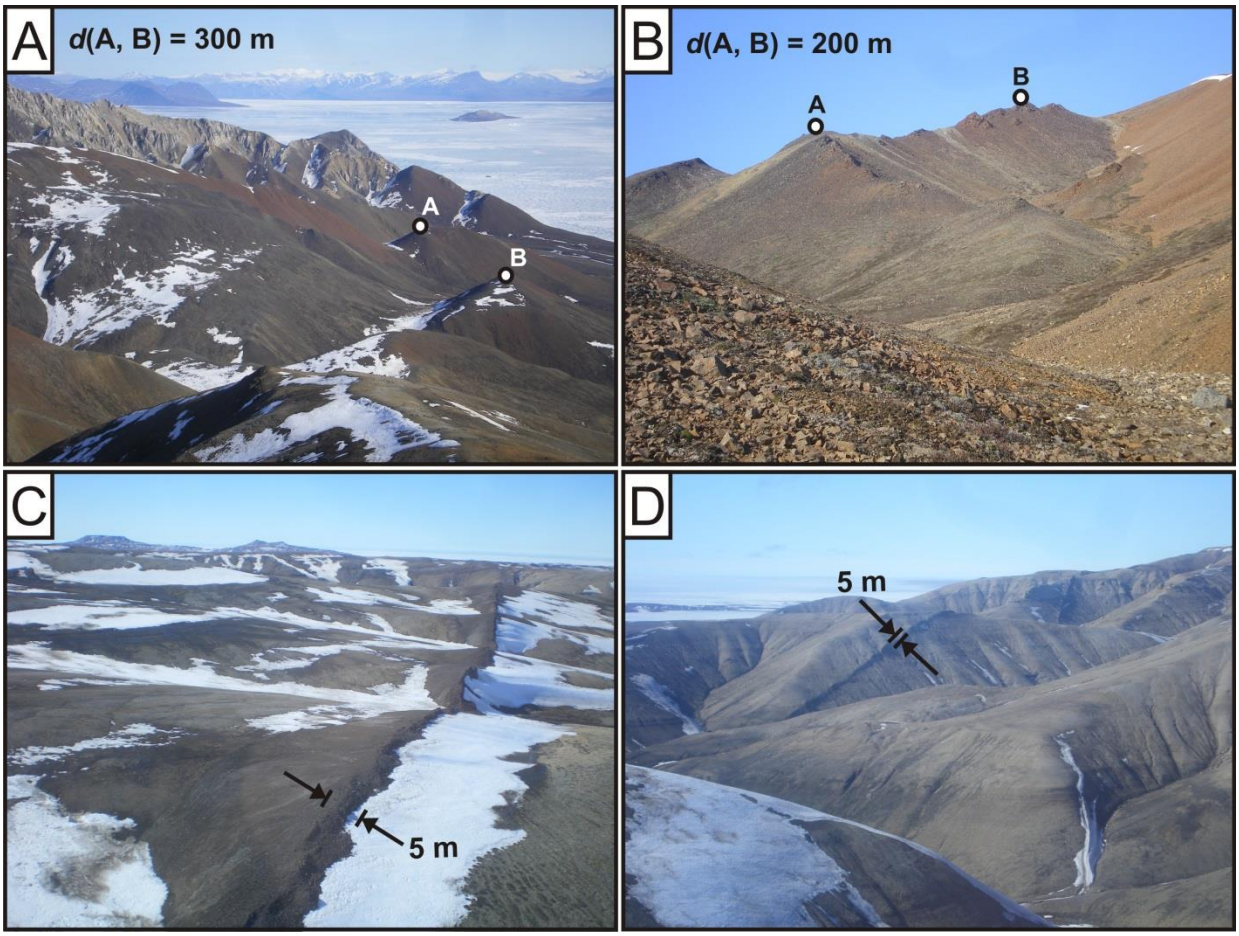

Figure 5. Field photographs of the 2013 field area on west central Axel Heiberg Island. (A) Overview photograph taken towards the east. The tan-coloured slopes consist of evaporite from the East Fiord diapir while the dark brown slopes consist of mafic igneous intrusive rocks and sedimentary rocks. (B) Mid-range view showing the typical morphology of ridges in the detailed study area. Note the extensive talus aprons which mantle the ridge slopes. (C) Oblique aerial photograph of the overall study area, showing a dyke cross-cutting subdued topography from the bottom centre to the distant-right of the image. (D) Oblique aerial photograph to the west showing a dyke cross-cutting horizontal sedimentary strata in the distant centre. Scale measurements of A and B refer to distances between points via Google Earth© imagery. Scale measurements on width of dykes in C and D were made by visual interpolation from ground measurements on dykes displaying similar width.

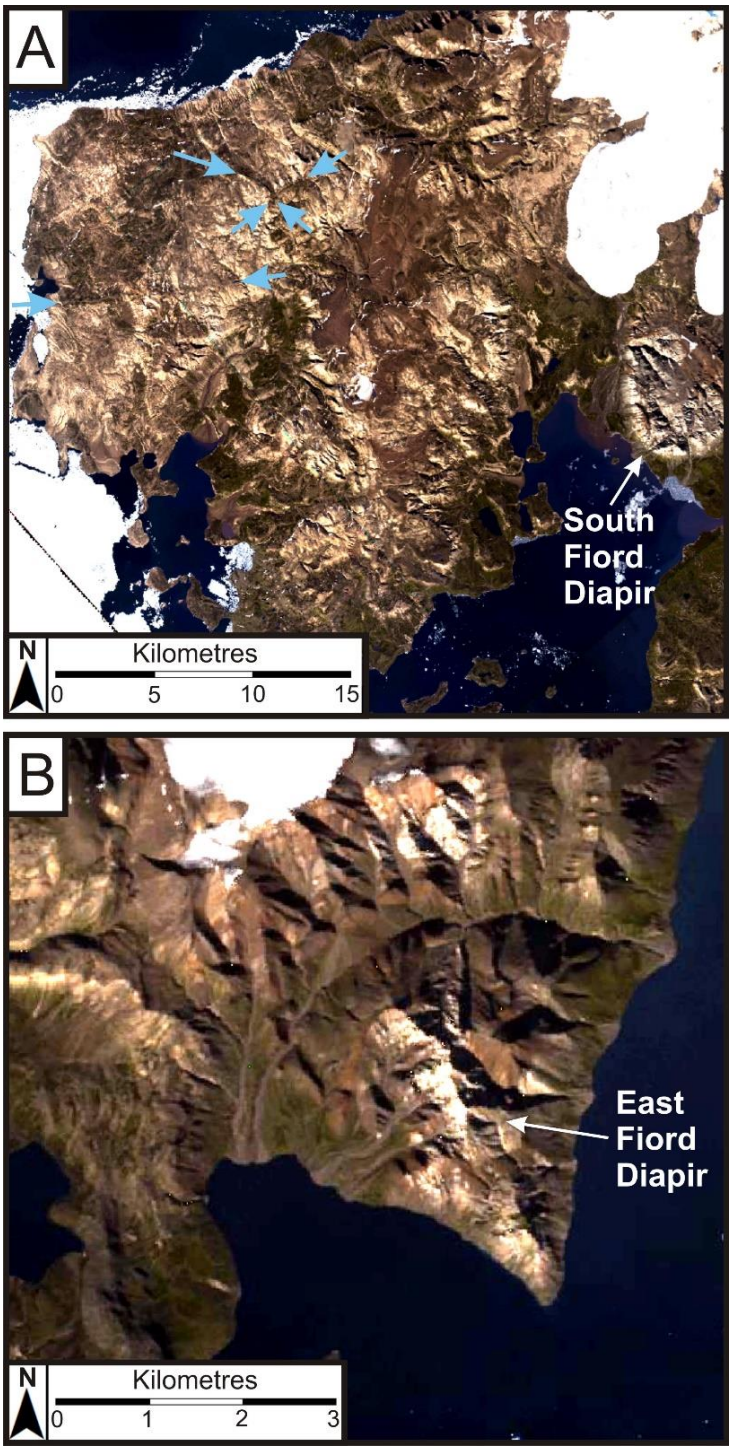

Figure 6. ASTER imagery of the 2013 Field Area. Dark brown represents mafic igneous rocks, light orange to tan colours represent sedimentary rocks, evaporite diapirs are displayed as whitish areas, and green areas denote vegetation. (A) Overall study area, blue arrows point to, and extend the strike parallel to selected dykes.
(B) Close up of the study area.

RESULTS AND DISCUSSION

Results from the composite ratio map (Figure 4) reveal that the South Fiord and East Fiord diapirs are bright red in colour when compared to the overall dark red baseline of the surrounding area, signified by the high [5] / [7] ratio of clays (note the kaolinite spectra in Figure 2). This suggests that the evaporite diapirs contain elevated clay content, and therefore metre-scale base metal gossans are likely to be present at these locations in contrast to the surrounding area. Small patches of diffuse green within the map area suggest increased concentrations of hydrothermal iron oxide components in these areas (Abrams et al., 1983; Kudamnya et al., 2014; Mia & Fujimitsu, 2012). However, it remains unclear whether these are indicators of gossans or simply reflect local variations in surficial soil chemistry. Landsat imagery has a resolution of 30 m per pixel. As a result, it is challenging to detect individual metre-scale gossans. Multispectral satellite imagery with higher spatial resolution is required to locate individual gossans. Furthermore, it is quite possible that some gossans may be buried beneath talus piles, which would render remote-sensing techniques more difficult to apply.

This study demonstrates that ASTER imagery is a useful tool for the first-order determination of mafic intrusion geometries, particularly dykes in sparsely-vegetated remote areas such as Axel Heiberg Island. ASTER imagery is especially effective for remote predictive mapping of poorly-vegetated volcanic terrain. In particular, the northwest quadrant of the peninsula in Figure 6A reveals that one dyke trends E-W while two others strike NE-SW and NW-SE as they cut sub-horizontal sedimentary sequences. In field areas exhibiting higher geological complexity, such as in the vicinity of evaporite diapirs (Figure 5A) or in areas with extensive talus piles (Figure 5B), relationships between intrusions and country rocks may be too unclear to resolve at the spatial resolution ASTER affords.

CONCLUSIONS

Applying ratios from spectral bands sensitive to Fe-oxide and clay reflectance on Landsat-7 TM imagery was used in this study to help predict where base metal gossans in the South Fiord and East Fiord areas may be present. As a result, the Abrams ratio map was employed to highlight regions that display spectral signatures of elevated Fe-oxides and clay, which are key indicators of the presence of gossanous deposits. On the basis of this work, base-metal gossans are predicted to be concentrated around evaporite diapirs, since diapirs show elevated spectral signatures of clay (Williamson et al., 2011).

Because Axel Heiberg Island is substantially unvegetated, and lithological units are not significantly influenced by a high-degree of tectonic complexion on the peninsula west of South Fiord Diapir it can be seen that much of the study area consists of sedimentary rocks (tan to light orange) with lava flows and dykes in dark red to brown. Geochemical studies on these igneous rocks as well as those of the detailed field area (e.g., Kingsbury et al., 2014b) along with isotopic and U-Pb dating will be used to understand the geochemical evolution, Ni-Cu-PGE potential and tectonic significance of HALIP in Arctic Canada and how it fits with dykes, sills and lava flows from correlatives in Russia and Norway.

ACKNOWLEDGEMENTS

The author wishes to thank Jeff Harris for sharing his knowledge of remote predictive mapping techniques; Marie-Claude Williamson, Stephen Day and Rick McNeil for their support during field work and for numerous discussions on site and at GSC Ottawa; and Jeffrey Shepherd for access to ASTER images of the study area. The author acknowledges financial and logistical support from the Polar Continental Shelf Program through PCSP Project 003-13; and an NSERC-CRD grant to Richard Ernst and Brian Cousens, the author's thesis supervisors at Carleton University. Special thanks to Guest Editors Helen Smyth and Benoit Saumur for

comments and suggestions that significantly improved the original manuscript.

REFERENCES

Abrams, M.J., Brown, D., Lepley, L., and Sadowski, R., 1983. Remote Sensing for Porphyry Copper Deposits in Southern Arizona: Economic Geology, v. 78, p. 591–604.

Drachev, S., and Saunders, A., 2006. The early Cretaceous Arctic LIP: its geodynamic setting and implications for Canada Basin opening, *in* Scott, R.A. and Thurston, D.K. eds., Proceedings of the Fourth International Conference on Arctic Margins, Anchorage, USA.

Jackson, M.P.A., and Harrison, J.C., 2006. An allochthonous salt canopy on Axel Heiberg Island, Sverdrup Basin, Arctic Canada: Geology, v. 34, p. 1045–1048.

Kingsbury, C.G., Williamson, M.-C., Day, S.J., and McNeil, R.J., 2014a. The 2013 Isachsen expedition to Axel Heiberg Island, Nunavut, Canada: a field report: Geological Survey of Canada, Open File 7539, 2014; 6 pages (1 sheet).

Kingsbury, C.G., Ernst, R.E., Cousens, B.L., and Williamson, M.-C., 2014b, Geochemical insights on the Early Cretaceous High Arctic LIP, *in* Geologicla Society of America Abstracts with Programs. Vancouver, BC., v. 46, p. 637.

Kudamnya, E.A., Andongma, W.T., and Osumeje, J.O., 2014. Hydrothermal mapping of Maru Schist Belt, north-western Nigeria using remote sensing tequnique: International Jounal of Civil Engineering, v. 3, p. 59–66.

Mia, B., and Fujimitsu, Y., 2012. Mapping hydrothermal altered mineral deposits using Landsat 7 ETM + image in and around Kuju volcano, Kyushu, Japan: Journal of Earth Systems Science, v. 121, p. 1049–1057.

Thorsteinsson, R., and Tozer, E.T., 1971. Geology, Middle Fiord, District of Franklin: Geological Survey of Canada, Map 1299A, scale 1:250,000.

Wilford, J., and Creasey, J., 2002. Landsat thematic mapper, *in* Papp, E. ed., Geophysical and Remote Sensing Methods for Regolith Exploration, CRCLEME Open File Report 144, p. 6–12.

Williamson, M.-C., Percival, J.B., Behnia, P., Harris, J.R., Peterson, R.C., Froome, J., Fenwich, L., Rainbird, R.H., Bédard, J.H., McNeil, R.J., Day, S.J., Kingsbury, C.G., Grunsky, E., McCurdy, M.W., Shepherd, J., Hillary, E. M and Buller, G., 2014. Environmental and economic impact of oxide-sulphide gossans, Northwest Territories and Nunavut: Geological Survey of Canada, Open File 74886, p. 10 (1 sheet).

Williamson, M.-C., Smyth, H.R., Peterson, R.C., and Lavoie, D., 2011. Comparative geological studies of volcanic terrain on Mars : Examples from the Isachsen Formation , Axel Heiberg Island, Canadian High Arctic: Geological Society of America Special Papers 483, p. 249–261.

NEAR SURFACE MANIFESTATIONS OF THE CONTROLS ON NI-CU-CO-PGE SULPHIDE MINERALISATION IN THE STRUCTURAL ROOTS OF LARGE IGNEOUS PROVINCES

Peter C. Lightfoot[1] and Dawn M. Evans-Lamwood[2]

[1]Vale Technology Development (Canada) Limited, Brownfield Exploration, Copper Cliff, Ontario, P0M 1N0 (email: Peter.Lightfoot@vale.com)

[2]Vale Newfoundland and Labrador Limited, 10 Fort William Place, Baine Johnston Centre, Suite 700, St. John's, Newfoundland and Labrador, A1C 1K4

INTRODUCTION

The history of discovery of large magmatic Ni-Cu-platinum group element (PGE) sulphide deposits has often been underpinned by discovery of a gossan or surface outcrop of mineralisation either through careful science or prospecting serendipity. Once the discovery is made, the creation of value through exploration is typically rooted in careful geoscience investigations. Notwithstanding the "holy grail", discovery remains attractive, and geologists continue to search remote areas for the surface manifestations of Ni-Cu-PGE sulphide ore deposits (Lightfoot, 2007).

Within this context, it is of critical importance that geologists and explorationists understand not only the characteristics of the target, but also favourable geological settings for the genesis and occurrence of magmatic Ni-Cu-PGE deposits. The presence of sulphide gossans often provide critical evidence for mineralisation that triggers further work leading to discovery of a deposit.

CONTEXT FROM THE VOISEY'S BAY NI-CU-CO SULPHIDE DEPOSIT, LABRADOR

The Voisey's Bay Deposit is located near the boundary of the Churchill and Nain Provinces in Labrador, Canada. The geology and geochemistry of the Voisey's Bay Intrusion is documented in Lightfoot et al. (2012a, b) and references therein. Figure 1 shows the recent state of mine development of the Ovoid Deposit and the narrower mineral zone to the west which comprises the Mini-Ovoid, that is a widened domain of the dyke that extends up the face of the open pit onto Discovery Hill. The original discovery gossan comprised strongly oxidized sulphide mineralisation within olivine gabbro and troctolite (Naldrett et al., 1996). The Ovoid Deposit was originally covered by a thin swamp underlain by 1-10m of glacial till; beneath the till cover, the Ovoid comprised of fresh sulphide at the bedrock interface and showed as a classic loop-textured style of mineralisation where large crystals of pyrrhotite are surrounded by chalcopyrite and pentlandite (Figure 2).

The distribution of magmatic Ni-Cu-PGE sulphide deposits and mineralisation in mafic intrusions is controlled by the geometry and structural setting of the magma chamber. The recognition that the Ovoid and the Eastern Deeps at Voisey's Bay are localized where a dyke-like conduit connects to a larger intrusive body has been a key observation that has underpinned much of the exploration activity (Figure 3). Geological evidence points to the development of the dyke, the Ovoid, and the Eastern Deeps chamber in a syn-magmatic dextral structure undergoing graben collapse (Lightfoot and Evans-Lamswood, 2015). Good evidence for syn-emplacement graben development is recorded in the detailed structural measurements of Evans-Lamswood (2000) and Evans-Lamswood et al (2000). Lightfoot and Naldrett (1999) suggested that the Eastern Deeps chamber is connected at depth to the eastern extension of the Western Deeps chamber (shown in Figure 3) by dyke-like structures that correspond to the Discovery Hill and Eastern Deeps dykes.

Figure 1. Aerial photograph showing the status of development of the Ovoid Deposit in 2012. The dyke extending towards the top right hand corner points to the original discovery site of a gossan. The wide domain of sulphide is the Ovoid Deposit, and the narrower zone of mineralsiation between the Ovoid and the dyke is the Mini-Ovoid zone. The location and general geology of the deposit is described in Lightfoot et al. (2012a).

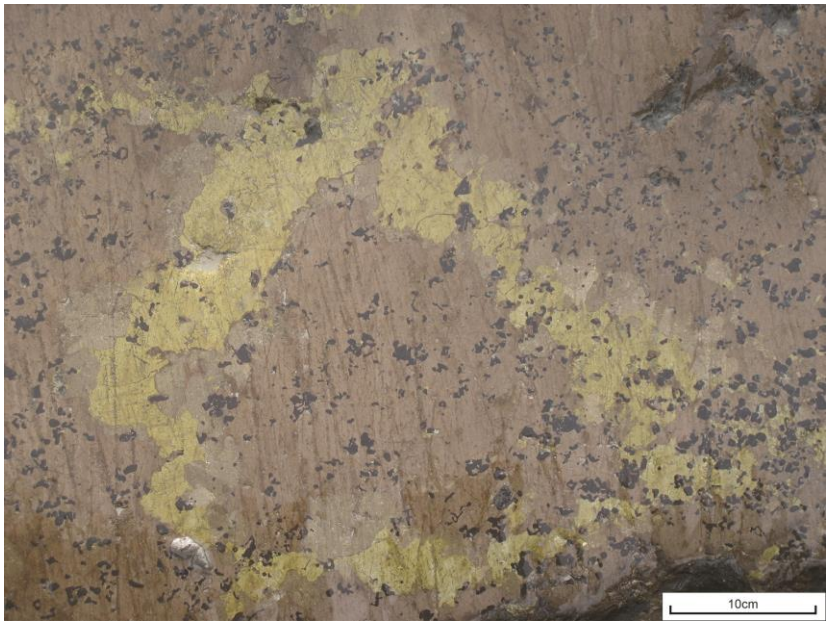

Figure 2. Massive sulphide mineralisation at surface, exposed beneath the till. The sulphide is entirely un-oxidised and shows the development of 25cm-1m loops of chalcopyrite and pentlandite containing large bodies of pyrrhotite.

Cruden et al. (2008) suggested that space creation for the emplacement of the intrusion was controlled by mid-crustal cauldron subsidence, a process geometrically analogous to caldera collapse, within an active rift zone. The combination of this model with the evidence for dextral transtension provides the basis for applying the scissor-fault model to the deposit as shown in Figure 4 (Lightfoot and Evans-Lamswood, 2015).

GLOBAL MODEL FOR NI-CU-PGE SULPHIDE DEPOSITS CONTAINED IN CHONOLITHS WITHIN TRANSCURRENT FAULT ZONES

The geological relationships in the Noril'sk Type intrusions indicate a localization of mineralisation within the thicker axial parts of magma conduits that follow and are modified by major structures like the Noril'sk Kharaelakh Fault (Lightfoot and Zotov, 2007; 2014). These intrusions have a cross-sectional morphology of chonolith tubes with flanking sills. The synformal structures developed adjacent to the Noril'sk-Kharaelakh Fault appear to control the locus of emplacement of the Noril'sk 1, Noril'sk 2 and Chernogorsk chonoliths (Lightfoot and Zotov, 2007; 2014).

Some of the best examples of mineralisation within intrusions adjacent to feeder conduits are found in China; the Hong Qi Ling Deposits in Jilin Province shows the juxtaposition of small mineralized mafic intrusions within structural corridors (Lightfoot and Evans-Lamswood, 2015). These relationships are also found in the Huangshan, Huangshandong and Jingbulake Intrusions in Xinjiang Province, where disseminated sulphides are localized at the base of differentiated intrusions above comagmatic dykes (Lightfoot and Evans-Lamswood, 2015).

The same intrusion geometry is developed at Jinchuan in Gansu Province where the largest sulphide Ni deposit in China is hosted in a small intrusion (Tang, 1992; 1993). Most of these small intrusions appear to be developed along regional strike-slip fault structures that create space for their emplacement. Many other small differentiated intrusions have diamond-shaped cross-sections and dyke-like keels; these include the Limahe and Qingquanshan Deposits in Sichuan Province and the Hong Qi Ling Intrusions in Jilin Province (Lightfoot and Evans-Lamswood, 2015). Another case of mineralisation controlled by magma conduits within strike-slip fault zones includes the Kalatongke Deposit in Xinjiang province.

Many other examples of small differentiated mafic-ultramafic intrusions with significant Ni-Cu-PGE sulphide deposits are associated with structure. The following examples share common features, including the space created within and adjacent to fault zones by the structures that link into mantle-penetrating fractures that localize magmatism in the roots of large igneous provinces (e.g. Lightfoot and Evans-Lamswood, 2013; 2015).

A. Diamond-shaped plan and funnel-shaped cross section

Jinchuan (Gansu, China), Hong Qi Ling #1 (Jilin, China), Jingbulake (Xinjiang, China), Kalatongke (Xinjiang, China), Huangshan (Xinjiang, China), Huangshandong (Xinjiang, China), Limahe (Sichuan, China), Qingquanshan (Sichuan, China), Lengshuiqing (Sichuan, China), Zhubu (Yunnan, China), Ban Phuc (Vietnam), Ovoid (Labrador, Canada), Discovery Hill (Labrador, Canada), Eastern Deeps (Labrador, Canada), Eagle (Michigan, USA), Double Eagle (Ontario, Canada), Aguablanca (Spain), Maksut (Kazakhstan), Santa Rita (Brasil), and Suwar (Yemen).

B. Pipe-like form

Baimazhai (Yunnan, China), Tongdongzi (Henan, China), Talnakh (Russia), Kharaelakh (Russia), Noril'sk I (Russia), Noril'sk II (Russia), Chernagorsk (Russia), Maslovskoe (Russia), Tamarack (Minnesota, USA), Current Lake (Ontario, Canada), Babel-Nebo (Western Australia), Nkomati (South Africa), Limoeiro (Brasil), Chibasong Jilin, China), Wellgreen (Yukon, Canada), and Voronezh (Russia).

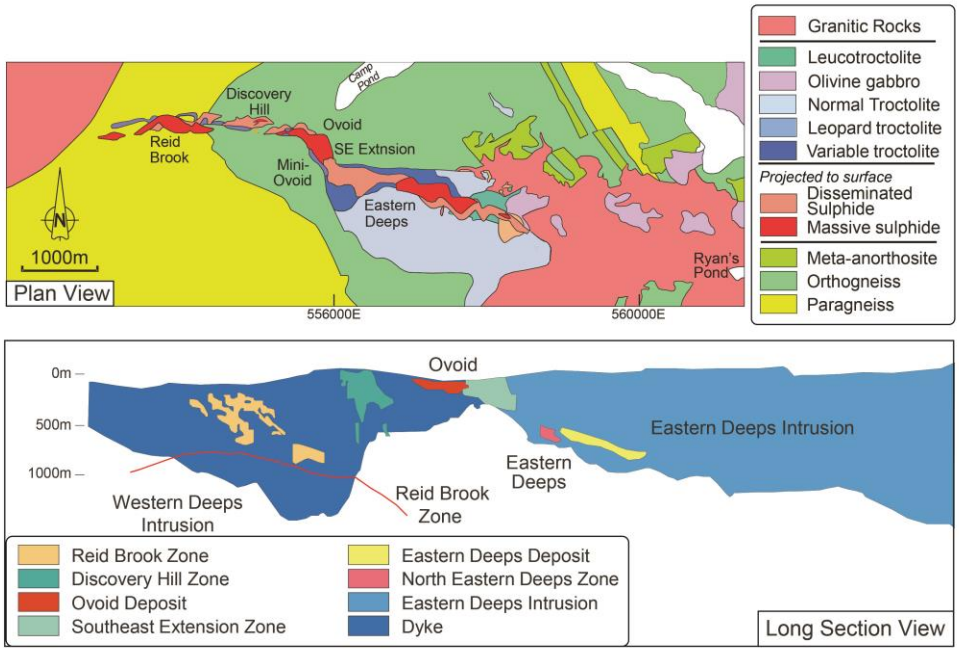

Figure 3. Plan view and long section showing the geological relationships in the area of the footprint of the Voisey's Bay Intrusion, and the projected location of sulphide mineralisation in plan view and long-section.

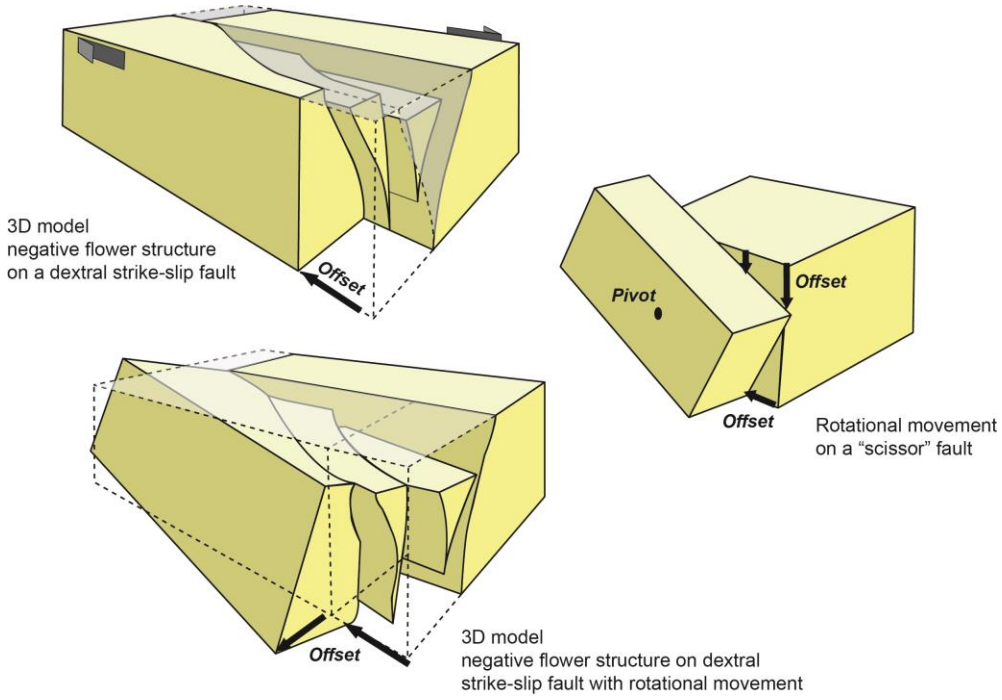

Figure 4. 3D block models showing how a combination of rotational movement on a scissor fault combined with dextral strike slip motion can creates the differing geometry of the Eastern Deeps (the large space opened towards the east) and the Discovery Hill dyke (smaller spaces opened towards the west).

C. Widened pipe-like conduits within dykes and structural discontinuities in dykes

Reid Brook and Eastern Deeps dykes at Voisey's Bay (Labrador, Canada), the Worthington and Copper Cliff Offsets of the Sudbury Igneous Complex (Ontario, Canada), and the Hong Qi Ling #7 Intrusion (Jilin, China).

We recognise a number of features of a class of small strongly differentiated intrusions hosting Ni-sulphide deposits:

1. A spectrum of Ni sulphide ore deposits are found in small intrusions with diamond-shaped outcrop patterns and funnel-shaped cross sections, narrow mafic magma tubes, or within widened domains in dykes. Collectively we refer to these intrusions as chonoliths.

2. The volume of magma relative to the volume of sulphide in many small intrusions is too low to support the formation of the observed deposits by in-situ sulphide saturation and segregation.

3. The massive sulphide ore bodies are sometimes located in the country rocks adjacent to the intrusions (e.g. Talnakh) or choke the feeder conduits (e.g. the Ovoid Deposit); the formation of these deposits by upgrading of the metal concentration in an open system is not supported by geological relationships (e.g. Lightfoot and Zotov, 2014).

4. The small intrusions are often strongly differentiated with mafic and ultramafic rock types developed, and the Ni-Cu-PGE sulphide mineralisation often has an elevated Ni tenor and a wide range in Ni/Cu ratio and PGE concentrations in sulphide.

5. The small intrusions tend to be spatially associated with regional structures that create space, and are localized by dilations and traps created by transtension in strike-slip fault zones.

We propose a model in which sulphide-laden magma ascended through a sub-vertical conduit system in a structural zone from a parental source/chamber at depth. The transportation of dense sulphide takes place through a conduit system undergoing transtension and/or transpression, which effectively pumps the sulphide through the conduit system.

These controls may also have been important in controlling the original geometry and primary ore localization in intrusions that have been extensively modified by deformation and metamorphism; examples include the komatiite channels and sub-volcanic intrusions of the Yilgarn (Western Australia), Thompson (Manitoba, Canada), Pechenga (Russia), and Raglan Belts (Quebec, Canada) (Lightfoot et al., 2012c). The development of gossans after sulphide mineralisation may be a useful exploration tool, but there are numerous examples of differentiated intrusions that have little mineralisation at the present level of subaerial erosion.

ACKNOWLEDGEMENTS

Permission from Vale to present this paper at Symposium no.4, GAC-MAC 2014, Fredericton, NB, is acknowledged. The authors appreciate reviews of this extended abstract by Guest Editors Helen Smyth and Benoit Saumur.

REFERENCES

Cruden, A.R., Evans-Lamswood, D.M., Burrows, D., 2008. Structural, tectonic and fluid mechanical controls on emplacement of the Voisey's Bay troctolite and its Ni–Cu–Co mineralisation; GAC Program with Abstracts, 33, p. 59.

Evans-Lamswood, D.M. 2000. Physical and geometric controls on the distribution of magmatic and sulfide bearing phases within the Voisey's Bay nickel–copper–cobalt deposit, Voisey's Bay, Labrador; Unpublished MSc thesis, Memorial University of Newfoundland, 212 pp.

Evans-Lamswood, D.M., Butt, D.P., Jackson, R.S., Lee, D.V., Muggridge, M.G., Wheeler, R.I., and Wilton, D.H.C., 2000. Physical controls associated with the distribution of sulfides in the Voisey's Bay Ni-Cu-Co deposit, Labrador; Economic Geology, v. 95, p. 749-770.

Lightfoot, P.C. 2007. Advances in Ni–Cu–PGE deposit models and exploration technologies, In Milkereit, B. (ed.), Proceedings of Exploration 07: Fifth Decennial International Conference on Mineral Exploration, pp. 629–646.

Lightfoot P.C. and Naldrett, A.J., 1999. Geological and geochemical relationships in the Voisey's Bay intrusion Nain Plutonic Suite Labrador Canada, In R.R. Keays, C.M. Lesher, P.C., and C.E.G. Farrow (eds.), Dynamic Processes in Magmatic Ore Deposits and Their Application in Mineral Exploration; Geological Association of Canada, v.13, p. 1-31.

Lightfoot, P.C. and Evans-Lamswood, D.M., 2013. Structural controls on Ni–Cu–PGE sulfide mineralisation in the roots of large igneous provinces; PDAC, Toronto. http://convention.pdac.ca/pdac/conv/2013/pdf/ts/lip1-lightfoot.pdf

Lightfoot, P.C. and Evans-Lamswood, D.M., 2015. Structural controls on the primary distribution of mafic-ultramafic intrusions containing Ni-Cu-Co-(PGE) sulphide mineralisation in the roots of large igneous provinces; Ore Geology Reviews, v. 64, p. 354-386.

Lightfoot, P.C., Keays, R.R, Evans-Lamswood, D.M., and Wheeler, R., 2012a. S saturation history of Nain Plutonic Suite mafic intrusions: origin of the Voisey's Bay Ni–Cu–Co sulphide deposit, Labrador, Canada; Mineralium Deposita, v. 47, p. 23-50.

Lightfoot, P.C., Evans-Lamswood, D.M., and Wheeler, R., 2012b. The Voisey′s Bay Ni-Cu-Co sulphide deposit, Labrador, Canada: Emplacement of silicate and sulphide-laden magmas into spaces created within a structural corridor; Northwestern Geology, v. 45, p. 17-28.

Lightfoot, P.C., Stewart, R., Gribbin, G., Macek, J., and Mooney, S., 2012c. Relative contribution of magmatic and post-magmatic processes in the genesis of the Thompson Belt Ni-Co sulphide ore deposits, Manitoba, Canada; Abstracts, International Conference on Nickel, Guiyang, China.

Lightfoot, P.C. and Zotov, I.A., 2007, Ni-Cu-PGE sulphide deposits at Noril'sk, Russia. Short Course; International Polar Year; Prospectors and Developers Association of Canada. Short Course Notes.

Lightfoot, P.C. and Zotov, I.A., 2014. Geological relationships between the intrusions, country rocks, and Ni-Cu-PGE sulphide ores of the Kharaelakh Intrusion, Noril'sk Region: Implications for the role of sulphide differentiation and metasomatism in ore genesis; Northwestern Geology, v. 47, p.1.

Naldrett, A. J., Keats, H., Sparkes, K., Moore, R., 1996. Geology of the Voisey's Bay Ni-Cu-Co Deposit, Labrador, Canada; Exploration and Mining Geology, v. 5, p. 169 – 179.

Tang, Z., 1992. Nickel Deposits of China; Chapter 6, In Mineral Deposits of China, v. 2, p. 52-99, Beijing Publishing House.

Tang, Z., 1993. Genetic model of the Jinchuan nickel-copper deposit, In Mineral Deposit Modelling, R.V. Kirkham, W.D. Sinclair, R.I. Thorpe, and J.M. Duke (eds.), Geological Survey of Canada, Special Paper 40, p. 389-401.

MLA-SEM EXAMINATION OF SULPHIDE MINERAL BREAKDOWN AND PRESERVATION IN TILL, VOISEY'S BAY NI-CU-CO DEPOSIT, LABRADOR: THE DISTRIBUTION AND QUANTITATIVE MINERALOGY OF WEATHERED SULPHIDE PHASES IN A TRANSECT FROM MASSIVE SULPHIDE THROUGH GOSSANOUS REGOLITH TO TILL COVER

Derek H.C. Wilton[1], Gary M. Thompson[2] and Dawn M. Evans-Lamswood[3]

[1]Department of Earth Sciences, Memorial University, St. John's, Newfoundland and Labrador, A1B 3X5 (email: dwilton@mun.ca)

[2]NSERC Industrial College Chair in Applied Mineralogy at the College of the North Atlantic, Prince Philip Drive, St John's, Newfoundland and Labrador, A1C 5P7

[3]Vale Newfoundland and Labrador Limited, 10 Fort William Place, Baine Johnston Centre, Suite 700, St. John's, Newfoundland and Labrador, A1C 1K4

INTRODUCTION

This research documents the breakdown of sulphide minerals in the Voisey's Bay deposits. Sulphide mineral destruction was the product of atmospheric oxidation coupled with migrating oxidized ground waters. The main rationale for the study was to observe whether the breakdown was sequential, and thus predictive. If predictive, then surface mapping of altered sulphide mineralization through the region could indicate whether a given altered zone is analogous to the Voisey's Bay (VB) mineralization. This portion of the study involved detailed MLA-SEM (Mineral Liberation Analyser – Scanning Electron Microscope) analyses of samples collected in a transect, along the wall of the Mini-Ovoid pit, from massive sulphide ore through gossanous regolith into the overlying till. This particular transect was undertaken because it provided a complete section from weathered bedrock through an altered zone (gossan) into overlying till.

The orthomagmatic Voisey's Bay Ni-Cu-Co deposits of northern Labrador are hosted by a troctolite dyke and chamber system which comprise the oldest (ca. 1.3 Ga) portions of the Mesoproterozoic Nain Plutonic Suite (Evans-Lamswood et al., 2000; Lightfoot et al., 2012). The deposits were discovered when a small gossan was sampled in 1993 by prospectors Al Chislett and Chris Verbiscki (Lightfoot and Evans-Lamswood; this volume). Subsequent geophysical surveys and diamond drilling lead to the discovery of the Ovoid ore body buried beneath 20 m of till; the Ovoid is currently being mined as an open pit. The deeper Eastern Deeps and Reid Brook deposits are scheduled for underground production by ca. 2017.

MLA-SEM ANALYSES

The instrument used to examine the samples was the *FEI Quanta 400* environmental Scanning Electron Microscope (SEM) equipped with a Bruker XFlash EDX Detector, in the CREAIT (Core Research Equipment and Instrument Training Network) facility, Bruneau Centre, Memorial University. The SEM is equipped with MLA software developed at the Julius Kruttschnitt Mineral Research Centre (JKTech), University of Queensland (Australia). The SEM electron gun uses a tungsten filament at an operating voltage of 25 Kv and a beam current of 103 nA. The working distance between sample and detector is 12 mm. Details on the instrument and operating systematics are described by Wilton and Winter (2012). A number of photomicrographs were taken of constituent minerals and their intergrowths in Back Scatter Electron (BSE) mode.

TRANSECT AND SAMPLE DESCRIPTION

A transect was completed in August 2011, along the north wall of the Mini-Ovoid open pit mine. Six samples were collected in a relative stratigraphy and numbered from OV-11-12 at the base in the slightly altered massive sulphide through to sample OV-11-09 in till. The stratigraphy of the samples is listed in Table 1.

Figure 1 provides an overview of the north wall transect and the locations of the collected samples. All of the material analysed was semi- to unconsolidated, except in the case of sample OV-11-11 which consisted of massive sulphide rock. The samples were prepared at the Bruneau Centre labs at Memorial University where portions of samples OV-11-07, 08, 09, 10 and 12 were mounted in epoxy pucks and polished, and a piece of sample OV-11-11 was sent to Vancouver Petrographics Limited for polished thin section preparation. The polished pucks and section were coated by graphite and analysed by the MLA-SEM. As previously stated, sample OV-11-11 was massive sulphide ore. Sample OV-11-12 was loose (completely unconsolidated), black, sandy material. Samples OV-11-10 and 08 were of light brown, semi-consolidated material with an overall sandy grain size and scattered pebble-size clasts. These samples resemble a highly weathered lithology. Samples OV-11-09 and 07 are semi-consolidated glacial diamict with an overall brown colour and local rusty and copper stained patches. There is a planar contact exposed between the highly weathered lateritic rock and till as shown on Figure 2.

Table 1. Stratigraphy of OV samples – Mini-Ovoid Transect

F	OV-11-009	Till; 3 m above OV-11-007
E	OV-11-007	Till cemented by gossan
D	OV-11-008	Lateritic host below Till
C	OV-11-010	Below Contact
B	OV-11-012	Black weathered material above
A	OV-11-011	Green weathered massive sulphide

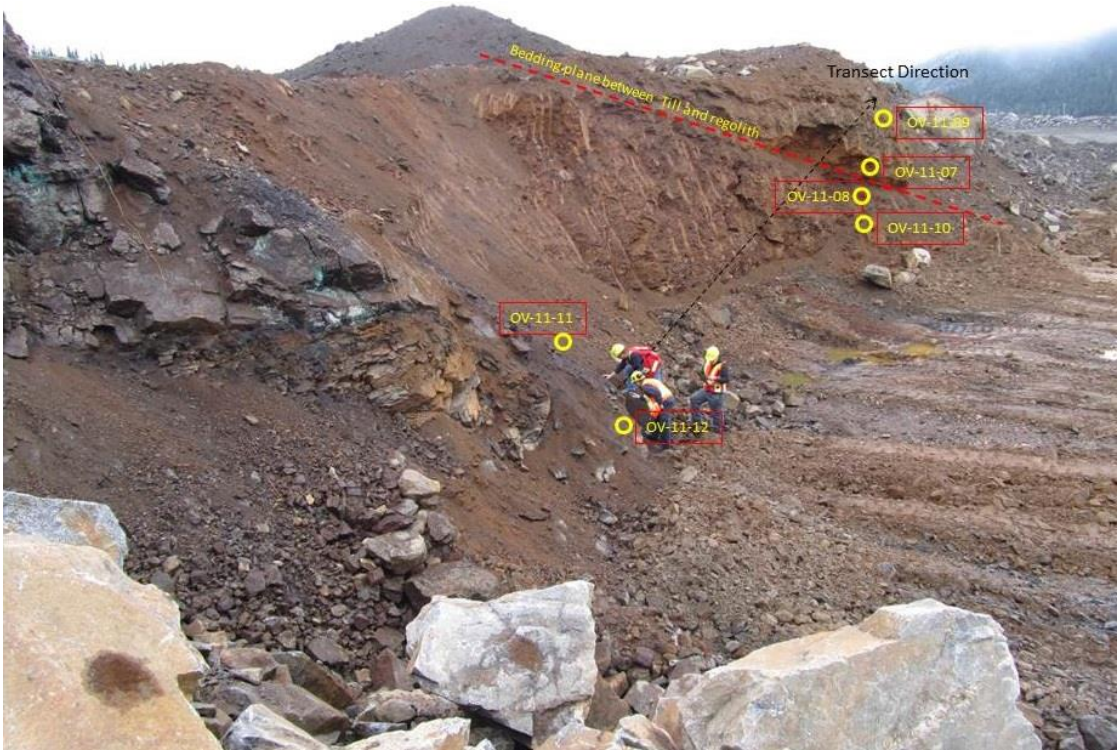

Figure 1. Sample locations at the Mini-Ovoid Pit wall transect.

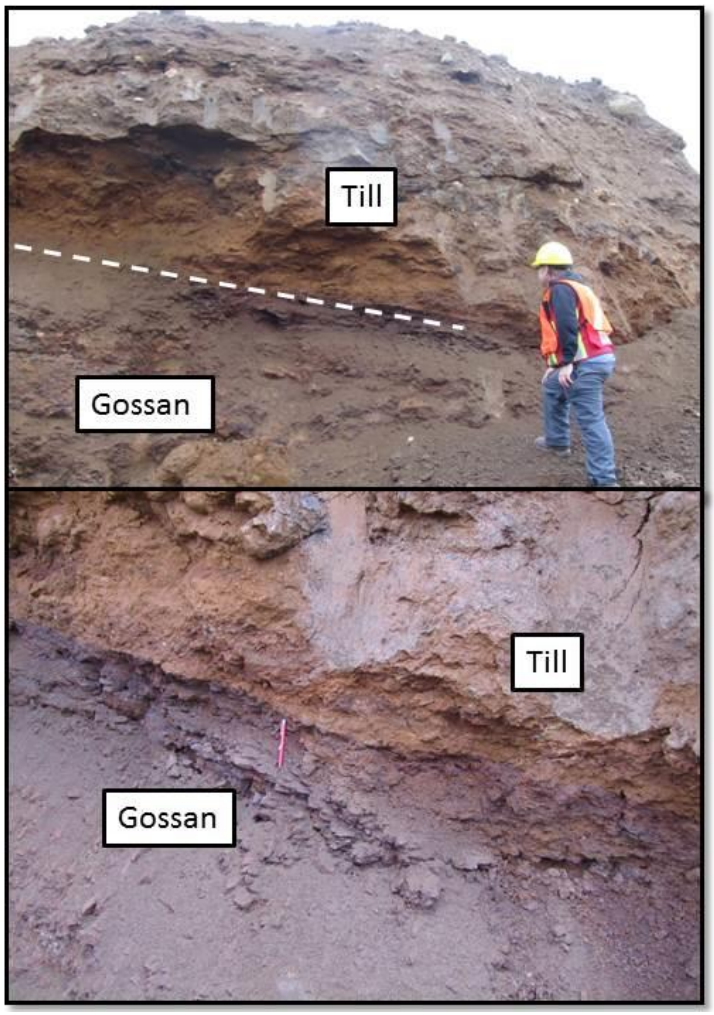

Figure 2. Contact between till and gossan/regolith; bottom is close-up of contact (note pen magnet for scale in lower plate).

BSE IMAGES

The BSE images constitute Figures 3 to 8. The massive sulphide sample (OV-11-11) consists predominantly of fractured pyrrhotite with large magnetite grains (Figure 3). Pentlandite is intensely altered along micro-stockwork fractures with remnant unaltered "islands" in the centres of more massive grains. Pyrrhotite and chalcopyrite are essentially unaltered. Sample OV-11-12 is completely different, consisting of unconsolidated granular, and up to 25-30%, acicular grains of dominantly oxidized iron sulphides, gossan and rare chalcopyrite (Figure 4); "gossan" in this study is defined as highly oxidized iron sulphide with a small to minor remnant S spectral peak. Massive gossan and intensely altered iron sulphide grains with botryoidal textures are common. Pyrrhotite, chalcopyrite and pentlandite are present as solitary grains, but in general the pyrrhotite and pentlandite grains have oxidized sulphide rims. Pentlandite grains, in particular, are extensively altered to the point that some grains exhibit an almost framboidal texture. Sphalerite is locally intergrown with chalcopyrite. Within sample OV-11-10 (Figure 5), most of the grains are equigranular with < 10% acicular grains. The equigranular grains average 200 µm across. The most common grains are intensely altered iron sulphides, along with botryoidal gossan grains. Iron oxide is highly mobile and in places forms

thin "finger" trails that surround and invade other grains. There are a number of solitary pyrrhotite grains, up to 100 µm long, and some rare, extremely altered pentlandite grains. Some pyrrhotite grains are incipiently altered along the trace of troilite exsolution lamellae. Chalcopyrite is present as fine grains in gossan "clumps" and as solitary grains up to 125µm across.

Sample OV-11-08 (Figure 6) is granular material composed of rounded grains that average 150-200 µm in diameter. Silicate minerals are common, and most grains are composite mixtures of silicates and rare sulphide, cemented by iron oxide. Pyrrhotite is present as minute grains in the gossanous masses and as rare solitary grains up to 200 µm across. There are also small chalcopyrite grains in gossanous masses and rare, minute pentlandite grains in the masses as well.

The material of sample OV-11-07 (Figure 7) is granular, but diamictic (i.e., non-sorted) with both 100-150 µm in diameter grains and fine clay. These grains are predominantly silicate with rare, minute pyrrhotite, chalcopyrite and pentlandite particles. Sample OV-11-09 (Figure 8) is a similar diamictite with silicate grains and clay; there are very rare, minute pyrrhotite, chalcopyrite and pentlandite particles.

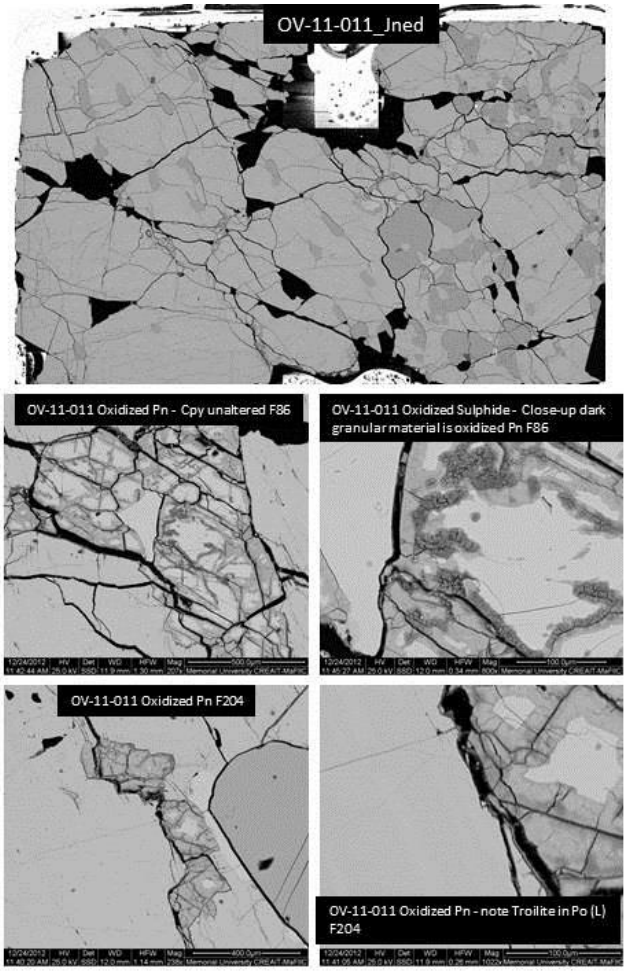

Figure 3. Back Scatter Electron (BSE) images of sample A. OV-11-11. The upper image is of the entire polished thin section (magnetite is slightly darker grey). Lower frames are close-up images of mineral intergrowths; note scale bar in lower right. Cpy = chalcopyrite, Pn = pentlandite, Po = pyrrhotite, F = Frame number.

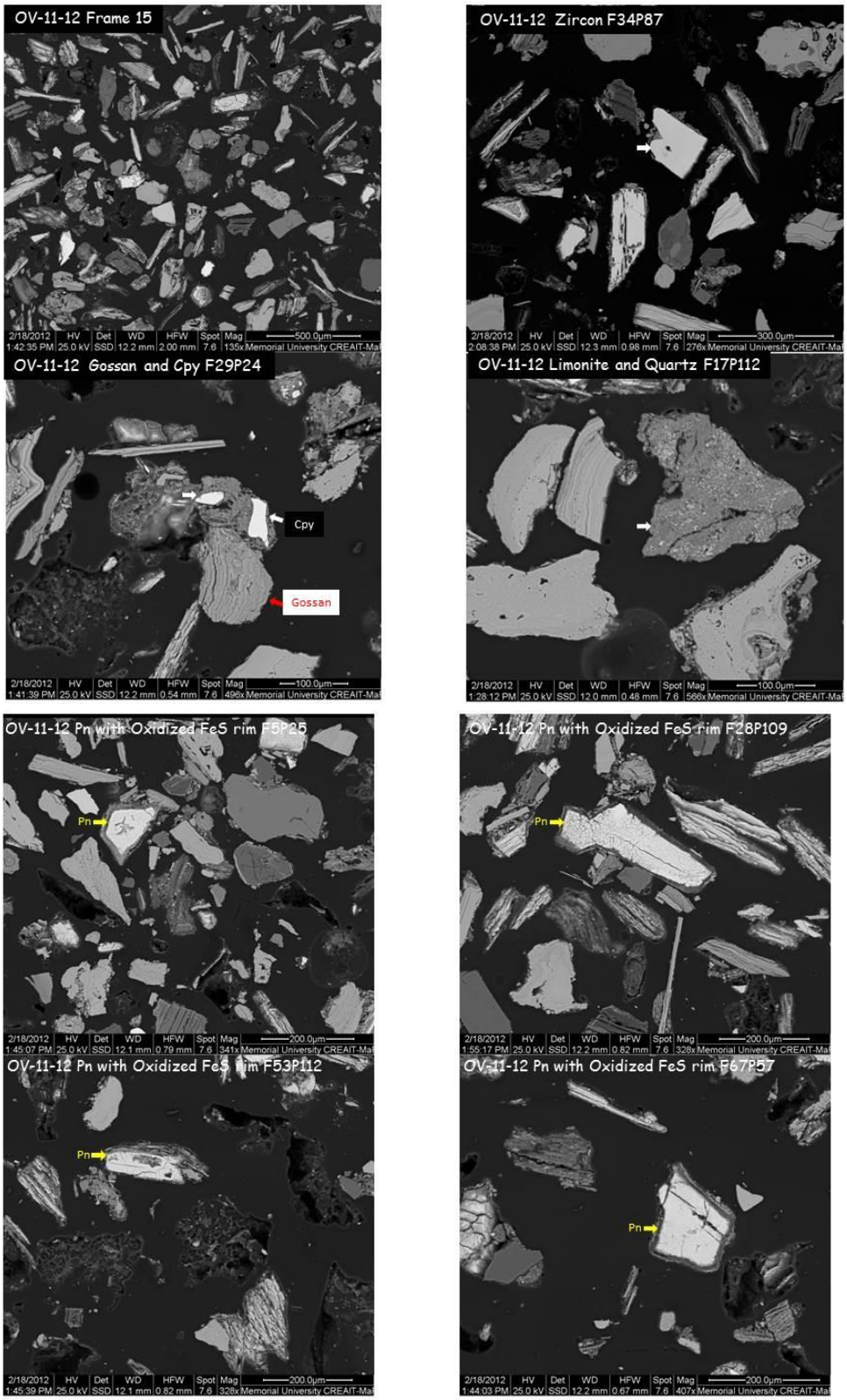

Figure 4. Back Scatter Electron (BSE) images of sample B. OV-11-12. The images are individual MLA frames of the sample grain mount; note scale bar in lower right. Cpy = chalcopyrite, F = Frame number, P = Particle number.

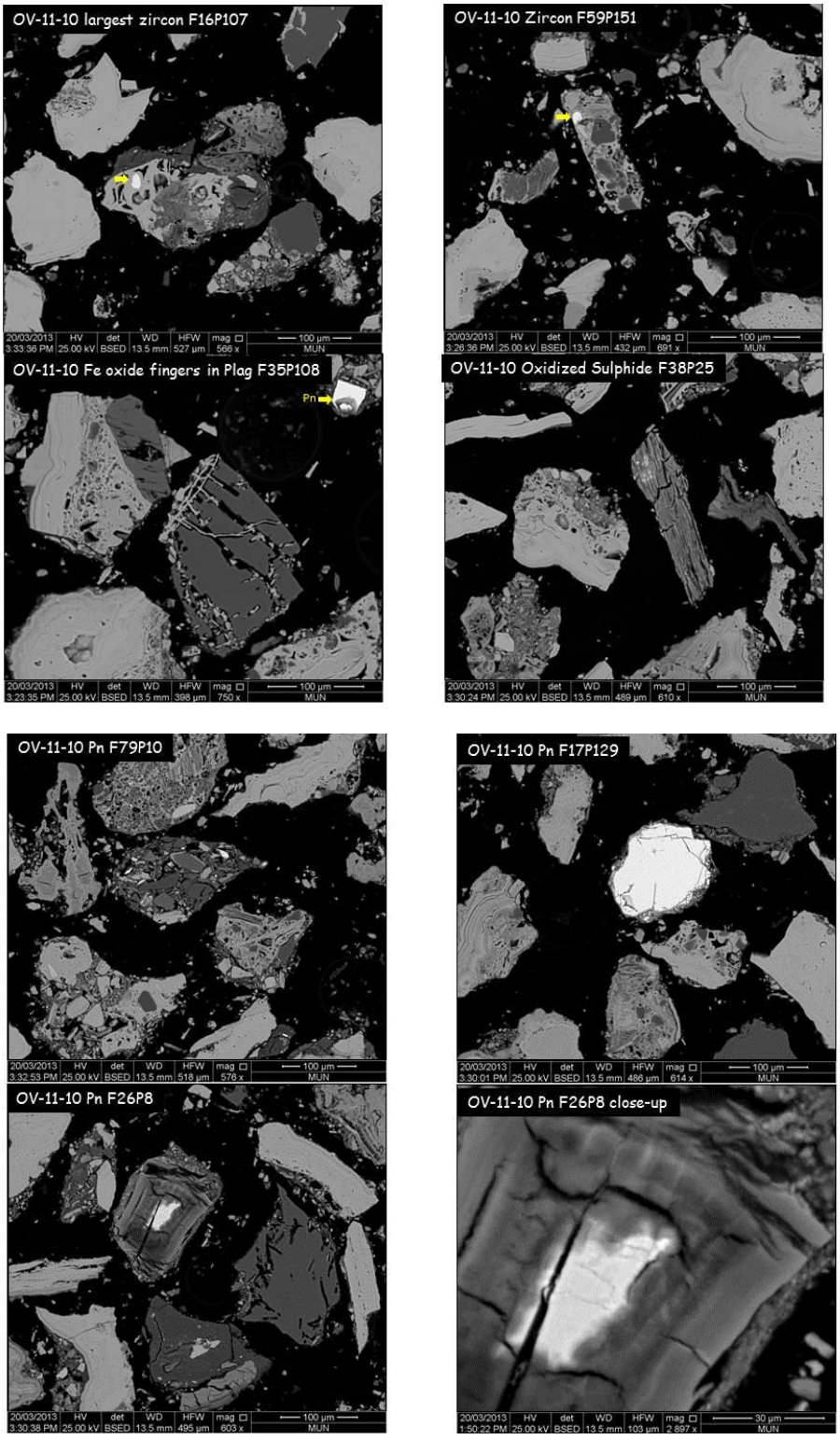

Figure 5. Back Scatter Electron (BSE) images of sample C. OV-11-10. The images are individual MLA frames of the sample grain mount; note scale bar in lower right. Pn = pentlandite, Fe = iron, Plag = plagioclase, F = Frame number, P = Particle number.

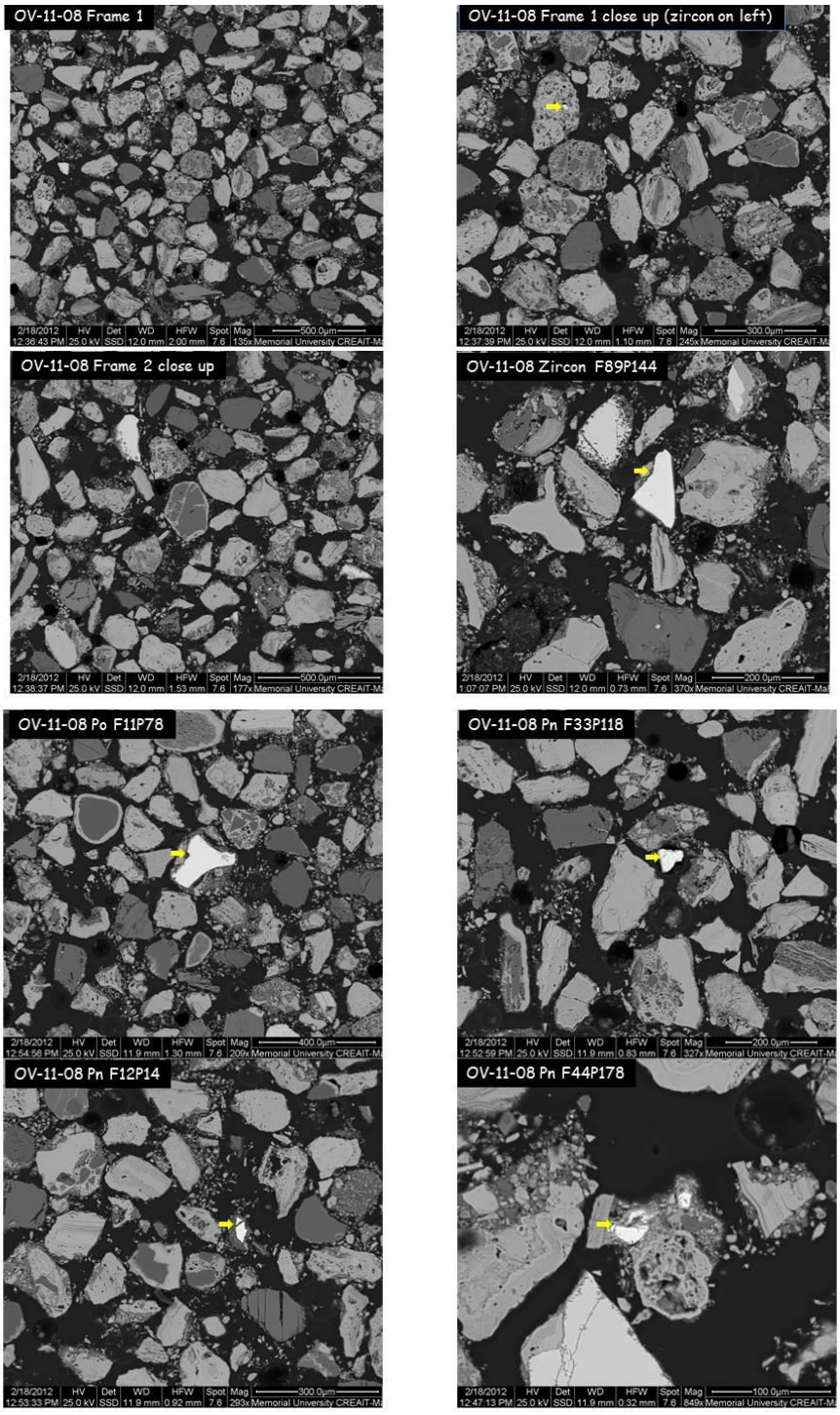

Figure 6. Back Scatter Electron (BSE) images of sample D. OV-11-08. The images are individual MLA frames of the sample grain mount; note scale bar in lower right. Pn = pentlandite, Po = pyrrhotite, F = Frame number, P = Particle number.

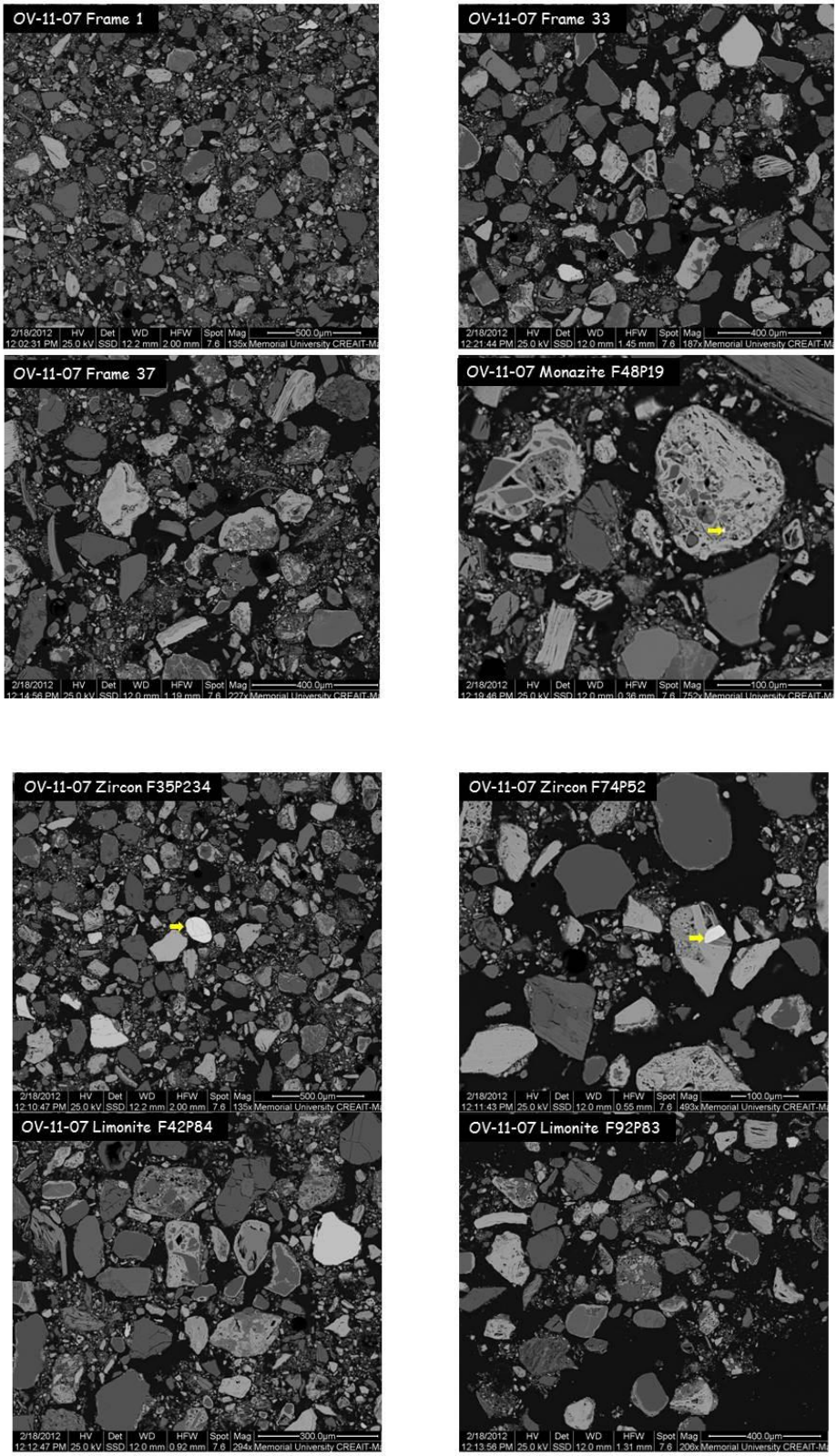

Figure 7. Back Scatter Electron (BSE) images of sample E. OV-11-07. The images are individual MLA frames of the sample grain mount; note scale bar in lower right. F = Frame number, P = Particle number.

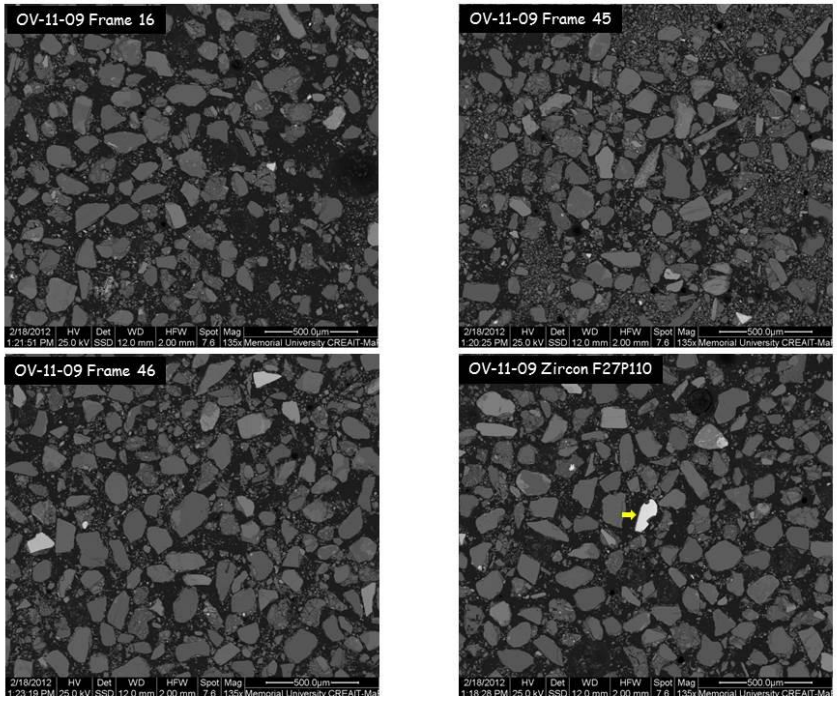

Figure 8. Back Scatter Electron (BSE) images of sample E. OV-11-09. The images are individual MLA frames of the sample grain mount; note scale bar in lower right. Cpy = chalcopyrite, Po = pyrrhotite, F = Frame number, P = Particle number.

In conclusion, OV-11-12, the sample immediately above the massive sulphide, is distinctly different from the others, not only mineralogically (i.e., enhanced pyrrhotite-chalcopyrite-pentlandite contents), but also texturally with the dominant acicular phases. OV-11-10 is transitional texturally (i.e., contains acicular material) between OV-11-12 and OV-11-08, containing some Ni- and Cu sulphides along with extensive gossan. Sample OV-11-08 has minimal sulphides, but abundant gossan. Till samples OV-11-07 and 09 are different again being diamictites with only rare sulphides.

MLA ANALYSES

Pie charts for the top ten mineral phases identified in each sample by the MLA viewer constitute Figure 9 which indicates that, similar to the BSE images, there are significant differences in the mapped minerals between the samples. OV-11-11, the massive sulphide is 83% pyrrhotite with 11% magnetite and lesser contents of chalcopyrite and pentlandite. In terms of pentlandite, the MLA defined a greater percentage (2%) of oxidized pentlandite than regular pentlandite (<1%), reflecting the innate destruction of this mineral. In sample OV-11-12, immediately overlying the massive sulphide, the predominant component (30% of the top ten phases) is gossan followed by oxidized Fe-sulphide, varieties of limonite and oxidized sulphides (pyrrhotite, pentlandite). In fact, no unaltered sulphide mineral could be identified in the top ten phases. Interestingly, magnetite only accounts for 1.73% of this sample and is not a top ten phase. In samples OV-11-10 and 08, gossan is the dominant phase, constituting >50% of the top ten minerals. Magnetite and limonites are important phases in these samples and silicates (biotite, feldspars, quartz) are amongst the top ten phases. There are no sulphide minerals in the top ten mapped phases.

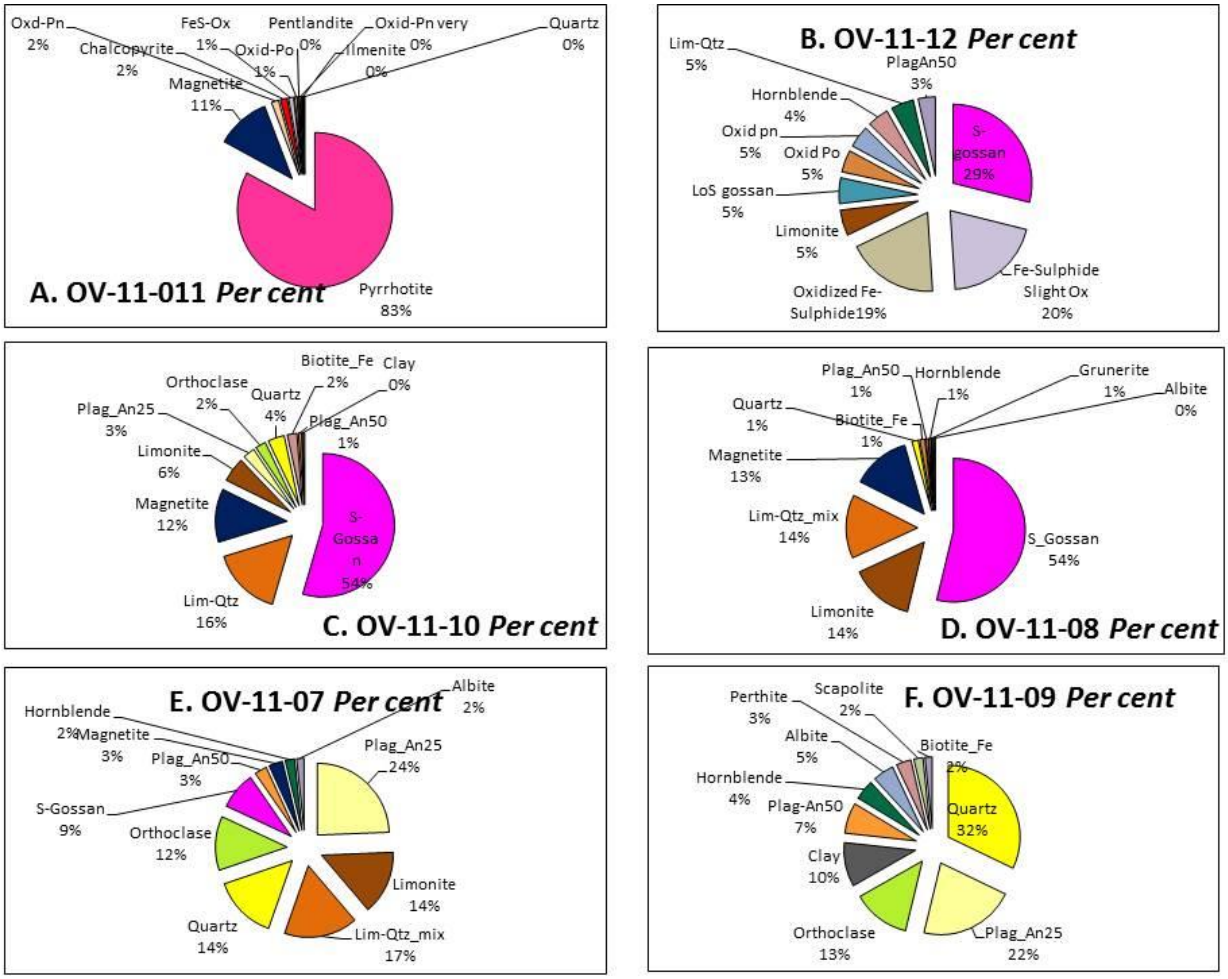

Figure 9. Pie charts indicating percentages of the top ten phases (by area) identified in each of the OV-11 transect samples by the MLA-SEM.

OV-11-07 and 09 predominantly contain rock-forming silicates (feldspars, biotite, quartz, hornblende) and magnetite as their top ten phases. OV-11-07 contains some gossan, because it directly overlies the altered rock. The uppermost sample in the transect, OV-11-09, contains clay as a top ten phase but there are no inherited gossan nor limonitic material within the upper glacial sediment.

CONCLUSIONS

1. In summary, the suite of samples from OV-11-12 to 08 are consistent with representing a weathered, paleo-regolith, and do not represent a modern gossan. Samples OV-11-07 and 09 are till overlying the regolith and indicate that the regolith probably formed before the Quaternary glaciations. The regolith could represent weathering well into the Neogene and Paleogene times, but much more research is required before the age of the regolith can be defined.

2. The study also confirmed that pentlandite is much more strongly altered (oxidized) in the natural environment than either chalcopyrite or pyrrhotite.

ACKNOWLEDGEMENTS

This work was funded by Vale Ltd. and a GeoExplore Grant from the Research and Development Corporation of Newfoundland and Labrador (RDC). Special thanks to Frank Blackwood and Kara Strickland. Brad King, Paul Loder and Glen House of Vale greatly aided in the sample collection. Discussions with Dr. Paul Sylvester were invaluable.

REFERENCES

Evans-Lamswood, D.M., Butt, D.P., Jackson, R.S., Lee, D.V., Muggridge, M.G., Wheeler, R.I., and Wilton, D.H.C., 2000. Physical controls associated with the distribution of sulfides in the Voisey's Bay Ni-Cu-Co deposit, Labrador.; Economic Geology, v. 95, pp. 749-769.

Lightfoot, P.C., Keays, R.R., Evans-Lamswood, D.M., and Wheeler, R., 2012. S-saturation history of Nain Plutonic Suite mafic intrusions: Origin of the Voisey's Bay Deposit, Labrador, Canada; Mineralium Deposita, v. 47, pp. 23-50.

Wilton, D.H.C., and Winter, L.S., 2012. SEM-MLA (Scanning Electron Microprobe–Mineral Liberation Analyser) research on indicator minerals in glacial till and stream sediments: An example from the exploration for awarauite in Newfoundland and Labrador; Quantitative Mineralogy and Microanalysis of Sediments and Sedimentary Rocks. Mineralogical Association of Canada Short Course Series v. 42, pp. 265-283.

ORECRETES LINKING GEOSCIENCES AND LIFE SCIENCES

Harald G. Dill
Federal Institute for Geosciences and Natural Resources,
D-30655 Hanover, Stilleweg 2, Germany
(email: haralddill@web.de)

INTRODUCTION

Supergene minerals range from oxygen-bearing minerals, originating from natural weathering in the gossan of pre-existing minerals, to artificial chemical compounds coating ancient smelter-slags, growing in tailing ponds or covering the walls of adits and galleries as a result of post-mining oxidation (Ettler et al., 2001; Bouzari and Clark, 2002; Manasse and Mellini, 2002; Dill et al., 2002; Yakovleva et al., 2003; Dill, 2008, 2009; Belogub et al., 2008). Even hazards provoked by man, such as blazes in settlements or industrial sites, may leave behind chemical compounds in the ashes and relicts that allow the reconstruction of the thermal event and identify processes in a way forensic experts used to do in a criminal case. However, not all of the types of supergene minerals identified are agreed upon and widely accepted by geoscientists as minerals sensu stricto (Nickel, 1995).

The colorful mineral aggregates originating from supergene mineralization that are texturally very much different from normal duricrusts are chemical residues denominated by Dill et al. (2013) as *metalliferous duricrusts* or *orecretes*. These technical terms are self-explanatory, and such encrustations are similar to the textbook examples of calcretes and gypcretes described by Goudie and Pye (1983) and Wright and Tucker (1991); however, duricrusts and orecretes can exhibit more variability in terms of chemical and mineralogical composition. Orecretes develop on or near the earth's surface in the oxidized zone and include oxicretes (oxide plus hydrate), carbocretes (carbonate), silicacretes (silica), halcretes (halogenides: Cl, J, F, and Br), sulcretes (sulfate plus APS minerals/aluminum phosphate sulfate minerals), phoscretes (phosphates), arsenocretes (arsenates), vanadocretes (vanadates) and some rare species accommodating Mo, Cr and Se in the anion complex. Orecretes may contain Pb, Cu, Zn, In, Fe, Mn, Ni, Co, W, REE, U, and Ag; these can be added as a suffix to the aforementioned terms (e.g., carbocretes-Cu containing malachite and azurite; vanadocretes-U made up of carnotite, tyuyamunite or francevillite). This varied spectrum of supergene minerals forms under near-ambient conditions at the interface of different spheres on the globe: atmosphere, biosphere, lithosphere, pedosphere, hydrosphere. There is a catena from geogenic to anthropogenic orecretes, with supergene oxidized minerals bridging the gap between geosciences and life sciences. The mineralogical composition and the physical-chemical regime is provided for some supergene mineralization observed in gossans, in areas previously subjected to mining, processing and smelting, as well as areas of historic disasters (Figure 1).

Three principal factors control the development of orecretes: parent material, landforms, and climate. As a result, the orecretes under study constitute a first-hand morphoclimatical marker available to geomorphologists and climatologists alike, as illustrated in a flow sheet on Figure 1. Using such rationale, climatologists are able to (1) gather insights on the recent past, and (2) predict what to expect in the near future with respect to shifts in morphoclimatic zones across the globe.

ORECRETES IN GOSSANS

More than 70 study areas across the globe, some of which contain more than one mineralized site, have been selected for a geomorphological and mineralogical study aiming to cover the various morphoclimatic zones from pole to pole (Dill et al., 2013). In this paper, the Nabburg-Wölsendorf fluorite mining district (Oberpfalz,

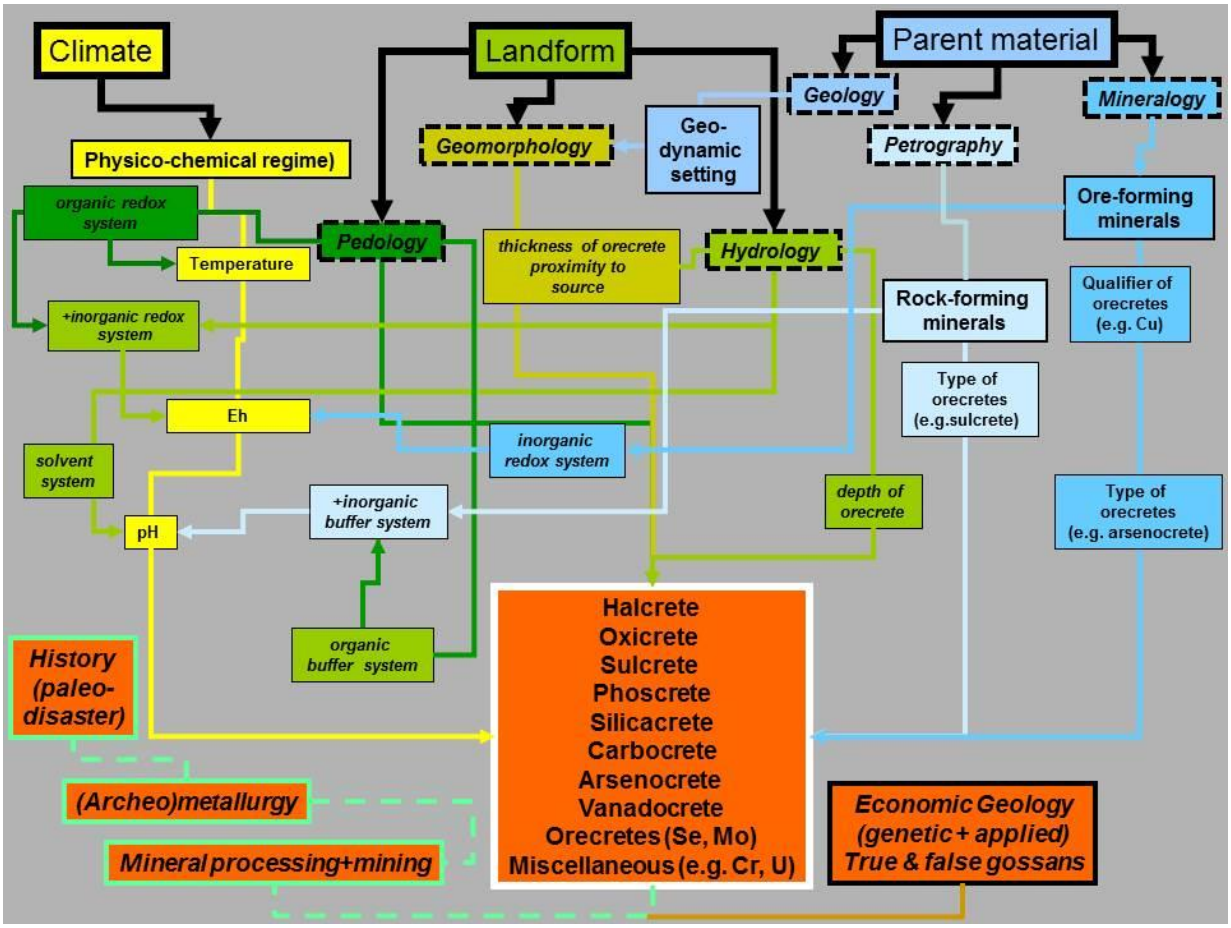

Figure 1. Flow sheet to illustrate the impact of various parameters in the fields of climate, geomorphology and parent material on the formation of orecretes. The various types of orecretes are listed in the central box and the life sciences and geosciences for which they are relevant are illustrated on the left- and right-hand side, respectively, of the central box.

NE Bavaria, Germany) has been selected as a case study for geogenic gossan mineralization.

A total of 28 out of 104 different mineral species recorded at this site accommodated Cu into their structure and were, therefore, classified as Cu minerals *sensu stricto* (Figure 2). Chalcopyrite is the most important primary copper mineral in the mining district. Descending meteoric fluids were the main carriers of Cu derived from the oxidation of chalcopyrite in the gossan. These fluids yielded a wide range of secondary sulfates, interacted with the granitic wall rocks where they dissolved silicates and phosphates, and decomposed sulfides with which chalcopyrite was associated. Ubiquitous carbon dioxide gave rise to carbocretes-(Cu). Unlike the previously mentioned secondary Cu minerals, Cu hydrosilicates are scarce, attesting to the presence of predominantly acidic fluids in the overall hydrological system. Supergene Cu mineralization is an integral part of the Plio-Pleistocene chemical weathering and the geomorphologic processes operating along the boundary fault of the uplifted NE Bavarian Basement. The hydraulic processes leading to carbocretes-(Cu), silicacretes-(Cu) and oxicretes-(Cu) may be chronologically constrained to the time interval of 0.2 to 4.2 Ma. The age (Figure 2) was inferred by means of U/Pb dating of uranocircite and torbernite building up the phoscretes-(U-Cu) deposits.

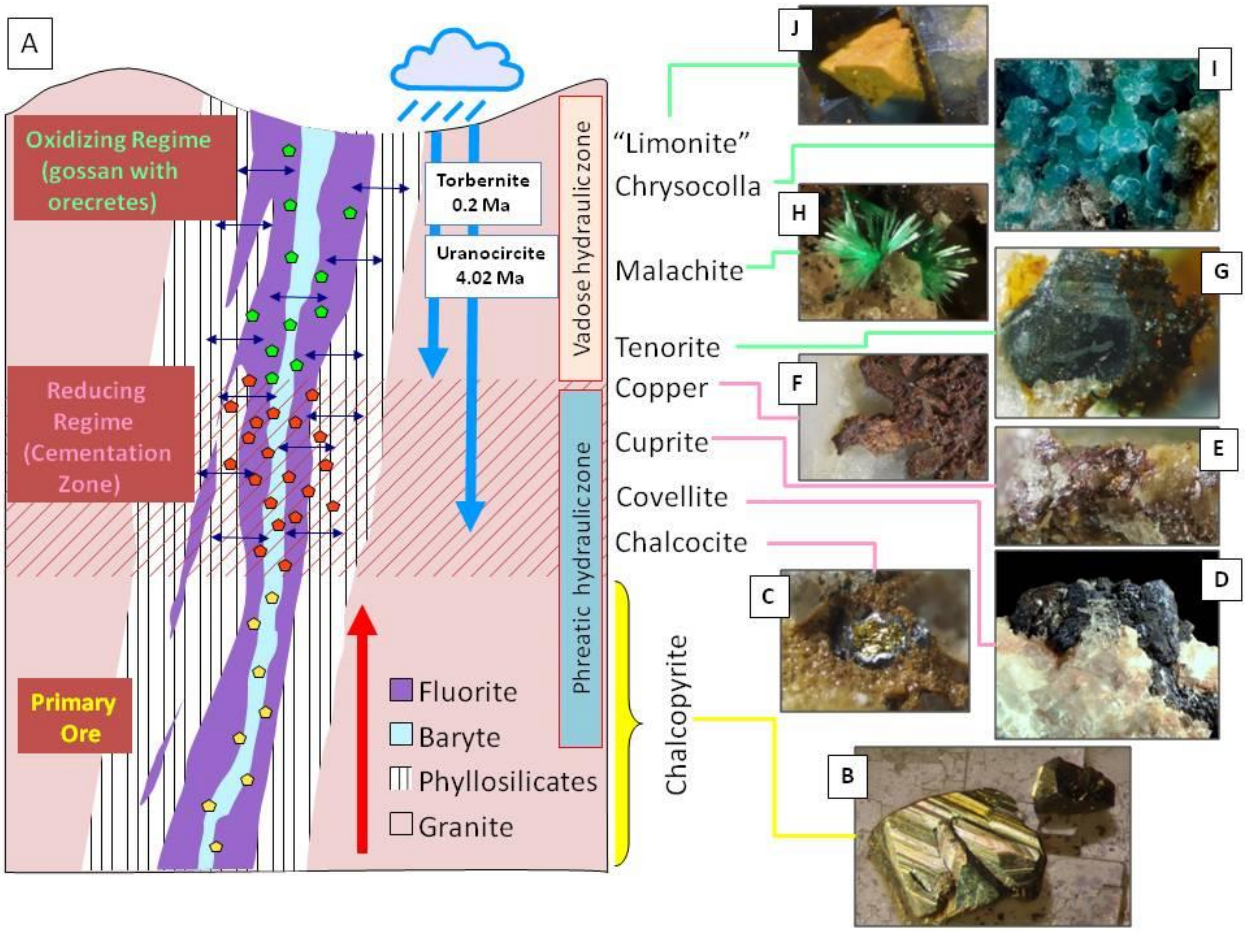

Figure 2. Secondary Cu minerals in F-Ba vein-type deposits of the Nabburg-Wölsendorf fluorite mining district, Germany. These represent examples of natural orecretes. The age of formation (white boxes) is based on U/Pb dating of silicacretes and phoscretes.
(A) Cartoon illustrating the tripartite subdivision of the fault-bound mineralization into primary ore originating from *per ascensum* (hypogene) mineralization, the gossan with the orecretes and the cementation zone, the latter two derived from *per descensum* mineralization (supergene).
(B) Chalcopyrite ($CuFeS_2$) growing on white fluorite, Erika Mine. Width of image 5 mm.
(C) Chalcocite (Cu_2S) coating chalcopyrite in yellow brown fluorite ("honey spar"), mine unidentified, Wölsendorf. Width of image 5 mm.
(D) Covellite (CuS) coating chalcopyrite in quartz mine unidentified, Wölsendorf. Width of image 5 mm.
(E) Cuprite (Cu_2O) forming reddish minerals with specks of native copper (metallic luster) and black tenorite, Roland Mine. Width of image 5 mm.
(F) Native copper (Cu) on quartz, Marienschacht Mine. Width of image 5 mm.
(G) Tenorite (CuO) pseudomorphosing chalcopyrite. The green tabular crystals are torbernite ($Cu(UO_2)_2(PO_4)_2 \cdot 12H_2O$), Roland Mine. Width of image 4 mm.
(H) Malachite ($Cu_2[(OH)_2(CO_3)]$) on quartz, Marienschacht Mine. Width of image 5 mm.
(I) Chrysocolla ($Cu_4H_4[(OH)_8|Si_4O_{10}] \cdot n\ H_2O$), Roland Mine. Width of image 5 mm.
(J) "Limonite" (goethite) (α FeOOH) pseudomorphosing chalcopyrite crystal between black fetid fluorite (left) and colorless fluorite (right), Marienschacht Mine. Width of image 5 mm.

ORECRETES IN MINING RESIDUES

Anthropogenic mining residues (post-mining mineral assemblage) result from descending meteoric waters in galleries and opencasts. The most recent mineralizations in underground mines are made up of poorly-crystallized, highly soluble sulphates, halogenides, phosphates, carbonates and compounds precipitated from oxalic acid. The various groups of minerals coating the walls of galleries or suspending from the ceiling in form of stalactites mainly differ from each other by the cations supplied by acid mine drainage (e.g., Cu, Zn, Fe) and their state of hydration, which is strongly controlled by aridity or evapotranspiration in the open mine workings.

As only carbon-bearing chemical compounds can successfully be used for ^{14}C dating, some of these are listed here by name and chemical formula:

Calcite [$CaCO_3$]
Malachite [$Cu_2(CO_3)(OH)_2$]
Whewellite [$CaC_2O_4 \cdot (H_2O)$]
Humboltite [$Fe(C_2O_4) \cdot 2(H_2O)$]
Moolooite [$Cu(C_2O_4) \cdot 0.5(H_2O)$]

These modern C-bearing minerals have derived from rotten timber used as roof support in underground mines and from excrements of animals, mainly bats, which became tenants of these man-made excavations when mining was abandoned. These poorly-crystallized mineral aggregates provide clear evidence for human activities, and may easily be distinguished from well-crystallized oxidic minerals that evolved for thousands or even millions of years in the gossan of the ore deposit described in the previous section.

A case in point is found within the ancient galleries of the Mega Livadi Mine, Greece, where blue to greenish acicular crystal aggregates were found coating walls and stopes. The underground workings provide insight on the occurrence of post-late Miocene gossan mineralization (Figure 3). In addition, anthropogenic mineralization, superimposed on post-late Miocene mineralization, can be distinguished from the latter and dated (Dill et al., 2010). Samples investigated by XRD and spectroscopy suggest a carbonate-humate mineralization with Cu and Fe as cations accommodated in the crystal lattice (Figure 3). Radio-carbon dating of this ventilation-related mineralization yielded an age of formation between 3325 and 2890 BC. Holocene Cu-Fe mineralization chronologically constrains the mining activities on the Isle of Seriphos to the early Bronze Age. The joint action of *per descensum* mineralizing fluids and ventilation in underground galleries caused these chemical compounds to precipitate.

In Cyprus, mining of copper started earlier than on the Isle of Seriphos. Obviously, people living on the islands of Crete and Cyprus were scouting the Aegean Sea in search of Cu ore that was easy to access at shallow depth and smelt, because of Cu ores located at a reasonable depth in Cyprus, where the ancient miners mainly mined the upper parts of the supergene ore in the deposit.

ORECRETES IN SMELTING RESIDUES AND CAUSED BY MAN-MADE DISASTER

Mineralogical, geochemical and microbiological processes in the tailing ponds (e.g. Matchless, Namibia) produce sulcretes, halcretes and phoscretes. The slag heaps investigated in Germany and the pyrometallurgical remains of Cu-enriched VMS deposits in Cyprus, have been covered with sulcretes since 1600 AC and the Chalcolithic Age. Archeometallurgy is not the end of the catena. In some areas, the mining residues were not only exposed to atmospheric processes but also to man-made physical-chemical processes such as blazes in the miner's settlements. Artificial processes gave rise to mixed sulcrete-phoscretes or pure phoscrete-bearing aggregates. The alteration of archeometallurgical remains by thermo-chemical processes during a fire-hazards caused by ancient settlers is shown in Figure 4 and described in a case history from southeast Germany.

In the municipal area of the town of Naila, iron slags were dumped and based upon relics of charcoal the smelting process has been constrained to the period of time between 1045-1275 AC. Two different sources can be singled out for the kiln feed. **Type I** ore is an iron ore exploited from near-surface supergene deposits or gossan enriched in oxicretes-(Fe) and carbocretes-(Cu) (Figure 4A). **Type II** is a dual-provenance ore with Cu, Fe, Ba and REE as marker elements. Cu-Fe ore has been derived from the chalcopyrite-siderite vein-type deposits found all across the southern urban area of Naila and mined by shafts underneath the gossan as hard ore. Anomalously high amounts of Ba indicate that the ore contained considerable amounts of barite, which is representative of the youngest stage of hydrothermal vein mineralization in the Central Frankenwald. Widespread monazite-(Nd) in parts of the slags is indicative of a kiln feed derived from mineralization in the reaches of the supergene alteration, which was active during the Neogene and caused the formation of rhabdophane-(Nd) (Figure 4C, 4D). Within the gossan, phoscretes-(REE) containing rhabdophane [$(Nd,Ce,La)PO_4 \bullet (H_2O)$] and oxicretes-(Fe) with goethite were dehydrated by pyrometallurgical processes to oxicretes-(Fe) abundant in wuestite, fayalite, magnetite and leuzite and phoscretes-(Nd) with apatite and monazite-(Nd) [$(Nd,Ce)PO_4$] (Figure 4A). The phosphates underwent an additional stage of alteration that resulted in the precipitation of strengite and phosphosiderite. The newly formed Fe (III)-phosphates reveal that the iron slags were deposited by the ancient settlers in dumps under well-aerated conditions, above the water level of the modern drainage system. Only at one site was a waste dump altered by an additional thermal event and affected by fire, a fact highlighted by the presence of coquimbite (Figure 4B).

CONCLUSIONS

On account of the variegated chemical and mineralogical compositions, orecretes are first-order specimens that contribute to the study of the Recent geomorphologic, climatological and hydrologic evolution of the globe (Figure 1), in a much better way than calcretes, gypcretes or ferricretes can. While the various chemical compounds allow for a precise determination of the physical-chemical regime (as illustrated in Eh vs. pH cross plots) analyses of the U/Pb, K/Ar, Ar/Ar ratios, or OSL studies and radiocarbon dating of silicates and C-bearing compounds can provide precise age information covering the period at the passage from geosciences into life sciences of mankind (Figs 2 and 3). In particular, the two case histories recorded from the Isle of Seriphos (Figure 3, gossan orecretes $\Rightarrow$ post-mining orecretes) and from Naila (Figure 4, gossan orecretes $\Rightarrow$ (archeo)metallurgical orecretes $\Rightarrow$ post-smelting/ mineral processing orecretes $\Rightarrow$ paleodisaster orecretes) show that a complex history can be preserved in orecretes. As far as applied economic geology is concerned, orecretes are prime targets to assist in the distinction between true and false gossans, thus contributing to a reduction of the risks and costs associated with mineral exploration.

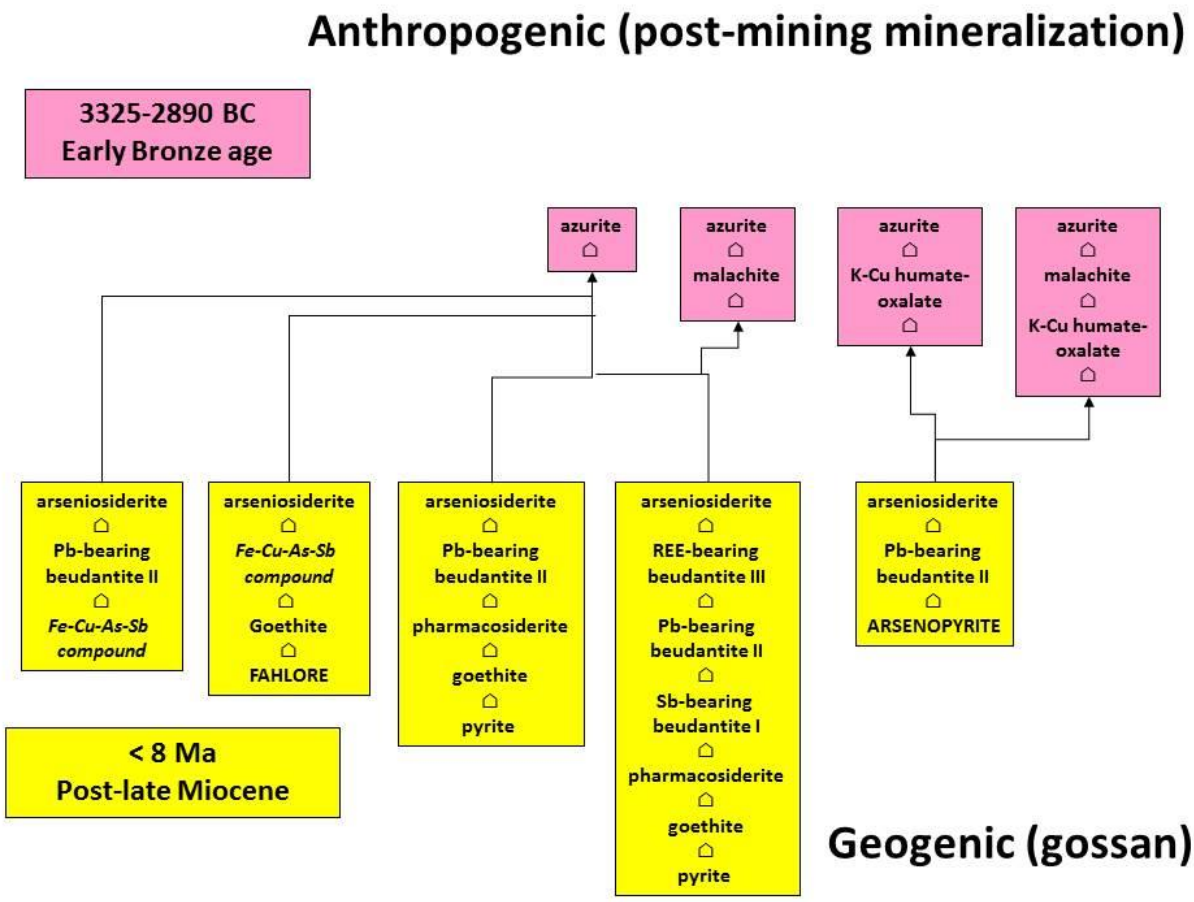

Figure 3. Transition from orecretes of a geogene gossan mineralization into man-made post-mining mineralization at the Mega Livadi Cu-Fe skarn deposit, Greece. Minerals listed in small characters have been identified by microanalytical techniques (SEM-EDX and XRD). Minerals in capital letters refer to the primary sulfide-arsenide mineralization whose minerals, excluding pyrite, can only be deduced from the morphology of solution cavities. Chemical compounds shown in *italics* record unknown minerals and/or mineral aggregates of uncertain composition. The arrows facing upward within the boxes denote that minerals below change into minerals above.

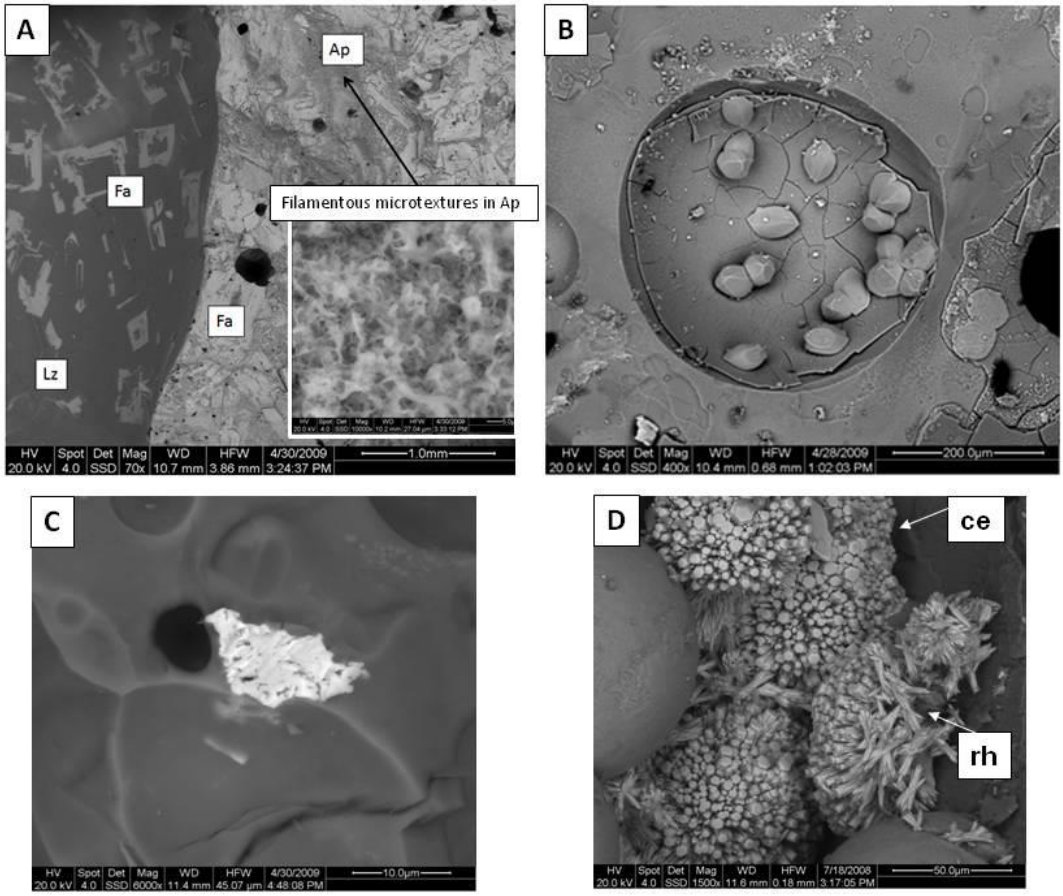

Figure 4. Scanning Electron Microscope (SEM) image of man-made archeometallurgical and paleodisaster orecretes (Naila, Germany).
(A) Zoned fayalite crystals (Fa) surrounded by leuzite (Lz). In the leuzite-fayalite intergrowth nests of apatite may be spotted (see inset for filamentous microtexture).
(B) Porous vitreous Fe-Si matrix with vugs filled with coquimbite. The Fe sulfate mineralization was emplaced in the course of a man-made fire.
(C) Relicts of monazite aggregates in a vitreous matrix.
(D) Rhabdophane (rh) and cerite (ce) from a gossan associated with a hydrothermal vein.
This geogene rare-earth mineralization is the source of the anthropogenic REE mineralization in smelting residues shown in Figure 4.

ACKNOWLEDGEMENTS

The author wishes to thank Marie-Claude Williamson for initiating the GAC-MAC Symposium 4 proceedings report; and Guest Editors Helen Smyth and Benoit Saumur for helpful comments on the original manuscript.

REFERENCES

Belogub, E.V., Novoselov, K.A., Yakovleva, V.A., and Spiro B., 2008. Supergene sulfides and related minerals in the supergene profiles of VHMS deposits from the South Urals; Ore Geology Reviews, v. 33, p. 239-254.

Bouzari, F., and Clark, A., 2002. Anatomy, evolution, and metallogenic significance of the supergene ore body of the Cerro Colorado porphyry copper deposit, I Region, Northern Chile; Economic Geology, v. 97, p. 1701-1740.

Dill, H.G., 2008. Geogene and anthropogenic controls on the mineralogy and geochemistry of modern alluvial-(fluvial) gold placer deposits in man-made landscapes in France, Switzerland and Germany; Journal of Geochemical Exploration, v. 99, p. 29-60.

Dill, H.G., 2009. Pyrometallurgical relics of Pb-Cu-Fe deposits in south-eastern Germany. An exploration tool and a record of mining history; Journal of Geochemical Exploration, v. 100, p. 37-50.

Dill, H.G., Pöllmann, H., Bosecker, K., Hahn, L. and Mwiya, S., 2002. Supergene mineralization in mining residues of the Matchless cupreous pyrite deposit (Namibia) – A clue to the origin of modern and fossil duricrusts in semiarid climates; Journal of Geochemical Exploration, v. 75, p. 43-70.

Dill, H.G., Melcher, F., Kaufholt, S., Techmer, A., Weber, B. and Bäumler, W., 2010. Post-Miocene and bronze-age supergene Cu-Pb arsenate-humate/ oxalate-carbonate mineralization at Mega Livadi–Serifos, Greece; Canadian Mineralogist, v. 48, p. 163-181.

Dill, H.G., Weber, B. and Botz, R., 2013. Metalliferous duricrusts ("orecretes") - markers of weathering: A mineralogical and climatic-geomorphological approach to supergene Pb-Zn-Cu-Sb-P mineralization on different parent materials; Neues Jahrbuch für Mineralogie Abhandlungen, v. 190, p. 123-195.

Ettler ,V., Legendre, O., Bodénan, F., and Touray, J.-C., 2001. Primary phases and natural weathering of old lead–zinc pyrometallurgical slag from Príbram, Czech Republic; Canadian Mineralogist, v. 39, p. 873-888.

Goudie, A.S., and Pye, K. 1983. Chemical Sediments and geomorphology-Precipitates and residua in the near-surface environment; Academic Press , London, 439 pp.

Manasse, A., and Mellini M., 2002. Chemical and textural characterization of medieval slags from the Massa Marittima smelting sites (Tuscany, Italy); Journal of Cultural Heritage, v. 3, p. 187-198.

Nickel, E.H., 1995. Definition of a mineral; Mineralogical Magazine, v. 59, p. 767-768.

Wright, V. P., and Tucker, M. E. 1991. Calcretes: an introduction; *In* V. P. Wright and M. E Tucker, (eds), Calcretes, International Association of Sedimentologists Reprint Series, v, 2, Blackwell Scientific Publications, Oxford, 1-22.

Yakovleva, V. A., Belogub E. V., and Novoselov, K. A., 2003. Supergene iron sulpho-selenides from the Zapadno-Ozernoe copper-zinc massive sulfide deposit, South Urals, Russia: a new solid-solution series between pyrite FeS_2 and dzharkenite $FeSe_2$; Mineralogical Magazine, v. 67, p. 355-361.

THE JAROSITE-RICH "GOLDEN DEPOSIT", NORTHWEST TERRITORIES, CANADA, AS AN ANALOGUE FOR MARS

Melissa M. Battler, Gordon R. Osinski, and Neil R. Banerjee
Centre for Planetary Science & Exploration, Western University, London, Ontario, N6A 5B7
(email: mbattle@uwo.ca)

INTRODUCTION

The jarosite-rich cold seep emplaced Golden Deposit (GD; Michel, 1977), in Northwest Territories, Canada, (65º11'58" N, 124º38'15" W) is visible from the air as a golden-yellow patch of unvegetated sediment, approximately 140 m long x 50 m wide (Figure 1). It appears as a patchwork of raised 1 – 3 m polygons, with water flowing from seeps into troughs between polygonal islands (Figure 2).

BACKGROUND: JAROSITE ON MARS

The GD has been investigated as an analogue to surficial deposits of the OH-bearing iron sulfate mineral jarosite that have been identified on Mars (Battler et al., 2013). Jarosite deposits have been observed in several places on Mars, such as Meridiani Planum (Christensen et al., 2004; Klingelhofer et al., 2004; Squyres et al., 2004) and Mawrth Vallis (Farrand et al., 2009; Michalski and Niles, 2011).

Jarosite is of particular interest as a paleoenvironmental indicator on Mars because it is thermodynamically stable under a majority of temperature and pressure conditions (e.g., air temperature and pressure at Gale Crater over the course of one Martian year (Mars Science Laboratory sol 1 – 668) ranged from -88° C to +11° C, and 732 to 925 Pa (Gomez-Elvira, 2014)) on present-day Mars (Navrotsky et al., 2005). As such, jarosite may contain chemical or textural indicators of Mars' history, including perhaps evidence of biological activity.

Martian jarosite deposition mechanisms are not known, but by comparing Martian sites to analogous sites on Earth, conditions of formation, and thus paleoenvironments on Mars during the time of deposition, may be postulated. The GD is of particular interest because its mineralogy and its syn-depositional environmental conditions (permafrost and arid surface conditions) are conceivably analogous to those in similar systems on Mars.

RESULTS

Laboratory-based ultraviolet–visible–near infrared (UV-Vis-nIR) spectral analysis performed at the University of Winnipeg on surficial samples from the GD indicate that these consist entirely of jarosite. However, mineralogy, as determined by X-ray diffraction (XRD; Western University) and confirmed by inductively coupled plasma emission spectrometry (ICP-ES following a lithium metaborate/tetraborate fusion and dilute nitric acid digestion; Acme Analytical Laboratories Limited), is pre-dominantly natrojarosite and jarosite, with hydronium jarosite, goethite, quartz, clays, and small amounts of hematite in some samples (Figure 3; Battler et al., 2013). Water chemistry analyses of the GD indicate that the water flowing from seeps and along polygonal troughs throughout the site is acidic and iron-bearing (Michel and van Everdingen, 1987; Battler et al., 2013). Water pH varies significantly over short distances depending on proximity to acid seeps, from 2.3 directly above seeps, to 5.7 several metres downstream from seeps within the deposit, and up to 6.5 in ponds proximal to the deposit. Details of these and other results have been reported by Battler et al. (2013).

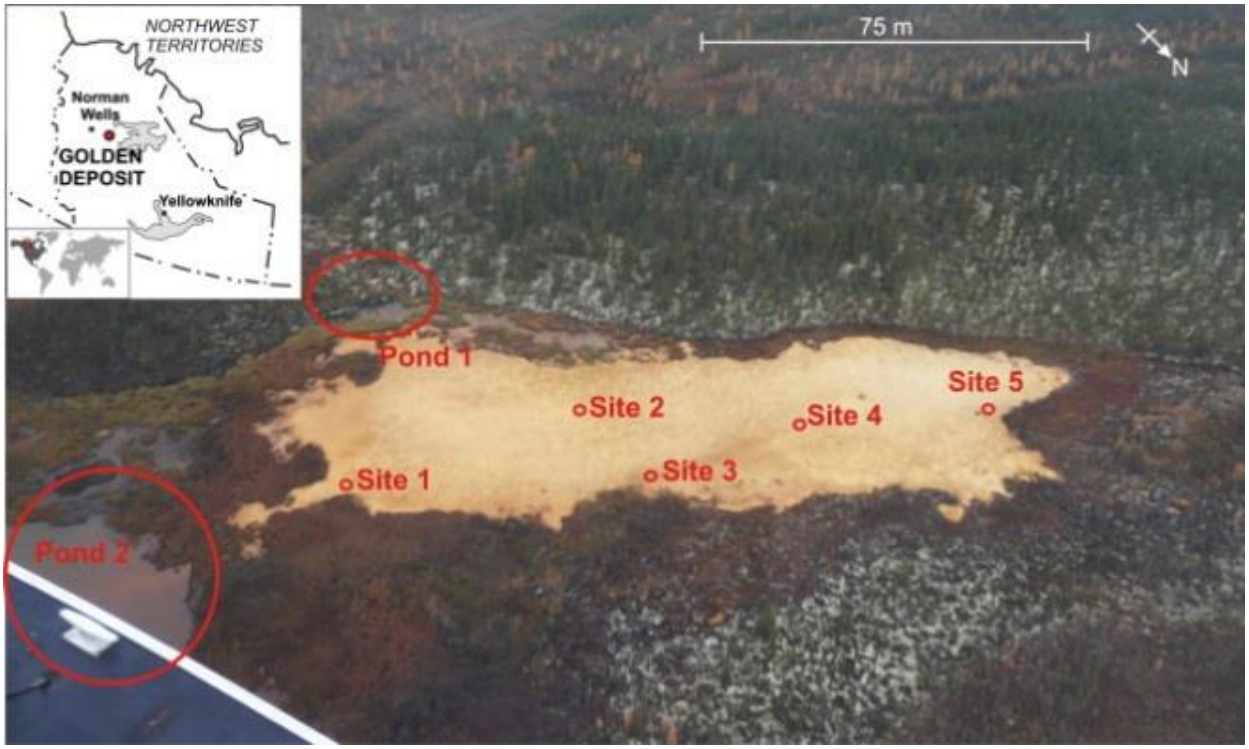

Figure 1. Aerial photograph of the GD; Sept. 2009. The inset map illustrates the approximate location of the Golden Deposit, south east of Norman Wells, in the Northwest Territories, Canada (Battler et al., 2013)

DISCUSSION

Spectral data indicate that GD is spectrally homogeneous; however XRD data indicate mineral heterogeneity at sub-meter and sub-centimeter scales. Therefore, Martian jarosite deposits may show more chemical and mineral variability than indicated by remote sensing data at the currently available spatial resolution. Although spectra with the relative spatial resolution of orbital imagery are useful for identifying major mineralogy and drawing coarse scale conclusions, ground-truthing is necessary to verify the detailed mineralogy of such deposits. Detailed mineralogical studies of analogue sites can yield information on the paleoenvironment and subsurface conditions, which may in turn be applied to develop hypotheses about the development of similar deposits on Mars (e.g., fluid chemistry, pH, Eh, habitability, organic preservation potential). The requirements necessary for the development of the GD include: (1) Fe-sulfides at depth; (2) groundwater circulation/upwelling; and (3).\ arid, oxidizing surface conditions. Although permafrost does not seem to be a requirement, it does not inhibit surficial jarosite precipitation. All of these requirements are (or were at some point) present on Mars (McSween and Treiman, 1998; Bibring et al., 2006), thereby suggesting similar mechanisms could have been responsible for the development of jarosite-rich deposits on Mars.

Finally, the GD may be of special interest as a terrestrial planetary analogue study site, as Mawrth Vallis is being considered as a landing site for the European Space Agency's 2018 ExoMars mission (LSSWG, 2014).

Figure 2. (A) Water flows through troughs around polygonal "islands". (B) Close-up of polygon centre. (C) Push core to 50 cm depth. (D) Jarosite-rich mud exposed several cm's beneath organic overburden, 20 m out from GD. (E) Evaporitic crust on vegetation and mud proximal to GD. (F) 60 cm deep trench in shale outcrop, west of GD. (G) Biofilaments in faster-flowing water (below scale bar). (H) Terraces near streamers also suspected to support microbial communities. (I) Active seeps with diameters from 1 cm (right) to 6 cm (middle). Photographs modified from Battler et al. (2013).

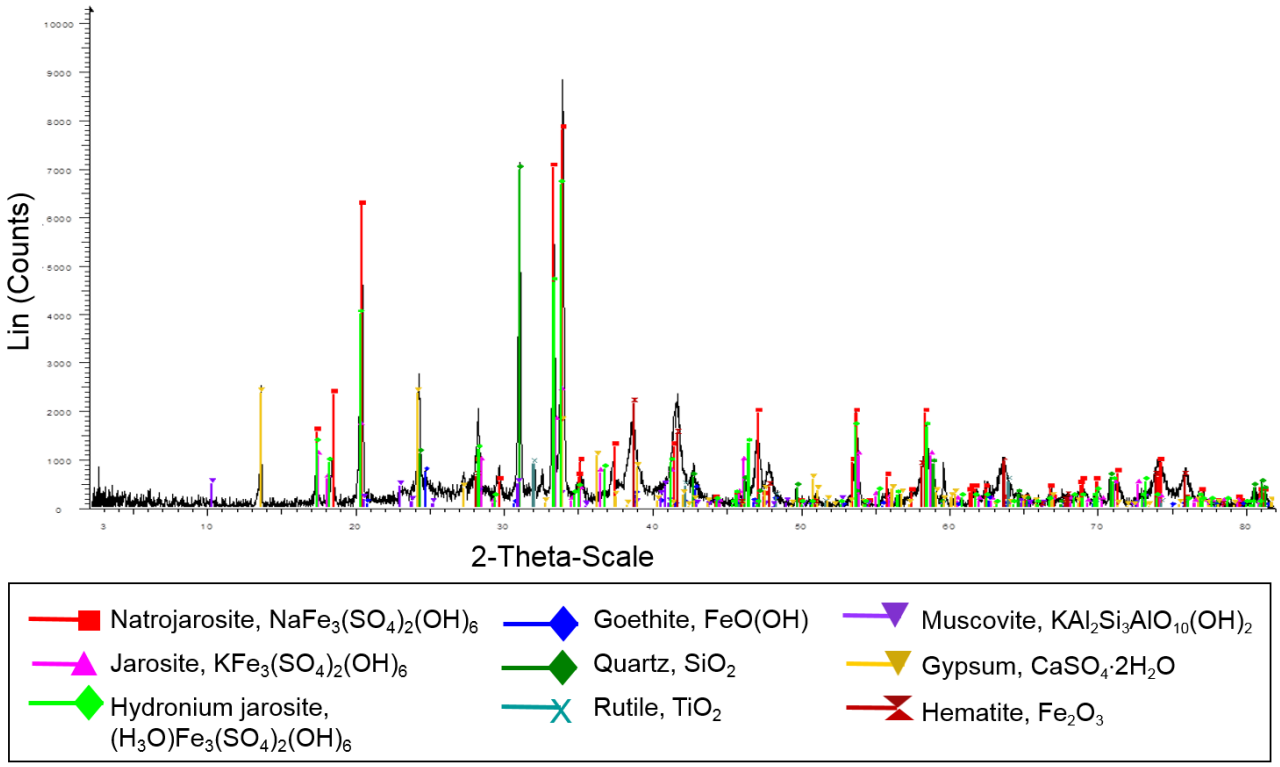

Figure 3. XRD pattern of a powdered sample collected beneath vegetation (sample site shown in Figure 2D) ~20 m out from the GD, indicating relative greater proportions of natrojarosite, jarosite, and hydronium jarosite, and relative lesser proportions of goethite, quartz, rutile, muscovite, gypsum, and hematite.

CONCLUSIONS

In summary, the jarositic cold seep emplaced GD, in the Northwest Territories, provides an excellent analogue to similar jarositic patches that have been identified on Mars. Martian jarosite may contain indicators (e.g., textural, chemical, biological) of former conditions, as this mineral is stable under a majority of temperature and pressure conditions on present-day Mars. Through comparing Martian jarosite sites to similar sites on the Earth, such as the GD, paleoenvironments on Mars during the time of deposition may be hypothesized. The GD appears as a brilliant golden-yellow patch of unvegetated polygonal sediment. UV–Vis–NIR spectral analysis detects only jarosite, however detailed mineralogy is predominantly natro-jarosite and jarosite, with hydronium jarosite, goethite, quartz, clays, and small amounts of hematite. The GD is of particular interest because mineralogy and environmental conditions at the time of deposition are conceivably analogous to jarosite deposits on Mars, and the mineralogy is more complex than what can be determined from orbital spectral data. Therefore, the GD may help to reveal potential Martian surface conditions at the time of deposition of similar jarosite deposits on Mars.

ACKNOWLEDGEMENTS

Thanks to Gordon Osinski and Neil Banerjee for supervising my PhD research and acting as mentors. Additional collaborators on the larger research project are also thanked: Darlene Lim, Alfonso Davila, Frederick Michel, Michael Craig, Matthew Izawa, Lisa Leoni, Gregory Slater, Alberto Fairén, and Louisa J. Preston. Roberta Flemming and Ed Cloutis are thanked for their XRD and spectroscopy expertise. Paul Mann, Kim Law, and Nicky Barry are thanked for their assistance in the lab and/or in the field.

This research was made possible by grants from the Canadian Space Agency and NSERC, a Northern Training Grant, and an NSERC Canadian Graduate Scholarship, a Lumsden Award, and support from the Canadian Astrobiology Training Program. Travel to GAC-MAC 2014 was sponsored by CPSX, Agnico Eagle Mines, SRK Consulting, and by the Environmental Earth Sciences Division and the Mineral Deposits Division of the Geological Association of Canada. All sponsors are thanked for their generosity.

REFERENCES

Battler, M.M., Osinski, G.R., Lim, D.S.S., Davila, A.F., Michele, F.A., Craig, M.A., Izawa, M.R.M., Leoni, L., Slater, G.F., Fairén, A.G., Preston, L.G., and Banerjee, N.R., 2013. Characterization of the acidic cold seep emplaced jarositic Golden Deposit, NWT, Canada, as an analogue for jarosite deposition on Mars; Icarus, v. 224, p. 382—398.

Bibring, J-P., Langevin, Y., Mustard, J.F., Poulet, F., Arvidson, R., Gendrin, A., Gondet, B., Mangold, N., Pinet, P., Forget, F., and the OMEGA team, 2006. Global mineralogical and aqueous Mars history derived from OMEGA/Mars Express data. Science; v. 312, p. 400–404.

Christensen, P.R., Wyatt, M.B., Glotch, T.D., Rogers, A.D., Anwar, S., Arvidson, R.E., Bandfield, J.L., Blaney, D.L., Budney, C., Calvin, W.M., Fallacaro, A., Fergason, R.L., Gorelick, N., Graff, T.G., Hamilton, V.E., Hayes, A.G., Johnson, J.R., Knudson, A.T., McSween Jr., H.Y., Mehall, G.L., Mehall, L.K., Moersch, J.E., Morris, R.V., Smith, M.D., Squyres, S.W., Ruff, S.W., and Wolff, M.J., 2004. Mineralogy at Meridiani Planum from the mini-TES experiment on the Opportunity Rover; Science, v. 306, p. 1733–1739.

Farrand, W.H., Glotch, T.D., Rice Jr., J.W., Hurowitz, J.A., and Swayze, G.A., 2009. Discovery of jarosite within the Mawrth Vallis region of Mars: Implications for the geologic history of the region; Icarus, v. 204, p. 478–488.

Gomez-Elvira, J. and REMS team, 2014. Mars Science Laboratory Rover Environmental Monitoring Station (REMS) Daily Reports. http://jpl.nasa.gov/msl/mission/instruments/environsensors/rems

Gorevan, S., Grant, J.A., Greeley, R., Grotzinger, J., Haskin, L., Herkenhoff, K.E., Hviid, S., Johnson, J., Klingelhöfer, G., Knoll, A.H., Landis, G., Lemmon, M., Li, R., Madsen, M.B., Malin, M.C., McLennan, S.M., McSween, H.Y., Ming, D.W., Moersch, J., Morris, R.V., Parker, T., Rice Jr., J.W., Richter, L., Rieder, R., Sims, M., Smith, M., Smith, P., Soderblom, L.A., Sullivan, R., Wänke, H., Wdowiak, T., Wolff, M., and Yen, A., 2004. The Opportunity Rover's Athena science investigation at Meridiani Planum, Mars; Science, v. 306, p. 1698–1703.

Klingelhöfer, G., Morris, R.V., Bernhardt, B., Schröder, C., Rodionov, D.S., de Souza Jr., P.A., Yen, A., Gellert, R., Evlanov, E.N., Zubkov, B., Foh, J., Bonnes, U., Kankeleit, E., Gütlich, P., Ming, D.W., Renz, F., Wdowiak, T., Squyres, S.W., and Arvidson, R.E., 2004. Jarosite and hematite at Meridiani Planum from Opportunity's Mossbauer spectrometer; Science, v. 306, p. 1740–1745.

LSSWG (ExoMars 2018 Landing Site Selection Working Group), 2014. Recommendation for the narrowing of ExoMars 2018 landing sites; European Space Agency, Issue 1, Reference EXM-SCI-LSS-ESA/IKI-004.

McSween, H.Y., and Treiman, A.H., 1998. Martian Meteorites; Reviews in Mineralogy and Geochemistry, v. 36, p. 6.1—6.53.

Michalski, J.R., and Niles, P.B., 2011. Formation of jarosite in the Mawrth Vallis region of Mars by weathering within paleo-ice deposits, *in* Proceedings of the Lunar and Planetary Science Conference 42, Houston, Texas. Abstract #1926.

Michel, F.A., 1977. Hydrogeologic studies of springs in the central Mackenzie Valley, Northwest Territories, Canada; M.Sc. Thesis, Department of Earth Sciences, University of Waterloo, Waterloo, Ontario, 185 p.

Michel, F.A., and van Everdingen, R.O., 1987. Formation of a jarosite deposit on Cretaceous shales in the Fort Norman area, Northwest Territories; Canadian Mineralogist, v. 25, p. 221–226.

Navrotsky, A., Forray, F., and Drouet, C., 2005. Jarosite stability on Mars; Icarus, v. 176, p. 250–253.

Squyres, S.W., Arvidson, R.E., Bell III, J.F., Brückner, J., Cabrol, N.A., Calvin, W., Carr, M.H., Christensen, P.R., Clark, B.C., Crumpler, L., Des Marais, D.J., d'Uston, C., Economou, T., Farmer, J., Farrand, W., Folkner, W., Golombek, M., Gorevan, S., Grant, J.A., Greeley, R., Grotzinger, J., Haskin, L., Herkenhoff, K.E., Hviid, S., Johnson, J., Klingelhöfer, G., Knoll, A.H., Landis, G., Lemmon, M., Li, R., Madsen, M.B., Malin, M.C., McLennan, S.M., McSween, H.Y., Ming, D.W., Moersch, J., Morris, R.V., Parker, T., Rice Jr., J.W., Richter, L., Rieder, R., Sims, M., Smith, M., Smith, P., Soderblom, L.A., Sullivan, R., Wänke, H., Wdowiak, T., Wolff,

M., and Yen, A., 2004. The Opportunity Rover's Athena science investigation at Meridiani Planum, Mars; Science, v. 306, p. 1698–1703.

GOSSANS OF THE CORNWALLIS DISTRICT, CENTRAL HIGH ARCTIC ISLANDS, CANADA

Elizabeth C. Turner
Department of Earth Sciences, Laurentian University, Sudbury, Ontario, P3E 2C6
(email: eturner@laurentian.ca)

INTRODUCTION

Gossanous showings have long been known from the Cornwallis District of the Canadian central high Arctic islands, Nunavut (Figure 1), a region containing Zn-Pb showings assumed to be related to the Polaris ore-body (20 Mt, 13% Zn, 4% Pb; mined between 1982 and 2002) (Dewing et al., 2007a). Although many of the showings in the area are not gossanous, those that are gossanous (Figure 2) are very conspicuous owing to the region's drab bedrock and Felsenmeer, and the almost complete lack of vegetation; the rusty weathering was known in the exploration community as "Arctic weathering".

REGIONAL CONDITIONS

The Canadian central high Arctic is underlain by epicratonic and passive-margin carbonate-dominated lower to middle Paleozoic rocks (Dewing et al., 2007b). Although bedrock exposures in the Cornwallis District are rare, the ubiquitous Felsenmeer consists of nearly in situ material that was frost-heaved from underlying bedrock and can, therefore, be regionally mapped. Glacially deposited material is sparse in the Cornwallis District owing to cold-based glaciation (Dyke, 1999; 2004). Deglaciation took place between 9 and 8.5 ka (Dyke, 2004). The modern climate in the Cornwallis District is arid, with annual average temperature well below 0°C.

Most of the Cornwallis District has subdued topography, with slightly higher plateaux underlain by lower to middle Paleozoic carbonate rocks of the Franklinian margin, and lower, wet areas underlain by mudrock and poorly lithified Devonian sandstone. Small drainages are only seasonally active, but larger rivers run throughout the summer and fall. Gossans are exposed in the well-drained plateau areas.

GEOLOGY

The geological history of the Cornwallis District includes semi-continuous lower to middle Paleozoic marine-dominated sedimentation punctuated by three episodes of deformation (Dewing et al., 2007a). The geometry and distribution of the resulting structures define three structural zones. Cambrian to Silurian strata were affected by subtle west-directed Late Silurian – Early Devonian deformation produced by far-field stresses associated with the Caledonian Orogeny, leaving north-trending fold axes and thrusts; these structures are most evident in the southern (Somerset Island) and central (Cornwallis Island) parts of the district. Late Devonian – Early Carboniferous south-directed compression associated with the Ellesmerian Orogeny produced west-trending folds and thrusts in the central (Cornwallis, Little Cornwallis, and easternmost Bathurst islands) and northern (western Devon Island) parts of the district. Early Carboniferous extension in the northern part of the district accompanied the development of the Sverdrup Basin (north of western Devon Island), reactivating older structures in the central and northern part of the district as normal faults.

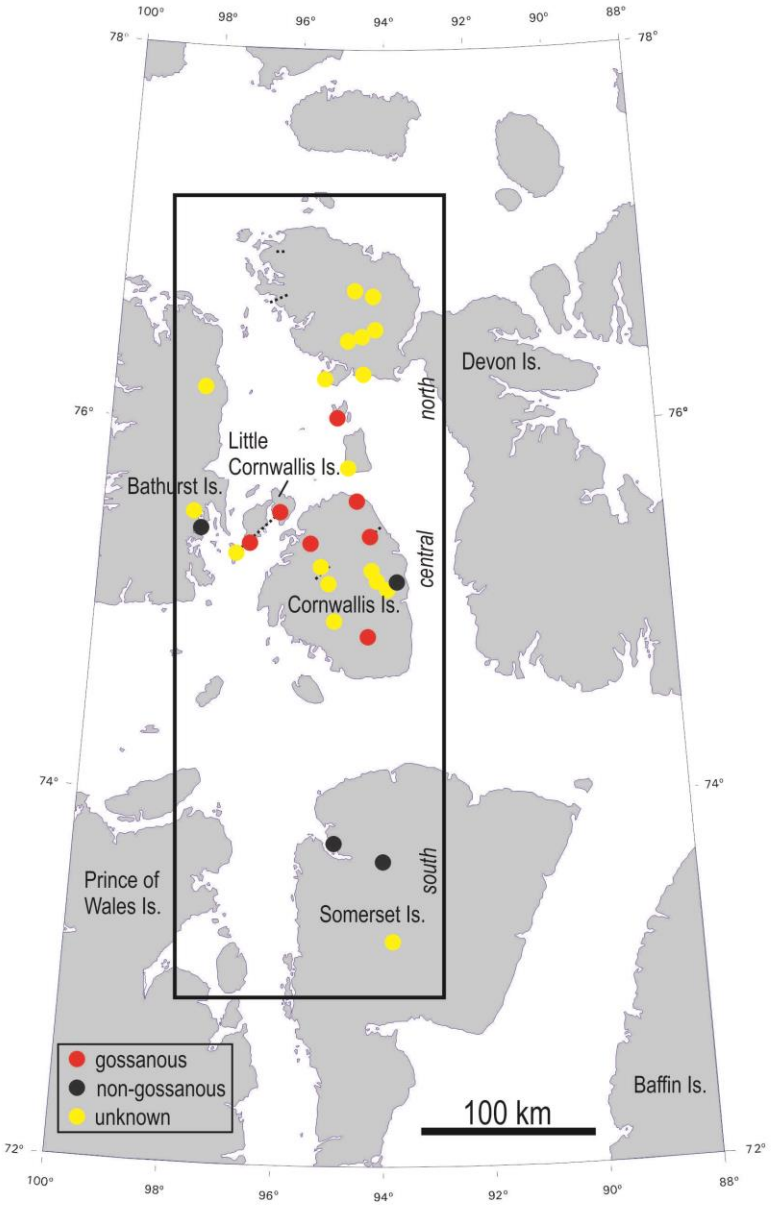

Figure 1. Distribution of some of the main showings in the Cornwallis District (black rectangle), after Dewing et al. (2007a).

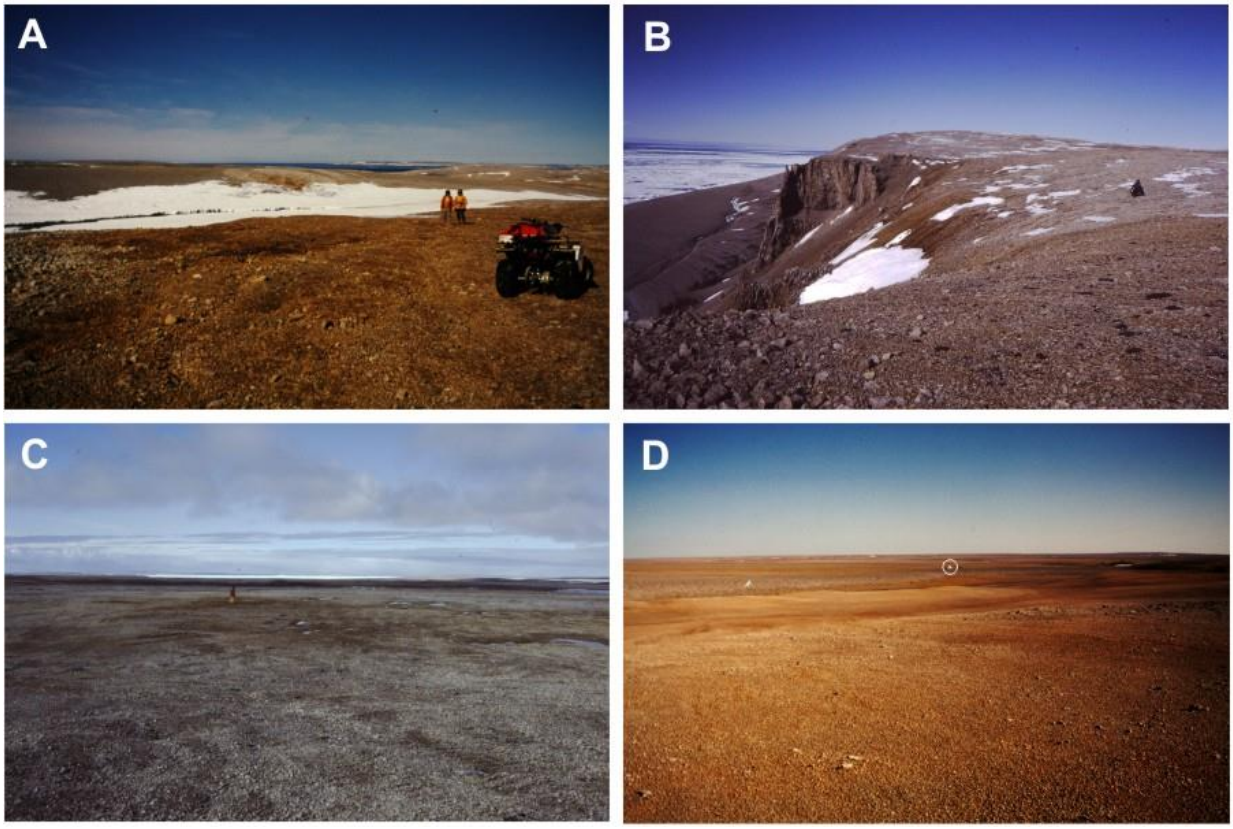

Figure 2. Gossanous showings of the Cornwallis District. (A) A gossan near Stuart River, northern Cornwallis Island. (B) A gossan on southwestern Dundas Island. Person on ATV for scale. (C) Eclipse gossan on eastern Little Cornwallis Island. Person for scale. (D) Part of an aerially extensive gossanous region near Bacon River, southern Cornwallis Island. Tent (circled) in background provides scale.

The Polaris Zn-Pb deposit formed in the late Devonian – Early Carboniferous (Christensen et al., 1995; Selby et al., 2005; contemporaneous with Ellesmerian deformation), but unpublished data (referred to in Dewing et al., 2007a), suggest the possible contribution of a separate, slightly younger Early Carboniferous mineralising event (i.e., contemporaneous with Sverdrup basin extension).

GOSSANOUS AND NON-GOSSANOUS SHOWINGS

The combination of three generations of structures and lithostratigraphic constraints dictates the location and size of gossanous and non-gossanous base-metal showings. Based on the compositions of known showings, there is no obvious spatial pattern in or structural control on the distribution of iron-bearing (and therefore gossanous) versus non-iron-bearing showings. Gossans are generally most abundant in the central part of the district, where their surface exposures range from metres to kilometres wide.

Obvious stratigraphic preferences are expressed in the distribution of gossanous and non-gossanous showings. In the southern region, the few known showings are predominantly in the Ordovician - Silurian Allen Bay Formation and are non-gossanous. On Cornwallis and Little Cornwallis islands (central region), showings are predominantly in the Ordovician Thumb Mountain Formation, the host rock of the Polaris deposit; this region contains the well-known "Arctic weathering" gossans. On northwestern Devon Island (northern region) showings are predominantly in O-S Allen Bay and Devonian Blue Fiord formations; few are gossanous.

CONCLUSIONS

The distribution of base-metal sulphide showings and of gossans produced by weathering of iron-containing showings in the Cornwallis District has structural, stratigraphic, and geographic biases. Gossanous base-metal showings of the Cornwallis District are most abundant and conspicuous in the central part of the district (Cornwallis and Little Cornwallis islands; gossans metres to kilometres wide), where showing distribution is constrained by (a) stratigraphy (predominantly Thumb Mountain Formation) and (b) structure, namely a combination of south-trending fold axes and reactivated Caledonian-aged faults, west-trending Ellesmerian fold axes and reactivated wrench faults extending away from Ellesmerian thrust faults.

Although the controls on spatial distribution of known base-metal sulphide bodies in the Cornwallis District are now adequately understood, the regional metallogeny of the Cornwallis District remains to be addressed. Three aspects remain unclear: (1) the presence or absence of iron in the showings and for the abundance of gossans in the central part of the district; (2) the weathering history that produced gossans, and (3) the geochemical and mineralogical nature of the gossans and their associated surface waters.

ACKNOWLEDGEMENTS

Regional research in the Cornwallis district was undertaken under the auspices of Canada-Nunavut Geoscience Office Arctic Zinc project. GSC colleague K. Dewing was the co-proponent of this field project. Sincere thanks go to hard-working and tolerant field companions too numerous to list.

REFERENCES

Christensen, J.N., Halliday, A.N., Leigh, K.E., Randell, R.N., and Kesler, S.E., 1995. Direct dating of sulphides by Rb-Sr: A critical test using the Polaris Mississippi-Valley-type Zn-Pb deposit; Geochimica et Cosmochimica Acta, v. 59, p. 5191-5197.

Dewing, K., Sharp, R.J., and Turner, E.C., 2007a. Synopsis of the Polaris Zn-Pb-Cu District, Canadian Arctic Islands, Nunavut, *in* Mineral Resources of Canada: A Synthesis of Major Deposit-types, District Metallogeny, the Evolution of Geological Provinces, and Exploration Methods, Goodfellow, W. (ed.), Geological Association of Canada, Mineral Deposit Division Special Paper 5, p. 655-672

Dewing, K., Turner, E.C., and Harrison, J.C., 2007b. Geological history, mineral occurrences and mineral potential of the sedimentary rocks of the Canadian Arctic archipelago, *in* Mineral Resources of Canada: A Synthesis of Major Deposit-types, District Metallogeny, the Evolution of Geological Provinces, and Exploration Methods, Goodfellow, W. (ed.),. Geological Association of Canada, Mineral Deposit Division Special Paper 5, p. 733-753.

Dyke, A.S., 1999. Last glacial maximum and deglaciation of Devon Island, Arctic Canada: support for an Innuitian ice sheet; Quaternary Science Reviews, v. 18, p. 393-420.

Dyke, A.S., 2004. An outline of North American deglaciation with emphasis on central and northern Canada, *in* Quaternary glaciations - extent and chronology, part II. North America, Ehlers, J and Gibbard, P.L. (eds.), Developments in Quaternary Science, v. 2, p. 373-424.

Selby, D., Creaser, R.A., Dewing, K., and Fowler, M., 2005. Evaluation of bitumen as a ^{187}Re-^{187}Os geochronometer for hydrocarbon maturation and migration: A case study from the Polaris MVT deposit, Canada, Earth and Planetary Science Letters, v. 235, p. 1-15.

MORPHOLOGY OF GOSSANS IN THE CANADIAN ARCTIC ISLANDS

Jeanne B. Percival, Marie-Claude Williamson, Rick J. McNeil, Stephen J.A. Day, Jeff R. Harris
Geological Survey of Canada, 601 Booth Street, Ottawa, Ontario, K1A 0E8
(email: Jeanne.Percival@nrcan.gc.ca)

INTRODUCTION

Chemical and physical weathering of bedrock and surficial materials may produce secondary minerals that vector to their primary mineral sources, such as potential buried ore deposits. The classic gossan, for example, includes a sulphide-depleted and silica-enriched leach cap, underlain by the main gossan zone enriched in Fe-oxides, Fe-oxyhydroxides and other secondary minerals. This overlies mineralized bedrock or surficial material containing primary sulphide minerals (Figure 1). Their formation is attributed to chemical weathering and supergene enrichment (Petruk, 2000). In this study, gossans were examined from two sites in the Canadian Arctic Archipelago (Figure 2): Victoria Island, Northwest Territories and Axel Heiberg Island, Nunavut. These gossans were investigated during a three-year study funded by Natural Resources Canada's Environmental Geosciences Program. One of the main objectives of the study was to demonstrate that Arctic gossans constitute natural analogues of mine wastes derived from base metal or PGE-type deposits. Study protocols included (1) the identification of gossan zones using satellite imagery (Harris et al., 2015); (2) mapping and sampling in the field (Kingsbury et al., 2013; Williamson et al., 2014); (3) laboratory analyses to determine the mineralogy and geochemistry of gossans (Peterson et al., 2014); (4) and complementary analysis of stream sediments and local streams (McNeil et al., 2015; Williamson et al., 2015).

Preliminary results show that Arctic gossans can display various morphologies and attributes. The nature of Arctic gossans is strongly controlled by the presence or absence of evaporites and interaction with permafrost. We therefore propose a classification scheme for gossans that reflects differences in morphology, chemical reactivity and host rock lithology. The results underscore the importance of including the study of gossans in northern mapping projects to enable their discovery, classification, and sampling for detailed mineralogy and geochemistry, and to elucidate their modes of formation.

VICTORIA ISLAND GOSSANS

The study area on Victoria Island is characterized by the presence of flood basalts and associated intrusive rocks. The Franklin Large Igneous Province (FLIP) consists of sills, dykes and flood basalts emplaced in Neoproterozoic sedimentary rocks that are exposed in the Minto Inlier, central Victoria Island (Bédard et al., 2012). Figure 3 is a simplified geological map of the Minto Inlier that shows the location of two gossans (yellow triangles 1 and 2) that lie within the Wynniatt and Kilian formations, respectively. The former consists of shallow-water carbonates and mudrock and the latter of sandstone and evaporitic rocks (Rainbird et al., 2014). Both occurrences are found in proximity to Franklin sills associated with the southern lobe of the Natkusiak Formation flood basalts (Williamson et al., 2013).

Location 1

The L1 gossan is a 75-m topographic high capped by a poorly consolidated gossan overlying pyritic sands (Figure 4A). Several concentric zones of variably-coloured, rubbly material were discovered in the gossan (Figure 4B). Quartz and pyrite are found in the central grey zone. This zone is surrounded by gypsum, quartz and jarosite in the yellow, somewhat oxidized zone that is, in turn, surrounded by hematite and amorphous Fe-oxides in the outermost strongly oxidized, brown-orange zone.

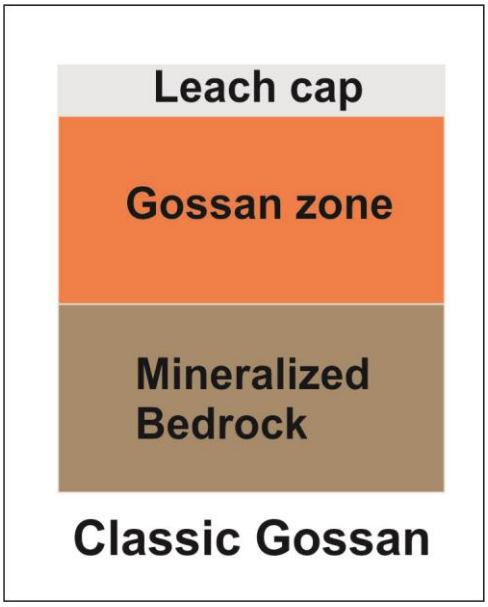

Figure 1. Schematic illustration of a classic gossan model showing the leach cap overlying gossanous zone and mineralized bedrock. Thicknesses of each unit are not drawn to scale and vary in nature.

Location 2

The L2 gossan developed below a 20+ m thick mafic sill in contact with a basal rheomorphic breccia. Figure 5A shows the extent of the gossanous soil developed beneath the sill. The contact between the sill and breccia is marked by a thin (10 cm) sulphide layer (pyrite (Figure 5B); Williamson et al., 2014). Pits were hand dug in areas of grey soil (Figure 5C) that reveal crude stratification (Figure 5D). Remarkably, the oxidation zone is inverted when compared to the classic gossan profile shown in Figure 1. No clear evidence of mass wasting was observed but this possibility cannot be ruled out. The oxidized layers are comprised of goethite, gypsum, jarosite and minor to trace sulphur with some samples containing minor bassanite. The measured depth to permafrost is 80 cm (Figure 5D).

AXEL HEIBERG ISLAND

The High Arctic Large Igneous Province (HALIP) comprises widespread mafic igneous rocks of Cretaceous age emplaced in the Sverdrup Basin, a rift basin that contains a thick succession of marine and non-marine clastic, carbonate and evaporitic rocks (Embry, 2011; Harrison and Jackson, 2014). Figure 6 shows the location of five gossans that lie within HALIP rocks in the Strand Fiord-Expedition Fiord region of Axel Heiberg Island (Harrison and Jackson, 2011). The gossans occur in sedimentary and evaporitic rocks that are spatially associated with HALIP volcanic rocks, sills, and dykes (Williamson et al., 2011; 2014).

Locations 3 and 4

Field work near the head of East Fiord revealed the presence of two gossans (L3 and L4, Figure 6). The L3 gossans are typically associated with relict sulphide chimneys or "mounds" embedded in the Agate North Diapir (AND). The best-preserved example observed in the AND consists of a conical, sulphide-rich structure that is 5 m long in cross-section (Figure 7A). Alteration zones of whitish-yellow to ocher alteration associated with relict mounds of sulphide-rich basaltic breccia are commonly found along the west-facing wall of the AND (Figures 7B and 7C). On-site mineralogical analysis using a portable X-Ray diffractometer and follow-up laboratory analyses confirmed the presence of the secondary sulphates copiapite, fibroferrite and jarosite in gossans associated with the basaltic breccia (Williamson et al., 2011).

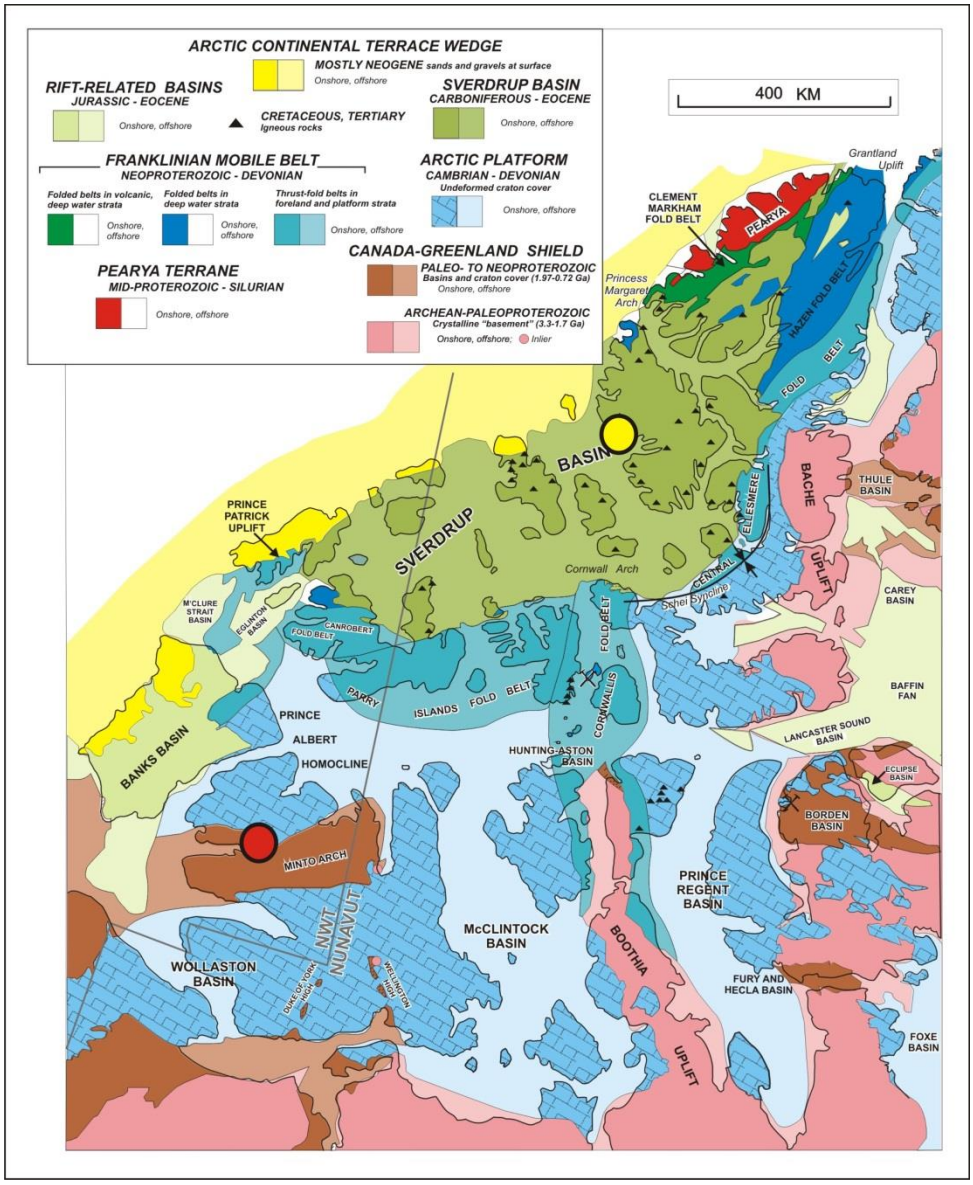

Figure 2. Location of the study areas (filled circle): red, Victoria Island, Northwest Territories; yellow, Axel Heiberg Island, Nunavut.

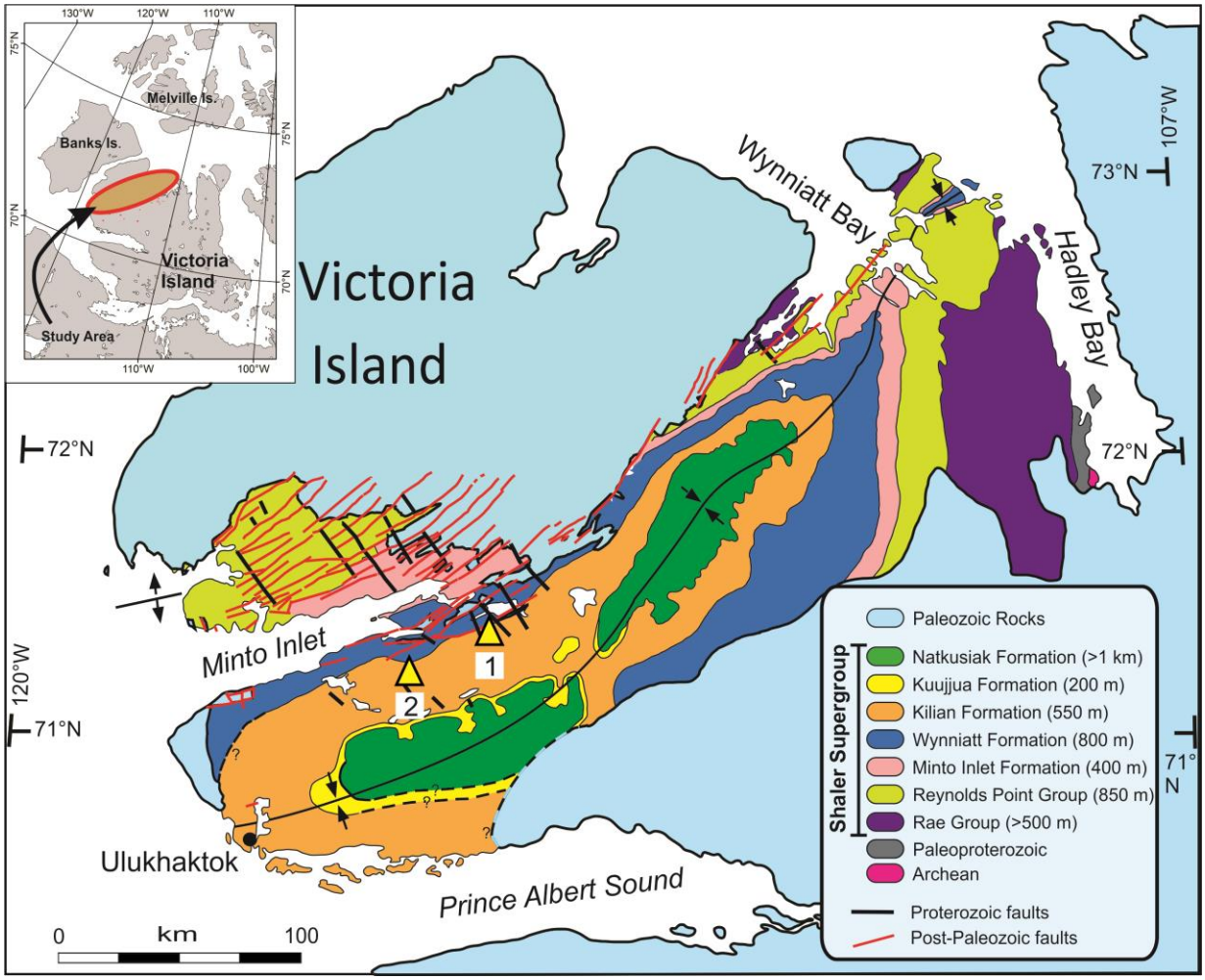

Figure 3. Simplified geological map of central Victoria Island, Northwest Territories, showing the location of gossans sampled in the Minto Inlier (yellow triangles): Location 1, Gossan Hill; Location 2, Sill Gossan (after Thorsteinsson and Tozer, 1962; Bédard et al., 2012). Sediment thickness is shown in brackets in the legend

.

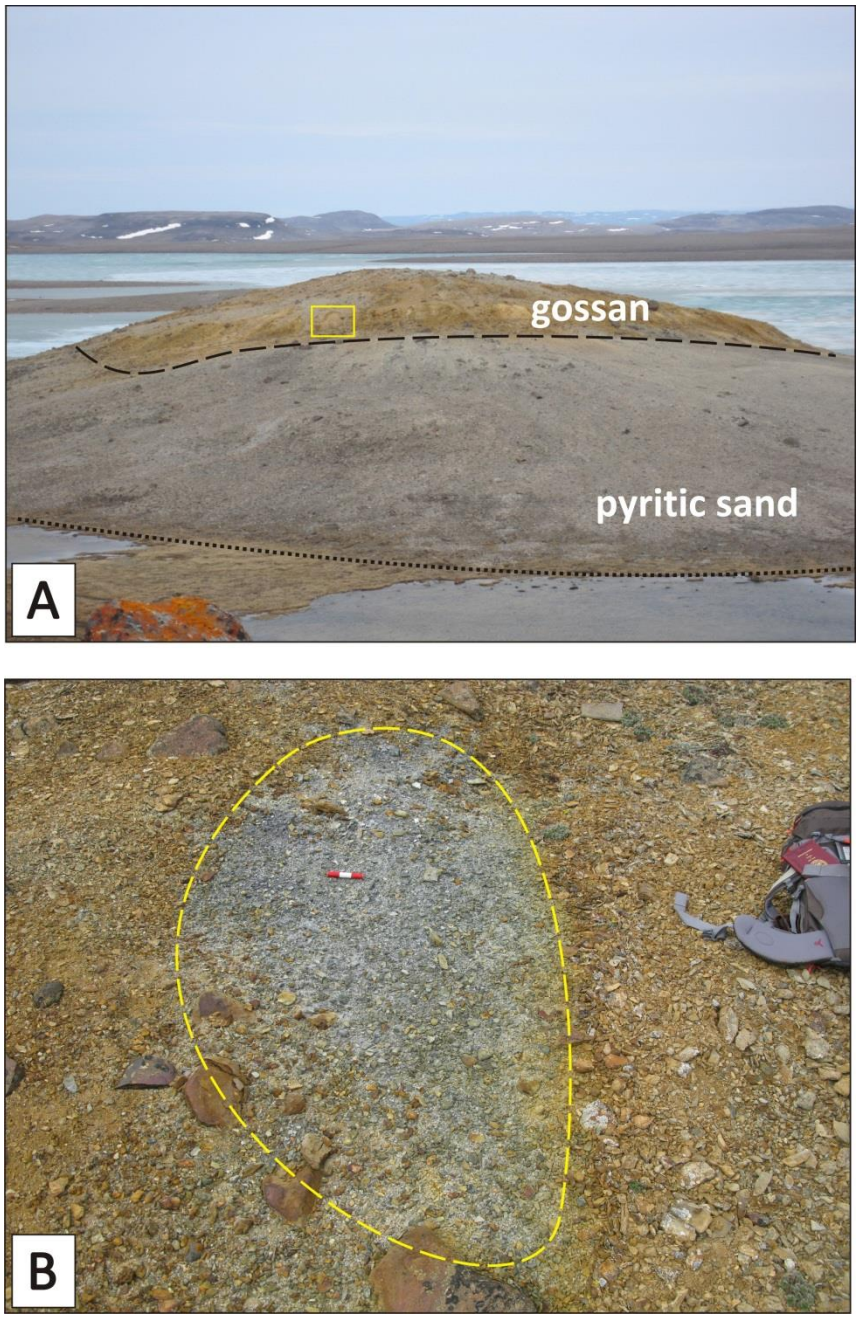

Figure 4. (A) View of the L1 gossan looking North. The hill rises approximately 75 m above the surrounding tundra and is 400 m long at the base (Peterson et al., 2014). The deposit consists of loosely-consolidated pyritic sands capped by gossanous soil. The contact between these two units is shown by the dashed line. The yellow square shows the approximate size of circular alteration zones. (B) Close-up view of one of several alteration zones mapped in the L1 gossan. The dashed line shows the contact between grey pyritic sand and the oxidized, yellow to rust-coloured material at the periphery. The scale at centre is 7.62 cm long.

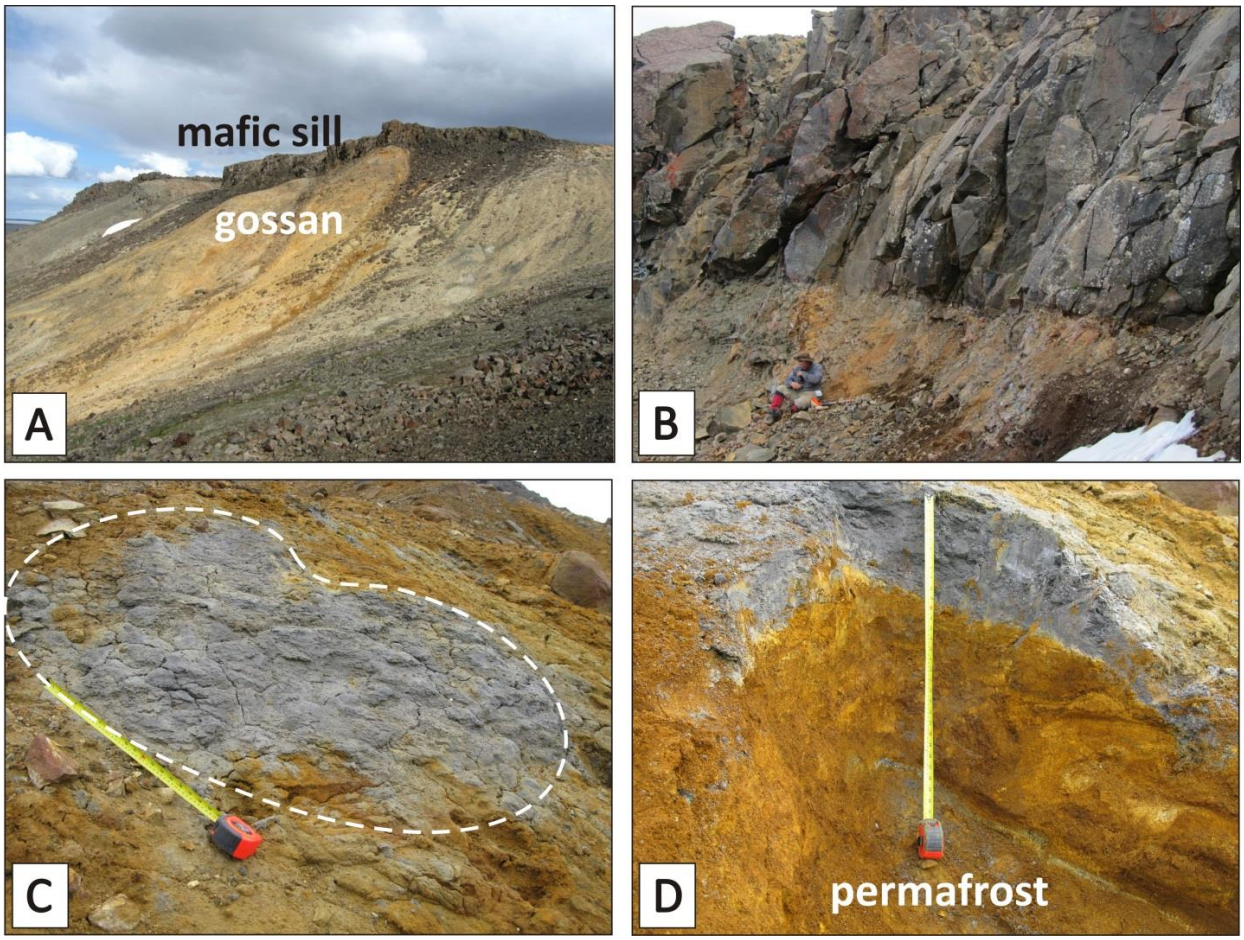

Figure 5. (A) Aerial view of the L2 gossan looking southeast. The scree slope consists of loosely-consolidated pyrite sands and gossanous soil overlain by a gabbro sill and complex rheomorphic breccia. (B) View of the contact between the massive sill and the underlying rheomorphic breccia. (C) Plan view of alteration zone where the pit was dug. The measuring tape is 51 cm long. (D) Close-up of the L2 gossan showing inverted stratigraphy when compared to Figure 1. Depth to permafrost is 80 cm (modified from Williamson et al., 2014).

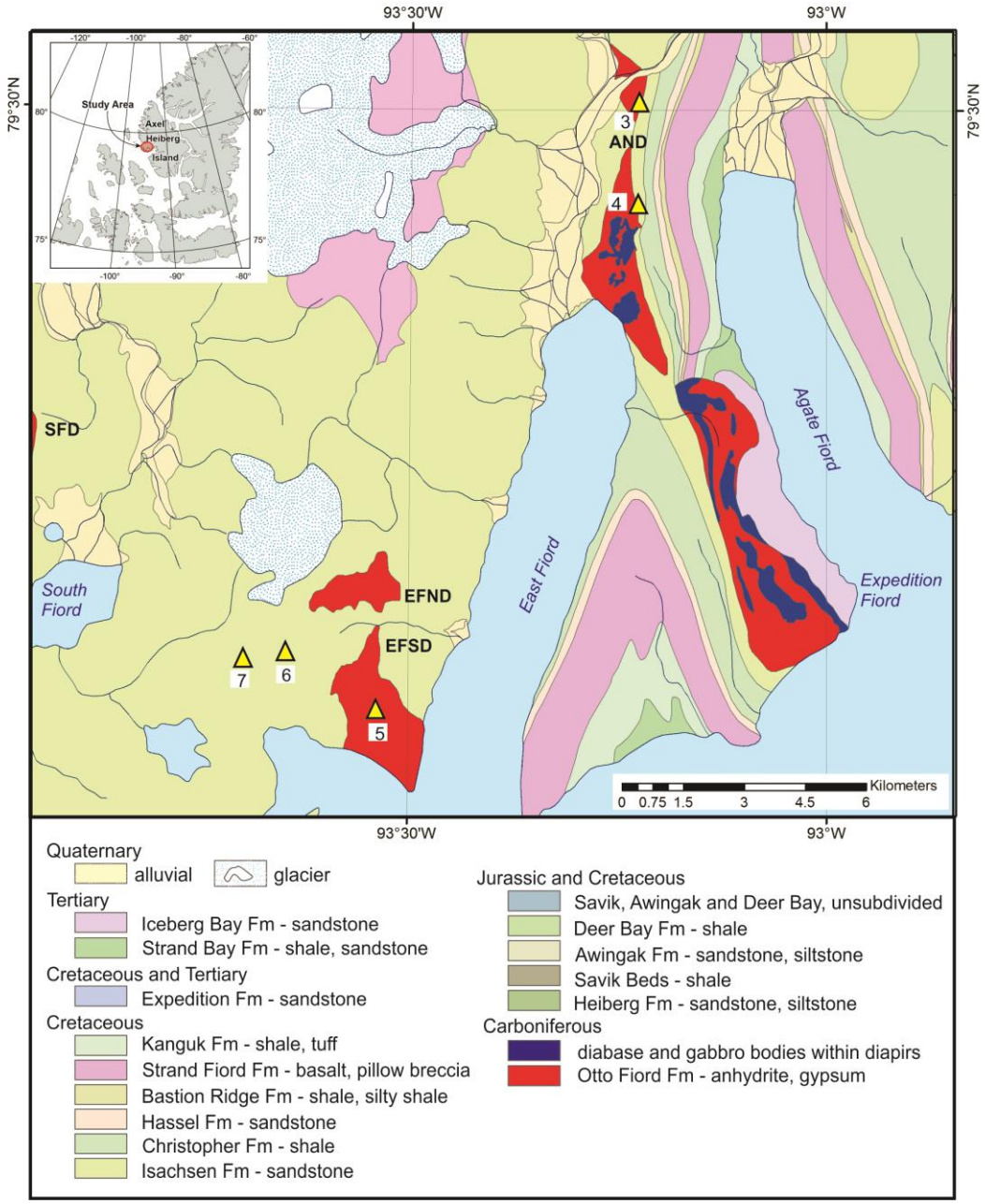

Figure 6. Simplified geological map of Axel Heiberg Island, Nunavut, showing the location of five gossans sampled in the Strand Fiord-Expedition Fiord area (yellow triangles). Note that three of the five gossans are located within evaporite diapirs: Agate North Diapir (AND); East Fiord North Diapir (EFND); and East Fiord South Diapir (EFSD). Bedrock geology from Harrison and Jackson (2011).

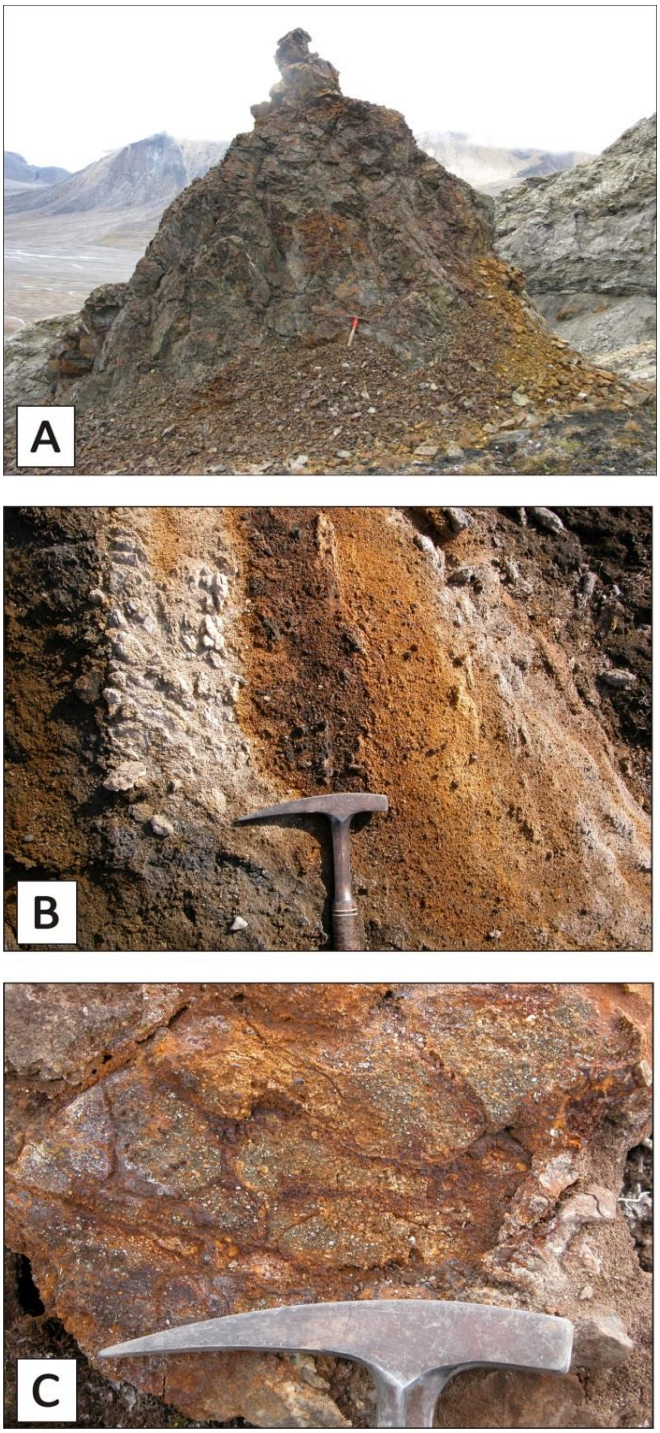

Figure 7. L3 gossans are located in the Agate North Diapir (AND) at the head of East Fiord. The gossans are associated with constructional edifices that resemble mounds or chimneys and are ~ 5 m long at the base. The mounds consist of sulphide-rich breccias and oxides that do not react with the underlying permafrost. (A) Field photograph of L3 mound with a roughly conical shape. The hammer is 30 cm in length. (B) Close-up of several alteration zones located within the AND. (C) Sulphide-rich breccia from L3 mound (Williamson et al., 2011).

The L4 gossans were discovered within poorly-consolidated sandstones of the Isachsen Formation along the eastern wall of the AND (Figure 8). Figure 8A illustrates the spectacular exposure of the gossan at this locality. L4 gossans show a classic profile that includes a bright yellow to orange upper layer (goethite and hematite) overlying a pale grey layer (clays) that is reactive with permafrost (Figure 8B; compare with Figure 1). At this site, permafrost occurred at a depth of 1 m. The top layer consists of a black, friable crust of unknown composition.

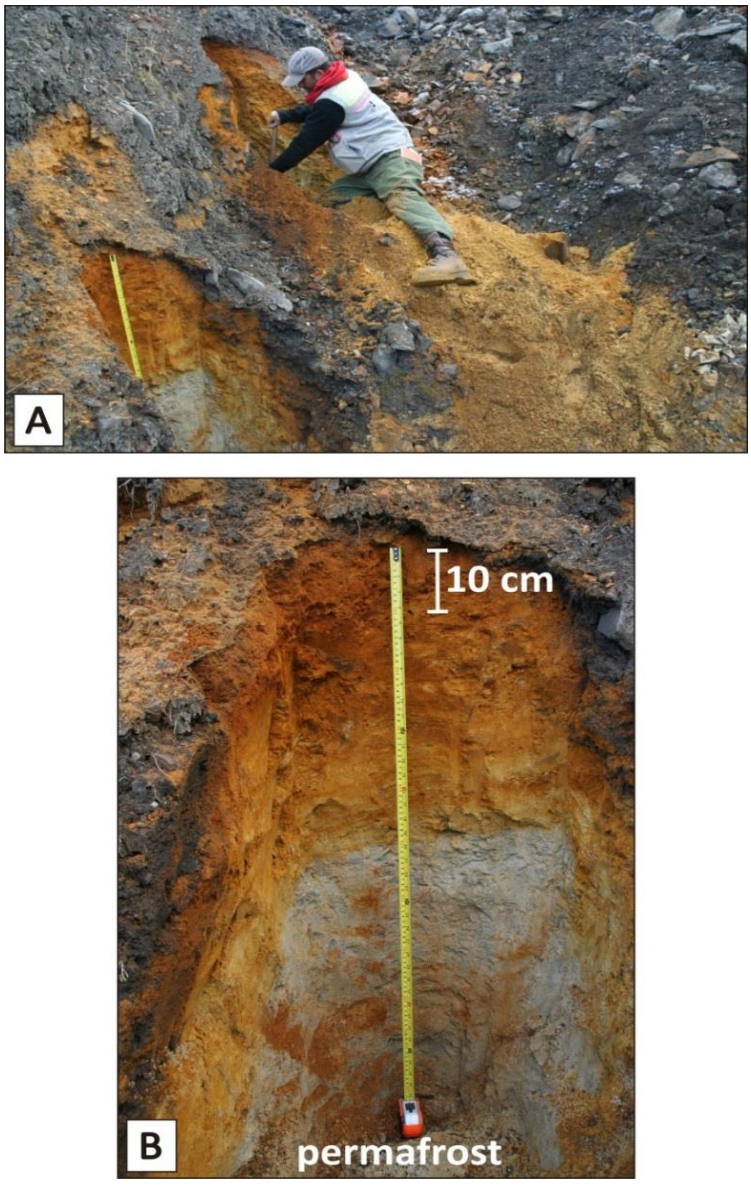

Figure 8. L4 gossans are located in the Agate North Diapir (AND) at the head of East Fiord. (A) Gossan developed in poorly-consolidated quartzitic sandstones of the Isachsen Formation. R.C. Peterson is sampling the gossan. The tape measures 50 cm. (B) L4 displays a classic gossan profile. The tape measures 1 m from leach cap to permafrost (Fig. 9A of Williamson et al., 2011). The top layer consists of a black, crust-like material of unknown composition.

Locations 5 and 6

Field work near South Fiord, Axel Heiberg Island, revealed the presence of three additional gossans (Figure 6). Location 5 consists of partially preserved sulphide mounds found within the South East Fiord Diapir (Figure 9). The L5 structures are ~ 5 m long at the base and consist of a (1) poorly-preserved mafic breccia, (2) siliceous 'apron' and (3) gossanous soil in evaporite host rocks that is not reactive with permafrost (Figure 9A). In contrast, the L6 gossan is a thick deposit that developed within poorly-consolidated shales located beneath a mafic sill, and is reactive with permafrost (Figure 10A). Many of its features, with the exception of its poor stratification and shale host (Figure 10B), are comparable to the L2 gossan on Victoria Island (Figure 5).

Figure 9. L5 gossans were discovered within the East Fiord South Diapir (EFSD). (A) Overview of L5 gossan morphology: the structures are ~ 5 m long at the base and consist of a poorly-preserved mafic breccia, silica-rich 'apron' and gossanous soil in evaporite host rocks. (B) Close-up view of the sharp contact between breccia and evaporite. The scale is 7.62 cm long. (C) Close-up view of the gossanous soil at the base of the structure. The hammer is 30 cm long.

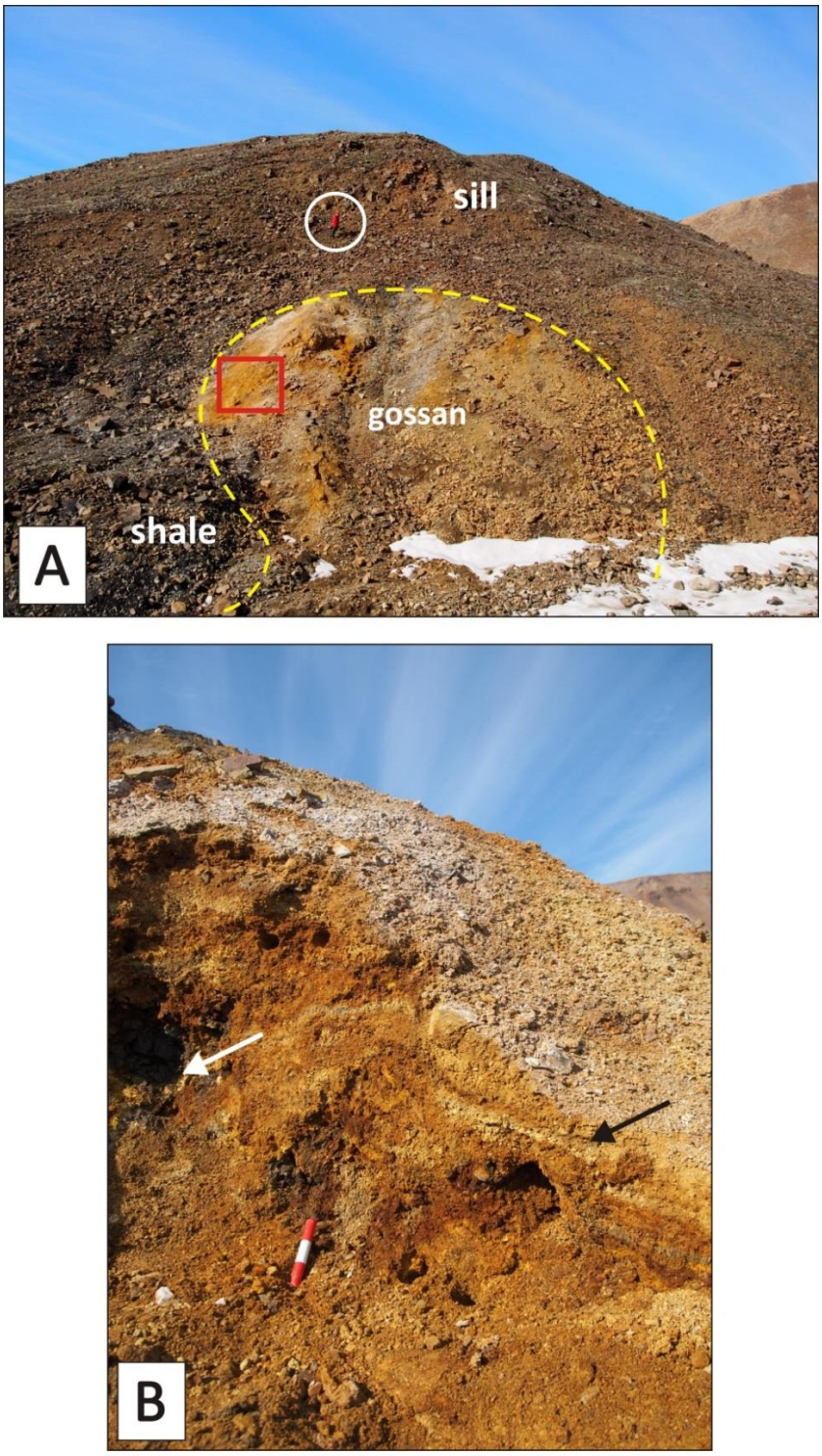

Figure 10. The L6 gossan is located near the glacial terrace chosen as base camp during the 2013 Isachsen Expedition to South Fiord (Kingsbury et al. 2013; Williamson et al., 2014). (A) View of the gossan outcrop (yellow dashed line) and host rocks consisting of shale and mafic sill. The field assistant is shown by a white circle at the base of the sill. The yellow square shows the location of the trench where samples were collected. (B) Close-up of coarse layering in the gossan (black arrow) and of small "pockets" where nodules are preserved (white arrow).

Location 7

The most enigmatic of all the gossans discovered in the South Fiord area is exposed at Location 7 (Figure 6). The L7 gossan consists of a thick deposit associated with shales and overlain by volcanic rocks of the Walker Island Member, in the Isachsen Formation (Figures 11A, 11B). The deposit consists of thinly stratified sediments and is reactive with permafrost (Figure 11 C).

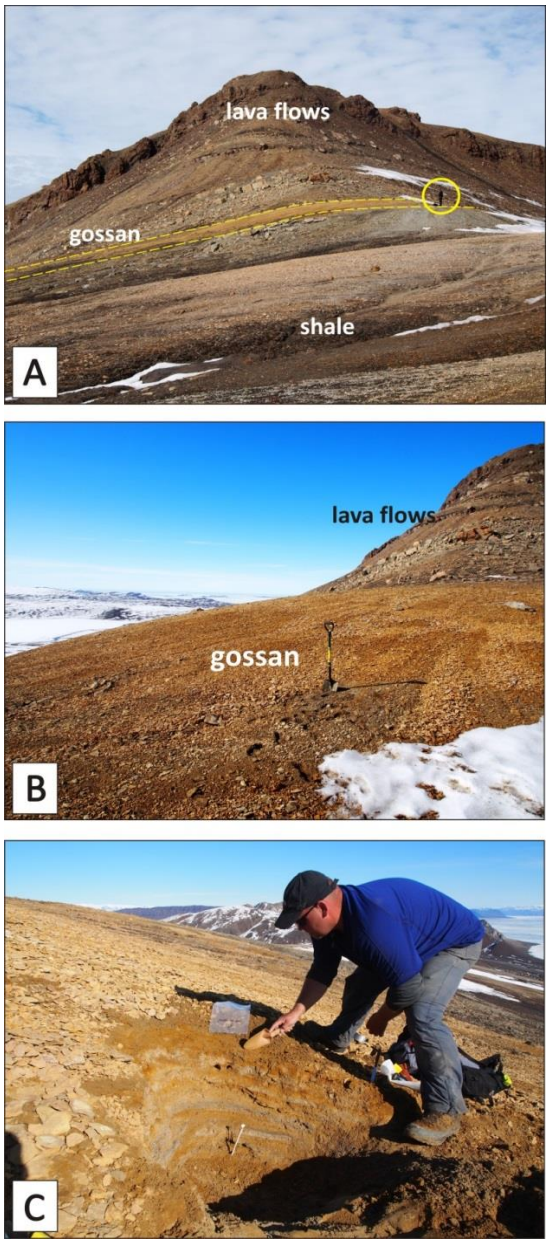

Figure 11. The L7 gossan on a ridge of volcanic rocks belonging to the Walker Island Member of the Isachsen Formation. (A) Panoramic view of the volcanic succession, gossan (dashed line; geologist in yellow circle) and shale. (B) Close-up of the gossan located at the base of the volcanic succession (shovel for scale). (C) A trench dug into the gossan revealed the presence of thin, coherent and laterally continuous layers of alternating orange, yellow and grey sediments.

DISCUSSION

The morphological attributes of gossans L1 to L7 are summarized in Table 1. In all cases, goethite, jarosite and gypsum predominate. Importantly, the gossans vary in size, their morphology is complex, and in some cases, the observed stratigraphy does not match the classic gossan profile (Figure 1). The deposits are found in a range of host rocks that include shale, sandstone, mafic sills, volcanic and evaporitic rocks. According to Elberling and Langdahl (1998), base metal gossans in arctic regions can react with underlying permafrost on a seasonal basis. Therefore, oxide-sulphide gossans record a complex acid-rock generation process in which freeze–thaw cycles promote the chemical weathering of sulphide-rich rocks accompanied by the production of reactive gossanous soil. The surficial deposits and underlying permafrost thus provide an opportunity to study alteration processes and mineral reactions that have been underway in the arctic environment for extended periods of time (e.g., since the last glaciation).

Based on this concept and observations in the field (e.g., loosely consolidated material, presence of acidic soils), the gossans were subdivided into reactive and non-reactive types (Table 2). Gossans L1, L2, L4, L6 and L7 were classified as Type 1 based on reactivity with permafrost, classic gossan profile, and the association with sedimentary host rocks. L2 is classified as Type 2 based on reactivity, an inverted profile and the clear association with mafic igneous rocks. L3 and L5 are non-reactive gossans associated with sulphide-rich breccias of igneous origin in evaporitic rocks. Therefore these deposits are classified as Type 3.

Table 1. Location and morphological attributes of gossans

LOCATION	GOSSAN PROFILE	HOST ROCK	FACIES	REFS
L1	Classic, reactive	Sedimentary	Complex	[1,2]
L2	Inverted, reactive	Igneous	Stratified	[2,3]
L3	Mound, nonreactive	Evaporite	Complex	[2,4]
L4	Classic, reactive	Sedimentary	Stratified	[2,4]
L5	Mound, nonreactive	Evaporite	Complex	[2,5]
L6	Classic, reactive	Sedimentary	Complex	[2,5]
L7	Classic, reactive	Sedimentary	Stratified	[2,5]

References: [1] Peterson et al. (2014); [2] Williamson et al. (2014); [3] Percival and Williamson (2013); [4] Williamson et al. (2011); [5] Kingsbury et al. (2013)

Table 2. Classification of gossans based on their attributes.

ATTRIBUTES	REACTIVE		NON-REACTIVE
CLASSIFICATION	**Type 1**	**Type 2**	**Type 3**
MORPHOLOGY	Classic	Inverted	Chimney
HOST ROCK	Sedimentary	Igneous	Evaporite
	L1	L2	L3
	L4		L5
	L6		
	L7		

At L1, Victoria Island, the presence of jarosite indicates formation under acidic conditions, usually a pH between 2 and 3 (Jambor, 2003). The subsurface material is comprised of similar mineralogy with discrete sulphur occurring in the yellowish samples. Permafrost occurs about 10 cm below the surface. Peterson et al. (2014) proposed that the L1 gossan developed post-glacially and may represent the vestiges of a hot spring system. Percival and Williamson (2013) and Percival et al. (2014) suggested that cyclical freeze-thaw action along with vertical pumping of fluids, upwards and outwards, could produce the concentric zones of rubble and concomitant oxidation of the pyritic sands (Figure 4B). This model would be similar to the "piston effect" of Shvartsev (1965, 1970) and that of Shilts (1973) describing a "diapiric" effect for mud boils in permafrost terrains (cf., McMartin and Campbell, 2009). A similar process may lead to the formation of concentric zones of pyritic sand at L2 (Figure 5B). The pyrite-rich breccia and mineralized contact above L2 may provide fresh pyrite on a cyclical or seasonal basis due to mass wasting along the hillside (Percival and Williamson, 2013; Percival et al., 2014). Thus, the unoxidized grey layer in L2 may contain fresh pyrite and is undergoing weathering. A forthcoming examination of these layers will allow us to establish if permeability is a factor to be considered in the inversion of gossan profiles.

The sulphide minerals associated with L3 gossans are found in structurally complex areas or 'chaotic zones' located at the periphery of evaporite diapirs where mafic igneous rocks or sandstone beds form a melange with anhydrite (Williamson et al., 2011). The growth of evaporite diapirs over time may have supplied conduits for the circulation of hot fluids through basaltic chimneys, now preserved as brecciated sulphide mounds (Figure 7). In contrast, L4 gossans appear to be associated with ephemeral springs that flow through the mafic rocks and deposit minerals in porous quartzarenites of the Isachsen Formation (Figure 8).

There is evidence that the L5 gossans in the East Fiord South Diapir (EFSD, Figure 6) may have formed from fluids circulating at the periphery of "rafts" of mafic igneous rocks mechanically transported in the diapir, much in the same way as observed in the case of L3 gossans. Figure 12 shows the structural relationships between a mafic sill, the host evaporite and the overlying gossan. The sill shows evidence of pinching and brecciation caused by the gradual rise of the evaporite diapir, providing a possible explanation for the conical shape of sulphide chimneys as the process evolves. Parts of the disrupted sill could become zones of weakness that enable circulation of hot fluids within the diapir. The entire unit may eventually break off into several fragments along these zones of weakness and lead to the formation of mounds such as those associated with the L3 and L5 gossans. Although the L6 gossan shows many similarities in scale and morphology with the L2 gossan on Victoria Island, the profile is not inverted. Finally, the areal extent and finely laminated, mineralogically diverse nature of the L7 gossan are remarkable attributes that warrant further investigation

CONCLUSIONS

Field observations and sampling of gossans at 7 localities in the Canadian Arctic Islands demonstrated the complex nature of these surficial deposits. The results of the study demonstrate that gossans can be grouped into 3 types based on stratigraphy, presence or absence of evaporite rocks, and reactivity with permafrost. The authors acknowledge that in the case of Axel Heiberg Island, the gossans represent a restricted sample in a region that likely contains hundreds of gossans. However, the proposed, first order classification scheme is a starting point. It is clear that in all cases, cryogenic (disintegration, dissolution, leaching) and oxidation processes are ongoing. The pumping action of fluids (piston effect or diapiric/mud boil activity) further enhances the above processes and the transport of materials down slope, similar to a solifluction process. Sulphide oxidation leads to acidic conditions (Jambor, 2003), which have been detected in pore waters and ice at all sites (Williamson et al., 2015) and to the formation of minerals such as gypsum, jarosite and goethite.

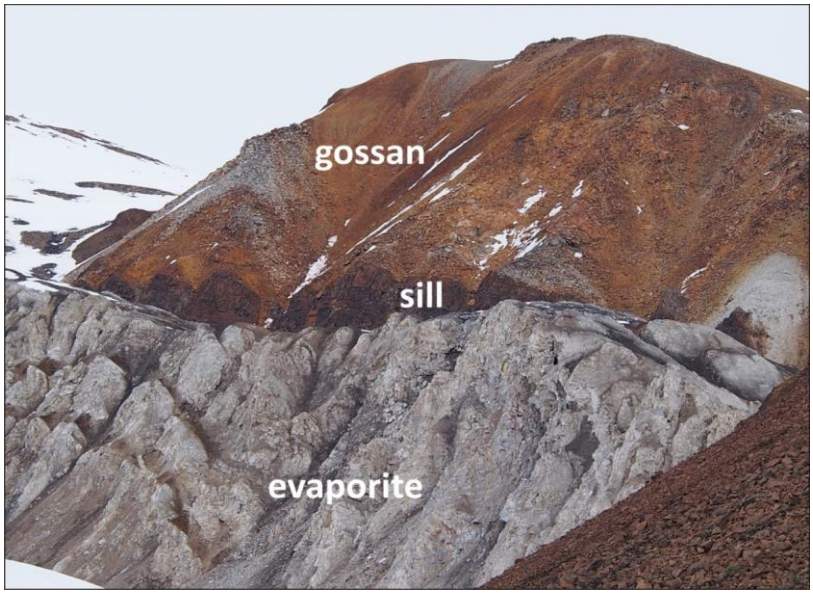

Figure 12. Panoramic view of the structural relationship between evaporite, mafic sill and overlying gossan at East Fiord South Diapir.

Oxide-sulphide gossans constitute natural analogues of mine waste in a permafrost environment that can increase our understanding of metal recycling, deposition, sorting, and burial as oxidation proceeds. The results of this study underscore the importance of including the study of gossans in northern mapping projects to enable their discovery, classification, and sampling for detailed mineralogy and geochemistry, and to elucidate their modes of formation.

ACKNOWLEDGEMENTS

The Arctic Gossans Activity was funded by the Environmental Geoscience Program of the Earth Sciences Sector-Geological Survey of Canada, Department of Natural Resources Canada. Field studies were carried out in collaboration with the Geomapping for Energy and Minerals (GEM 1) and Polar Continental Shelf Programs. Special thanks to Cole Kingsbury for assistance in the field and to Beth Hillary (GSC-Ottawa) for cartographic work. Comments by Guest Editors Helen Smyth and Benoit Saumur improved an earlier version of the manuscript. ESS Contribution no. 20130475.

REFERENCES

Bédard, J.H., Naslund, H.R., Nabelek, P., Winpenny, A.,Hryciuk, M., Macdonald, W., Hayes, B., Steigerwaldt, K., Hadlari, T., Rainbird, R.H., Dewing, K., and Girard, E., 2012. Fault-mediated melt ascent in a Neoproterozoic continental flood basalt province, the Franklin sills, Victoria Island, Canada; Geological Society of America Bulletin, v. 124, p. 723–736, doi:10.1130 /B30450.1

Elberling, B., and Langdahl, B.R., 1998. Natural heavy-metal release by sulphide oxidation in the High Arctic; Canadian Geotechnical Journal, v. 35, p. 895–901.

Embry, A.F., 2011. Chapter 36: Petroleum prospectivity of the Triassic–Jurassic succession of Sverdrup Basin, Canadian Arctic Archipelago; Geological Society of London, Memoirs, v. 35, p. 545-558, doi:10.1144/M35.36

Harris, J.R., Williamson, M.-C., Percival, J.B., Behnia, P., and MacLeod, R.F., 2015. Detecting and mapping gossans using remotely-sensed data, *in* Environmental and Economic Significance of Gossans, (ed.) M.-C Williamson; Geological Survey of Canada, Open File 7718, p. 3-13.

Harrison, J.C., and Jackson, M.P.A., 2011. Bedrock geology, Strand Fiord-Expedition Fiord, western Axel Heiberg Island, northern Nunavut (parts of NTS 59E, F, G, and H); Geological Survey of Canada, Map 2157A, 2 sheets, scale 1:125 000.

Harrison, J.C., and Jackson, M.P.A., 2014. Tectonostratigraphy and allochthonous salt tectonics of Axel Heiberg Island, central Sverdrup Basin, Arctic Canada; Geological Survey of Canada, Bulletin 607, 124 pp.

Jambor, J.L., 2003. Mine-waste mineralogy and mineralogical perspectives of acid – base accounting; *in* Environmental Aspects of Mine Wastes, Jambor, J.L., Blowes, D.W. Ritchie, A.I.M. (eds.); Mineralogical Association of Canada Short Course, v. 31, ch. 6, p. 117-145.

Kingsbury, C.G., Williamson, M.-C., Day, S.J.A., and McNeil, R.J., 2013. The 2013 Isachsen expedition to Axel Heiberg Island, Nunavut, Canada: A field report; Geological Survey of Canada, Open File 7539, 6 p. + poster (doi:10.4095/293842).

McMartin, I., and Campbell, J.E., 2009. Near-surface till sampling protocols in shield terrain, with examples from western and northern Canada, *in* Application of Till and Stream Sediment Heavy Mineral and Geochemical Methods to Mineral Exploration in Western and Northern Canada, Paulen, R.C. and McMartin, I (eds.); Geological Association of Canada, GAC Short Course Notes 18, p. 75-95.

McNeil, R.J., Day, S.J.A., and Williamson, M.-C., 2015. Stream sediment and water geochemical study, Axel Heiberg Island, Nunavut, Canada, *in* Environmental and Economic Significance of Gossans, (ed.) M.-C Williamson; Geological Survey of Canada, Open File 7718, p. 85-96.

Percival, J.B., and Williamson, M.-C., 2013. Mineralogy and economic potential of oxide-sulphide gossans, Canadian Arctic Islands; XV International Clay Conference (ICC), Rio de Janeiro, Brazil, July 2013 (Abstract).

Percival, J.B., Williamson, M.-C., McNeil, R.J. and Harris, J.R., 2014. Morphology of gossans in the Canadian Arctic Islands; Geological Association of Canada-Mineralogical Association of Canada Annual Meeting, Program With Abstracts v. 37, p. 219. ESS Cont. No. 20130475.

Peterson, R.C., Williamson, M.-C., and Rainbird, R.H., 2014. Gossan Hill, Victoria Island, Northwest Territories: An analogue for mine waste reactions within permafrost and implication for the subsurface of Mars; Earth and Planetary Science Letters, v. 400, p. 88–93 (doi: 10.1016/j.epsl.2014.05.010).

Petruk, W., 2000. Applied Mineralogy in the Mining Industry, 1st ed. Elsevier, The Netherlands, 268 pp.

Rainbird, R.H., Bédard, J.H., Dewing, K., and Hadlari, T., 2014. Geology, Kangiryuaqtihuk/ Minto Inlet, Victoria Island, Northwest Territories; Geological Survey of Canada, Canadian Geoscience Map 82 (preliminary), 1:50 000 (doi:10.4095/293460).

Shvartsev, S.L., 1965. Physicochemical processes in series of permafrost rocks, *in* Cryogenic Processes in Soils and Rocks, Nauka, Moscow, p. 132-140 (in Russian, GSC Translation No. 485).

Shvartsev, S.L., 1970. Certain features of the formation of the chemical composition of groundwater under the conditions of perennially frozen ground; Report of the Scientific and Technical Conference on Hydrogeology and Engineering Geology, v. 3, p. 161-167, Yerevan, USSR (in Russian, GSC Translation No. 2042).

Shilts, W., 1973. Drift prospecting; geochemistry of eskers and till in permanently frozen terrain: District of Keewatin; Northwest Territories; Geological Survey of Canada, Paper 72-45, 34 pp.

Thorsteinsson, R., and Tozer, E.T., 1962. Banks, Victoria and Stefansson Islands, Arctic Archipelago; Geological Survey of Canada Memoir, v. 330, 85 pp.

Williamson, M.-C., Smyth, H.R., Peterson, R.C., and Lavoie, D., 2011. Comparative geological studies of volcanic terrain on Mars: Examples from the Isachsen Formation, Axel Heiberg Island, Canadian High Arctic; Geological Society of America, Special Paper 483, p. 249-261.

Williamson, N., Bédard, J., Ootes, L., Rainbird, R., Cousens, B., and Zagorevski, A., 2013. Volcanostratigraphy and significance of the southern lobe Natkusiak Formation flood basalts, Victoria Island, Northwest Territories; Geological Survey of Canada, Current Research (Online) no. 2013-16, 12 pp., doi:10.4095/292706.

Williamson, M.-C., Percival, J.B., Harris, J., Peterson, R.C., Froome, J., Bédard, J., McNeil, R.J., Day, S.J., Kingsbury, C.G., Grunsky, E., McCurdy, M., Shepherd, J., Hillary, B., and Buller, G., 2014. Environmental and economic impact of oxide-sulphide gossans, Northwest Territories and Nunavut; Geological Survey of Canada, Open File 7486, 10 p. + poster. doi:10.4095/293922

Williamson, M.-C., McNeil, R.J., Day, S.J.A., McCurdy, M.W., Rainbird, R.H., and Grunsky, E.C., 2015. Environmental impact of gossans revealed by orientation surveys for base metals in the Canadian Arctic Islands, *in* Environmental and Economic Significance of Gossans, (ed.) M.-C Williamson; Geological Survey of Canada, Open File 7718, p. 74-84.

ENVIRONMENTAL IMPACT OF GOSSANS REVEALED BY ORIENTATION SURVEYS FOR BASE METALS IN THE CANADIAN ARCTIC ISLANDS

Marie-Claude Williamson, Rick J. McNeil, Stephen J.A. Day, Martin W. McCurdy, Robert H. Rainbird and Eric C. Grunsky
Geological Survey of Canada, 601 Booth Street, Ottawa, Ontario, K1A 0E8

INTRODUCTION

Gossans are found all across Canada's northern landmass in bedrock of widely varying composition and age. The deposits are routinely identified on 1:50,000 scale geological maps published by the Geological Survey of Canada (GSC). Previous studies have shown that some arctic gossans react with permafrost leading to a complex acid rock generation process in which freeze–thaw cycles ensure a continuous degradation of sulphide-rich rocks and expose reactive gossanous soil (Elberling and Langdahl, 1998). These processes were investigated during a 4-year activity funded by the Earth Sciences Sector's Environmental Geoscience Program to determine if reactive gossans constitute analogues of mine waste in permafrost. Field work was carried at sites where gossans interacted with the surrounding permafrost in two areas of the Canadian Arctic Archipelago: Victoria Island, Northwest Territories (2011), and Axel Heiberg Island, Nunavut (2013).

A unique aspect of the project was the geologic context: the targeted gossans were associated with mafic volcanic and intrusive rocks from two Large Igneous Provinces, the Franklin Large Igneous Province (FLIP) exposed in the Minto Inlier of central Victoria Island, and the High Arctic Large Igneous Province (HALIP) exposed in the central Sverdrup Basin, chiefly on Ellef Ringnes Island, Axel Heiberg Island and northern Ellesmere Island (Ernst, 2014). Both the FLIP and the HALIP are prospective for magmatic sulphide deposits (e.g. Bédard et al., 2012; Jowitt et al., 2014). The presence of comparable host rocks and the potential for economic indicators enabled an integrated approach to field work and the use of industry survey data. This portion of the study involved a comparison of stream water pH and geochemical data in areas located in proximity to known gossans. The objective was to determine if reactive gossans in sensitive areas of permafrost have a measurable environmental impact on local stream water and sediments. In this short paper, we report new field protocols to study reactive gossans and a preliminary interpretation of the pH and geochemical data. The supporting databases are available in GSC reports in preparation (see Williamson et al., in prep.). The new data demonstrate the environmental impact of gossans on local streams and highlight the importance of including detailed studies of these deposits in northern geoscience surveys.

ORIENTATION SURVEYS – PART 1

Victoria Island Survey in the FLIP

The Franklin Large Igneous Province comprises sills, dykes and flood basalts emplaced in Neoproterozoic sedimentary rocks exposed in the Minto Inlier, on central Victoria Island (Figure 2; Bédard et al., 2012; Ernst, 2014). Regional geochemical surveys were carried out by Great Northern Mining and Exploration (GNME) and the Geological Survey of Canada (GSC), between 2009 and 2011, to determine the Ni-Cu-PGE and Pb-Zn potential of the area. McCurdy et al. (2013) identified 5 areas of economic interest based on stream silt and water data collected at 121 sites (Figure 3). Areas 4 and 5 displayed elevated concentrations of Zn and Pb in both stream sediments and water. In addition, sphalerite and galena were detected in stream sediment heavy mineral concentrates. The presence of two gossans in Area 4 provided the first opportunity to investigate the potential effects of the deposits on stream water and sediment geochemistry in this region (Williamson et al., 2013a, 2013b).

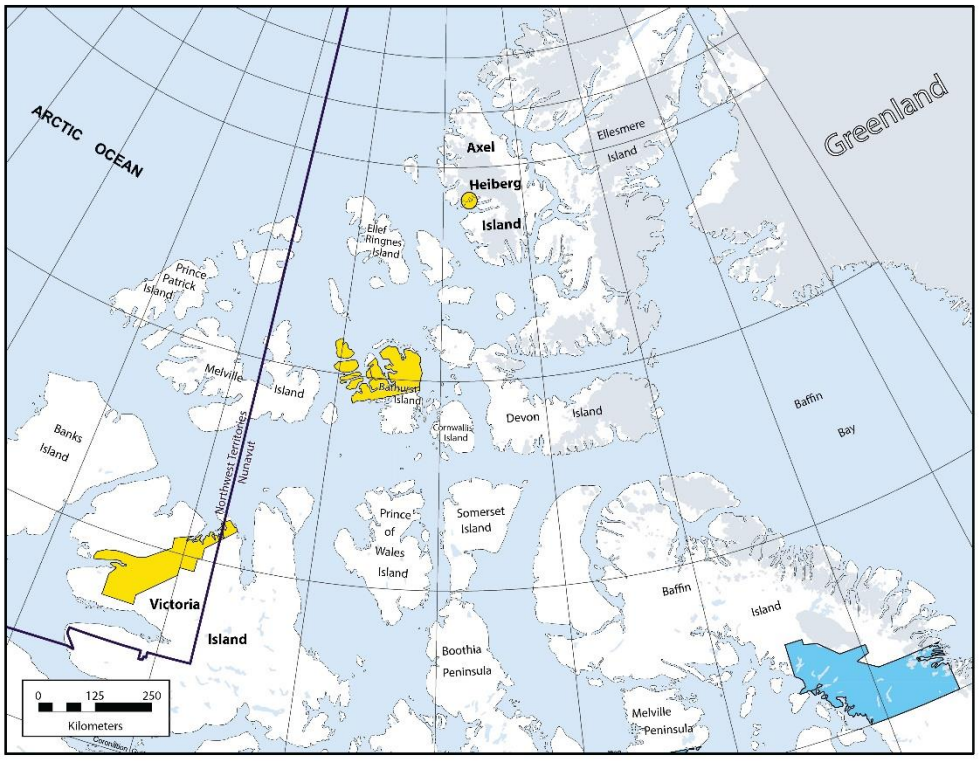

Figure 1. Map showing the current Geological Survey of Canada coverage of drainage geochemical surveys in the Canadian Arctic Archipelago. Stream surveys are shown in yellow and lake surveys are shown in blue. The study areas discussed in this paper include the Minto Inlier, on Victoria Island, NT, and western Axel Heiberg Island, NU.

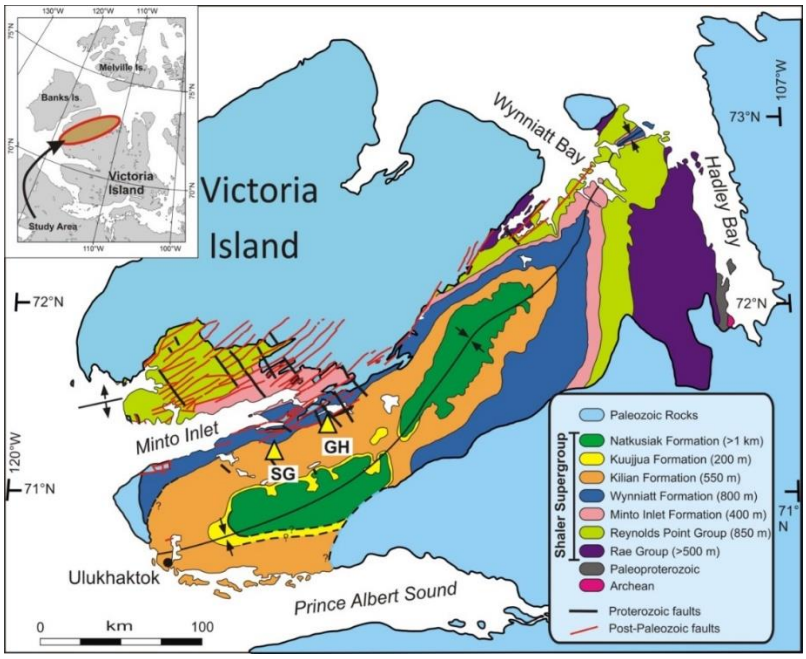

Figure 2. Simplified geological map of the Minto Inlier, central Victoria Island, showing the location of Gossan Hill (GH) and Sill Gossan (SG) in the Minto Inlier (yellow triangles) (after Thorsteinsson and Tozer, 1962; Bédard et al., 2012). Sediment thickness is shown in brackets in the legend.

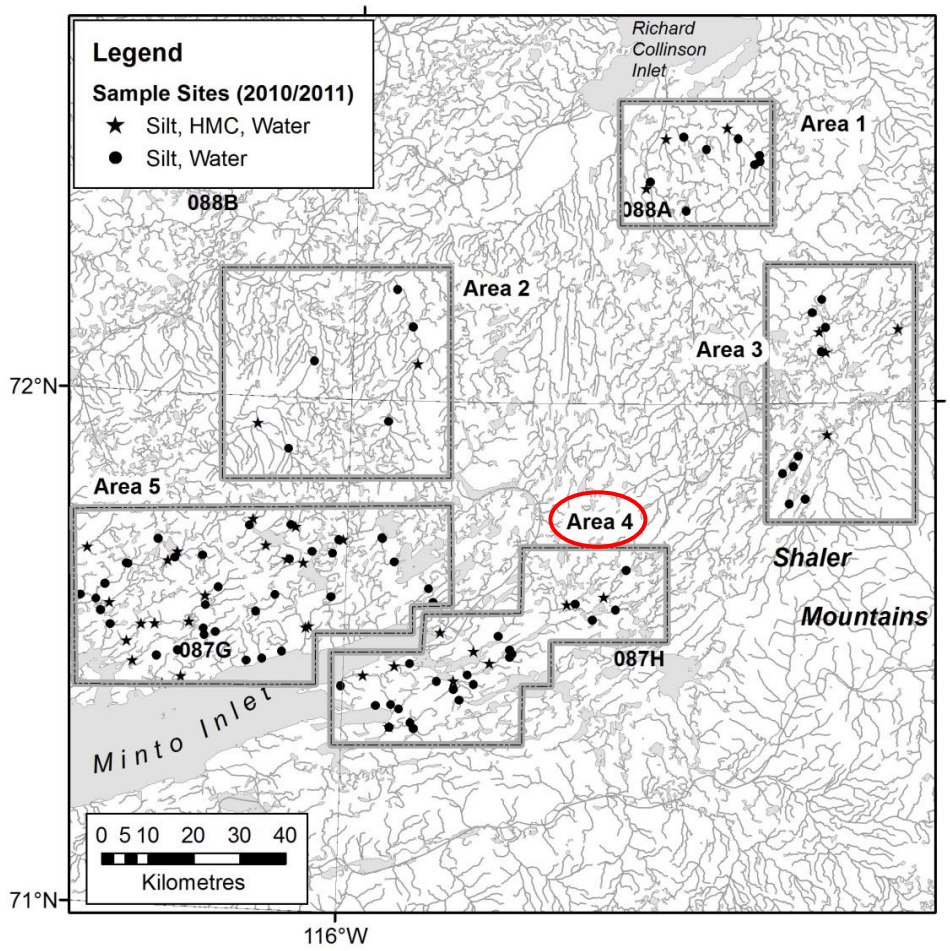

Figure 3. Location of GSC sample sites in Areas 1 to 5 on Victoria Island. The sample sites are grouped according to bedrock geology. The red circle show the area investigated for this study (from McCurdy et al., 2013).

Figures 4-7 show the results of the stream sediments surveys in the vicinity of the two gossans. Figure 4 shows the range of pH values obtained at stations sampled for a 1994 GSC regional geochemical stream survey (Friske et al., 2002). A first order, qualitative interpretation of the data in the vicinity of the Sill Gossan and Gossan Hill reveals pH data in the range 7.6-7.8 but these results are inconclusive. A surface map of pH values was generated using an Esri® ArcMap™ 10.1 Inverse Distance Weighting (IDW) algorithm with inverse distances raised to the power of 2 and a fixed search radius of 4,200 m. The use of the Esri® Kriging algorithm did not significantly alter the pattern of distribution. Figure 5 shows contoured pH values in a subset of stream waters from the 1994 survey of 893 streams. Although not specifically designed to identify point sources of mineralization, the regional geochemical data nevertheless highlight the drainage basins within which the two gossans are located. Water samples from streams adjacent to and downslope of the gossans show relatively low pH values, taking into account the presence of carbonate host rocks. Figures 6 and 7 show IDW concentration maps using the same parameters as the pH map for Fe (%) and S (%) across the study area, respectively. Both Fe and S are relatively high in stream silts sampled from streams adjacent to the westernmost Sill Gossan. Fe concentrations are close to the mean value of 2.59 % (Figure 6). Sulphur concentrations in proximity of Gossan Hill show a subtle but detectable increase (Figure 7). Based on these results, a new scientific hypothesis was generated, to test the environmental impact of gossans on local streams (Williamson et al., 2014).

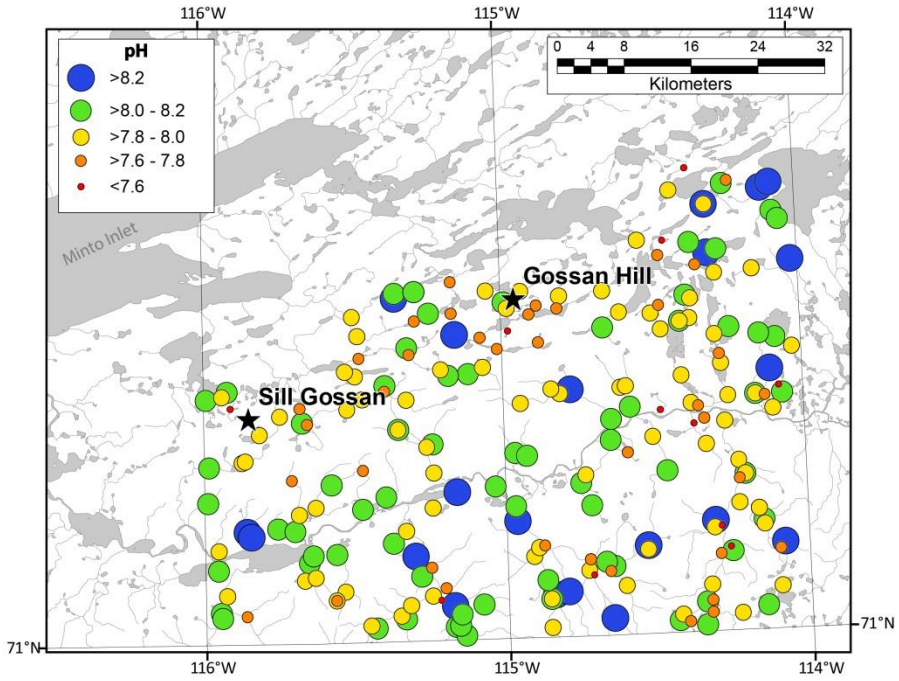

Figure 4. Water pH values measured at GSC stations sampled in Area 4 of McCurdy et al. (2013). Each circle represents a stream sediment and water sampling station from Friske et al. (2002).

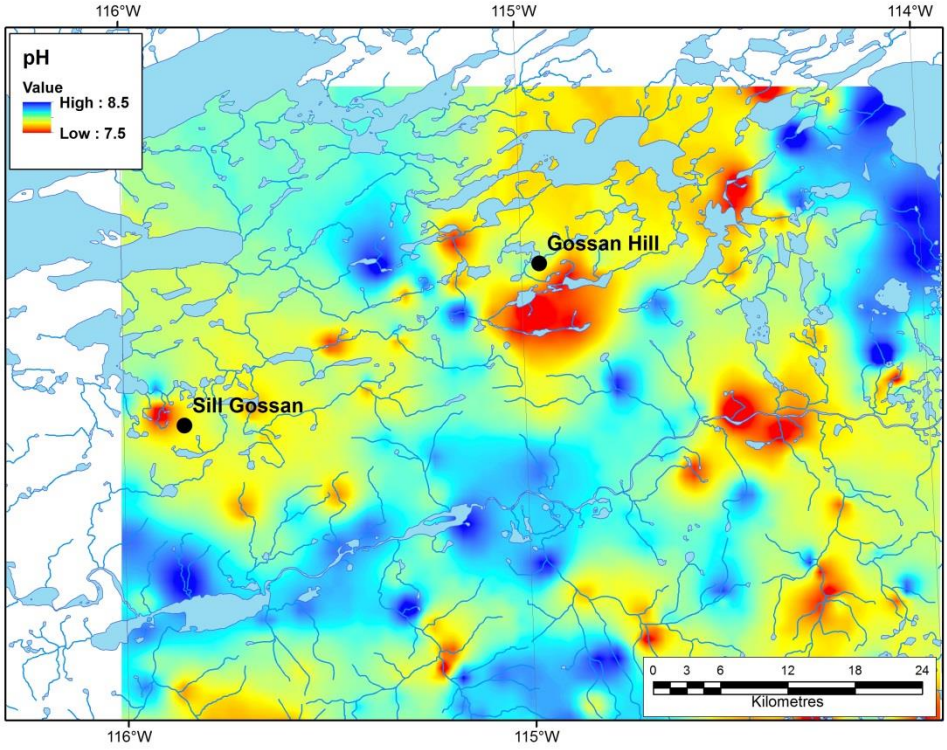

Figure 5. Surface map of pH values in stream waters in the study area generated using an Inverse Distance Weighting algorithm.

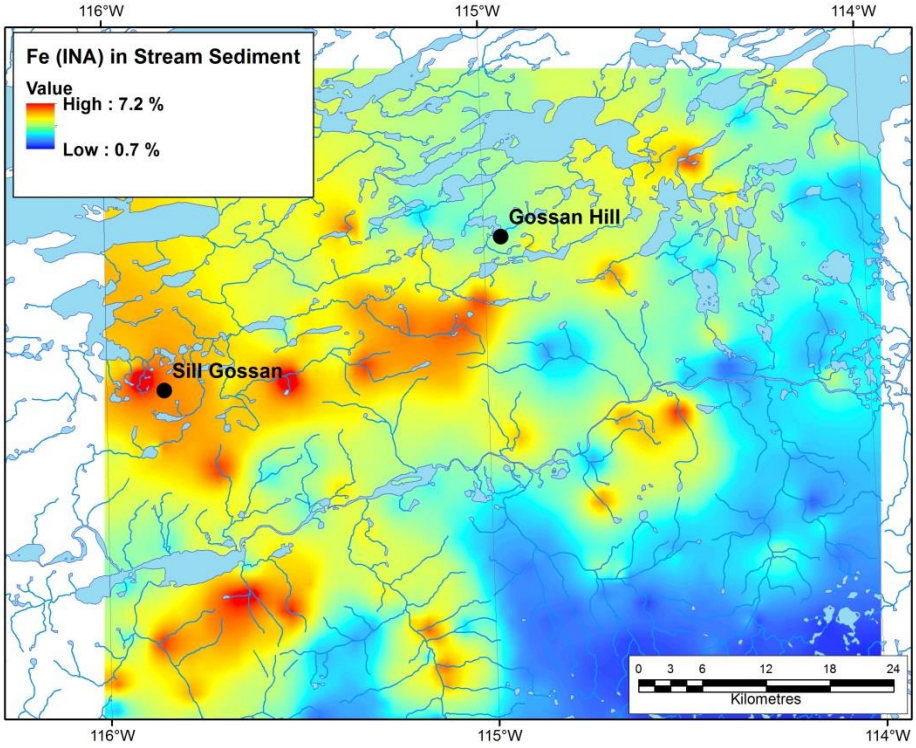

Figure 6. Surface map of Fe values in stream sediments determined by Instrumental Neutron Activation analysis.

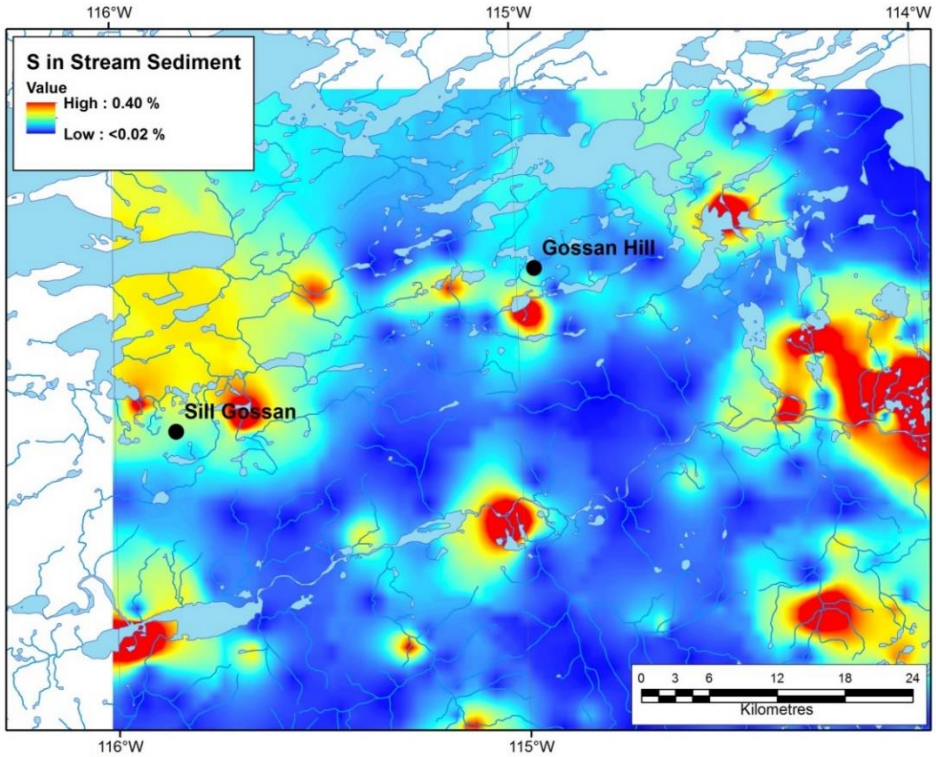

Figure 7. Surface map of S concentrations in stream sediments determined by digestion of the sediments in HCl-HNO3 followed by ICP-ES analysis.

ORIENTATION SURVEYS – PART 2

Axel Heiberg Island Survey in the HALIP

The High Arctic Large Igneous Province (HALIP) consists of volcanic rocks and associated intrusive rocks of Cretaceous age known to occur in the Canadian Arctic Archipelago, Franz Josef Land (Russia), Svalbard (Norway) and the Barents Sea (Ernst, 2014). The HALIP exposed on Axel Heiberg Island shares many attributes of the Franklin LIP, including its association with a sedimentary succession. However, some key differences include (1) the absence of carbonate rocks in the succession exposed on Axel Heiberg Island and (2) the greater number of gossan occurrences on Axel Heiberg Island. Many gossans occur within and/or at the periphery of evaporite diapirs (Williamson et al., 2011; 2014). Others are associated with volcanic and sedimentary rocks of the Isachsen Formation (Kingsbury et al., 2013). These field relationships are particularly evident in the Expedition Fiord area where salt diapirs and canopies modify the regional stratigraphy (Figure 8; Harrison and Jackson, 2014; Percival et al., 2015).

METHODS

The field protocol involves the collection of (1) soil samples, (2) silt and water samples and (3) silt, water and bulk samples along a valley transect that originates at a gossan (Figure 9). Figure 10A illustrates the sampling approach using Locality 7 of Percival et al. (2015) as an example. Once the stratigraphy is exposed, the pH at the top and bottom of the trench is measured *in situ* using a portable Kelway HB2 pH/moisture meter (Figures 10A and 10C). Repeat analyses are performed at GSC laboratories to reduce the errors in pH values caused by rapid soil dessication as the gossan is exposed to ambient conditions and direct sunlight. The pH values of stream waters are measured routinely with a portable YSI Pro Plus instrument that also records values of Eh, conductivity, dissolved oxygen and temperature (Figure 10B). A Hanna Combo pH/Conductivity portable meter is also used for first order assessments during traverses. The reader is referred to McNeil et al. (2015) for a detailed description of the GSC stream sediment and water survey protocols.

DISCUSSION

The sampling locations for gossans, bedrock and stream sediments are illustrated in Figure 11. The larger number of gossans available for study (8 stations vs. 2 on central Victoria Island) enabled a robust field test of the protocols illustrated in Figure 10. In addition, the integrated approach involving mineralogical and geochemical studies of bedrock, gossans and local streams allows a thorough investigation of the environmental and economic impact of gossans in this region of Nunavut (Williamson et al., 2014). Figure 12 illustrates the range of pH values measured in stream waters in the study area. The most obvious feature of the data is the buffering effect of evaporitic diapirs. As the measured conductivity values in stream waters increase from west to east in the study area, so do measured values of the pH (McNeil et al., in prep.). A second, important feature of the pH data is associated with gossans sampled further away from evaporitic diapirs. Remarkably, the lowest pH values (6.8-7.0, Figure 12) are from streams located in proximity to gossans exposed on ridges capped by mafic igneous rocks in an area of prominent faulting (Localities 6 and 7; Percival et al., 2015).

A preliminary comparison of results for both the Victoria Island and Axel Heiberg Island study areas suggest that some types of acid-generating gossans influence the pH of stream waters. In addition, the location of Gossan Hill and Sill Gossan in one of the economic prospectivity corridors of McCurdy et al. (2013) is considered to be significant and worthy of further investigation. Anomalously high abundances of sulphide minerals in the South Fiord study area of Axel Heiberg Island suggest that this region also constitutes a "prospectivity corridor" (McNeil et al., 2015). A detailed comparative study of Gossan Hill, Sill Gossan (Victoria Island) and Localities 6 and 7 (Axel Heiberg Island; Percival et al., this study) is underway to clarify the possible links between environmental impact of reactive gossans in permafrost and economic prospectivity

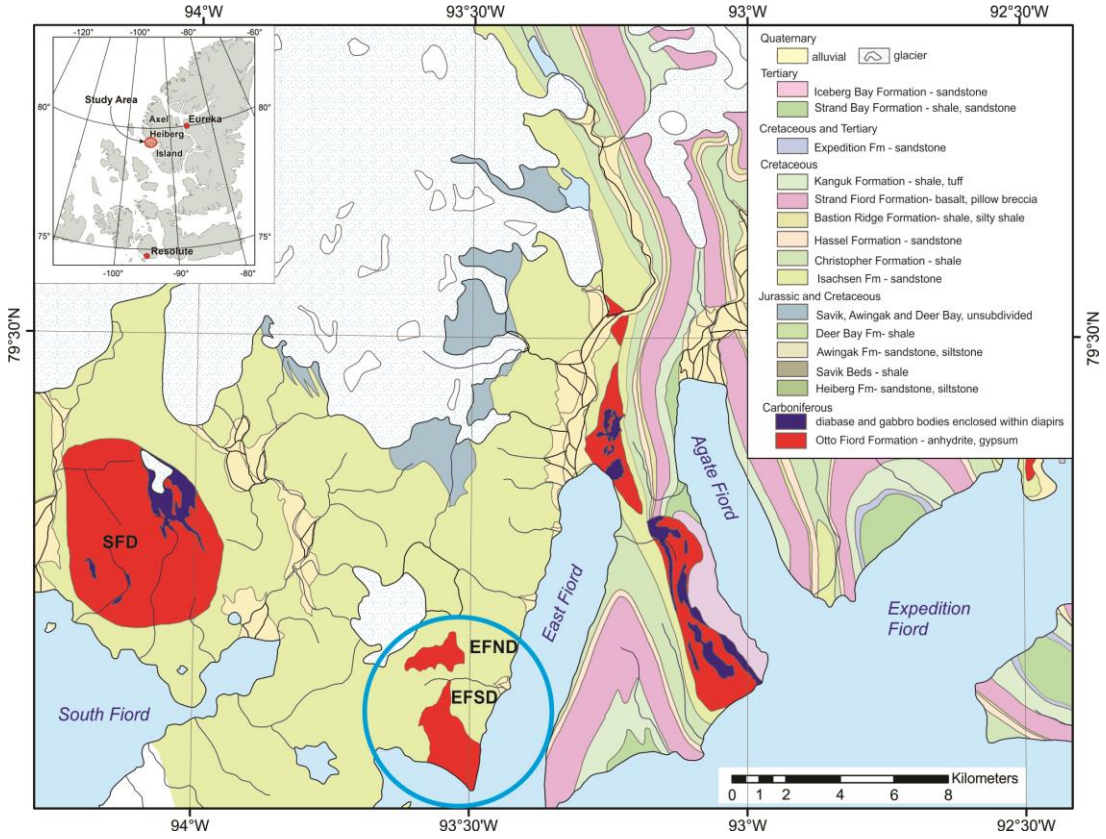

Figure 8: Simplified geological map of the Strand Fiord-Expedition Fiord area, Axel Heiberg Island (Harrison and Jackson, 2010). The 2013 study area is shown by the blue circle.

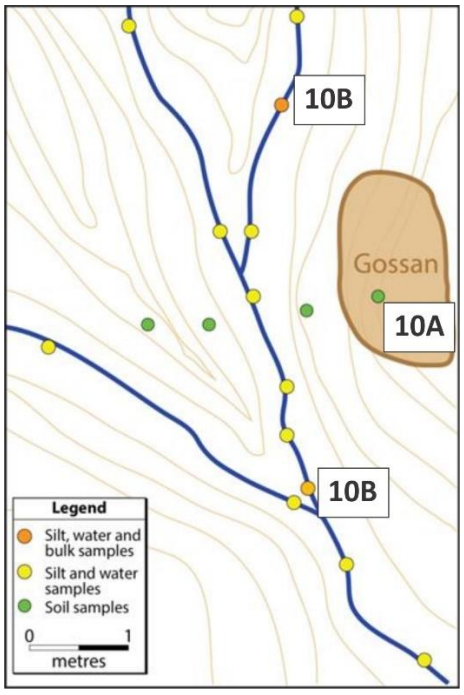

Figure 9. Idealized sampling plan of a detailed drainage study to identify the areal extent of the geochemical and mineralogical signature and dispersion down drainage of a known gossan. Labels are keyed to Figure 10.

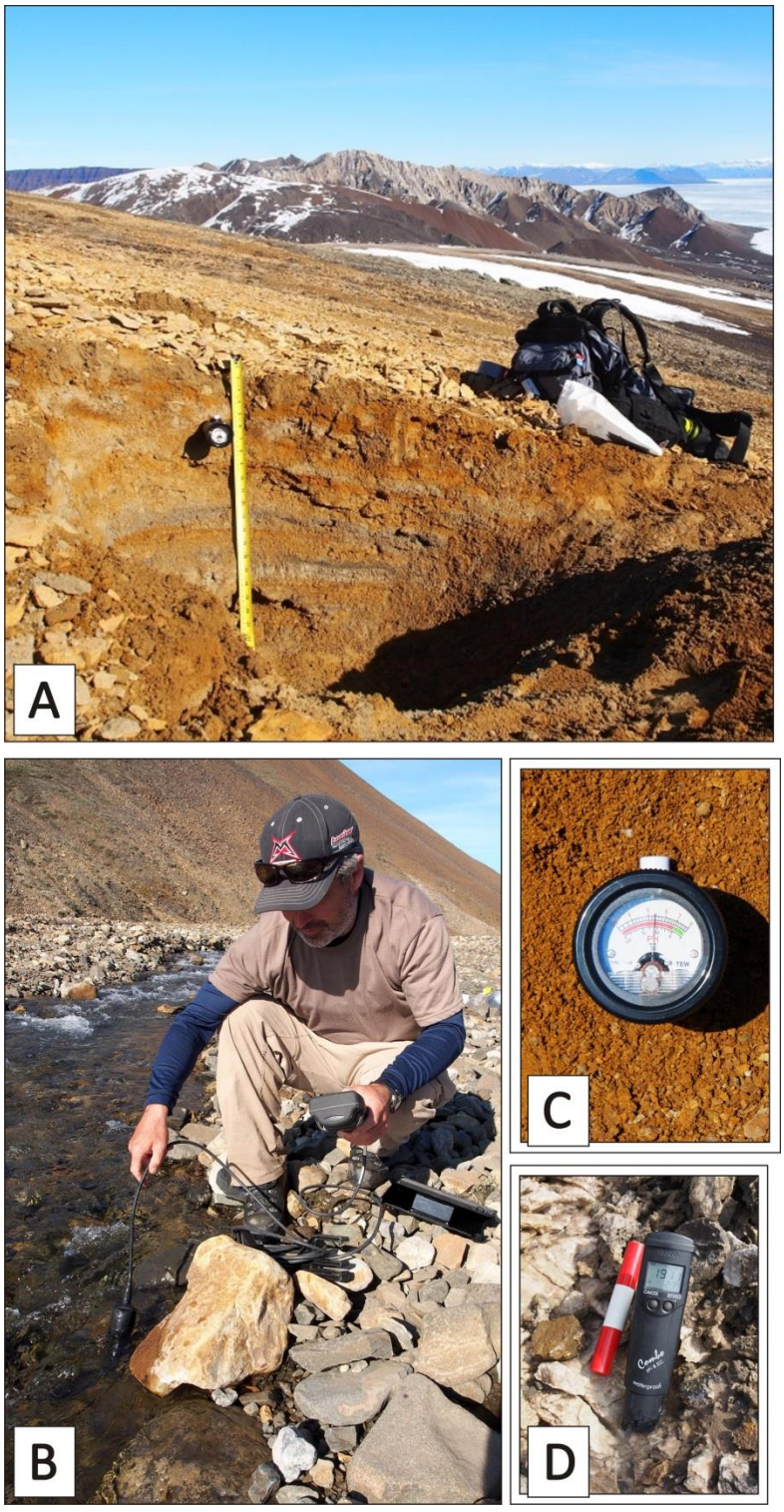

Figure 10. Field measurements of pH in gossans and stream waters (keyed to symbols in Fig. 9). (A) Field shot of a finely layered gossan sampled for mineralogy and geochemistry. Soil acidity is measured *in situ* using a portable Kelway HB2 pH/moisture meter (next to yellow tape). (B) The pH values of stream waters are routinely measured with a portable YSI Pro Plus instrument that also records values of Eh, conductivity, dissolved oxygen and temperature. (C) Close up of the Kelway HB2 pH/moisture meter in gossanous soil. (D) Rapid assessment of water temperature and pH during traverses was carried out using a Hanna Combo pH/Conductivity portable meter.

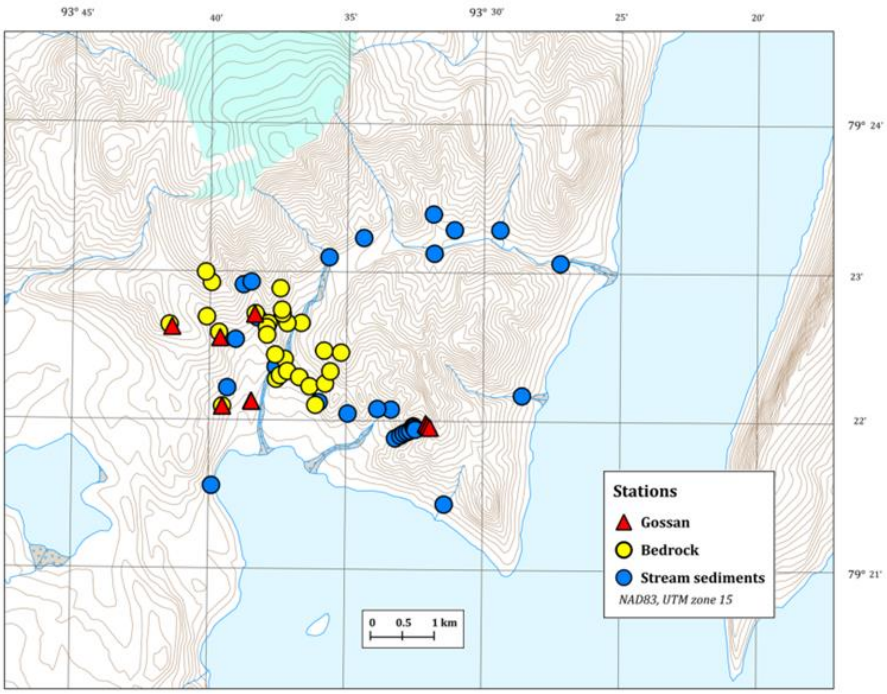

Figure 11. Topographic map of the 2013 study area showing the sampling stations for bedrock, gossans, and stream sediments.

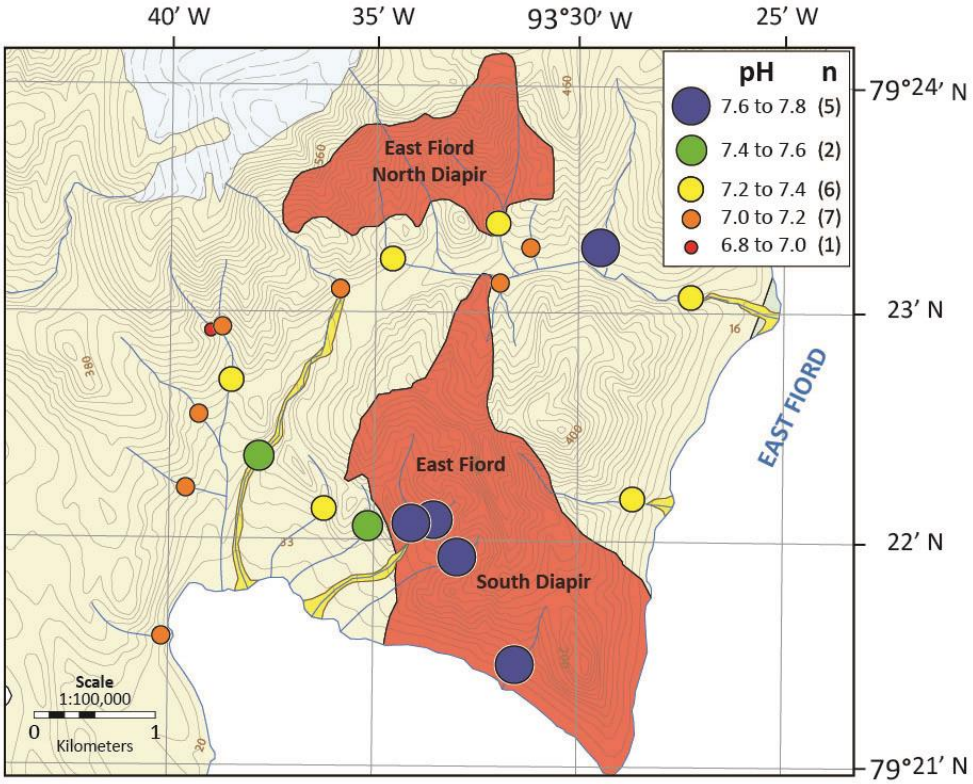

Figure 12. Topographic map of the 2013 study area showing pH values where stream waters were analysed. The East Fiord South and East Fiord North diapirs buffer stream water pH values as explained in the text.

CONCLUSIONS

This study, and the supporting geochemical data reported by McCurdy et al. (2013) and McNeil et al. (2015) for Victoria Island and Axel Heiberg Island, Canadian High Arctic, suggest that acid-generating gossans with reactive zones in permafrost influence the pH of stream waters on a local scale. The investigation led to several important observations and results:

(1) Reconnaissance geochemical databases resulting from mineral exploration and government-led surveys can be successfully merged for analysis and interpretation (Figures 4-7).

(2) The idealized sampling plan of a detailed drainage study in proximity to a known gossan (Figure 9) constitutes a valid, tested protocol for future studies of reactive oxide-sulphide gossans (Figure 10).

(3) Field studies that integrate bedrock mapping, sampling of gossans and stream sediment surveys on a local and regional scale offer the best range of data to evaluate the environmental impact of reactive gossans (Figures 11 and 12).

(4) The attributes of gossanous soils and sediments, nature of host rocks and structural setting are key features that determine both environmental impact and economic prospectivity.

(5) The results confirm the need for additional regional stream water and sediment geochemical surveys in Canada's North (Figure 1).

Overall, the new data unequivocally demonstrate the environmental impact of gossans and highlight the importance of including detailed studies of these deposits in northern geoscience surveys.

ACKNOWLEDGEMENTS

The Arctic Gossans activity was funded by the Environmental Geoscience Program of the Earth Sciences Sector, Geological Survey of Canada, Department of Natural Resources. Field work was carried out with aircraft and logistics support from the Polar Continental Shelf Program, in collaboration with the Geo-mapping for Energy and Minerals Program (GEM-Victoria Island Project, 2011) and the HALIP Research Group, Department of Earth Sciences, Carleton University (2013). The first author wishes to thank Jeff Harris, Jeanne Percival, Ron Peterson, Jean Bédard, Cole Kingsbury, Richard Ernst, Guy Buller, Jeffrey Shepherd and Beth Hillary for sharing their expertise during the course of the project. Comments by Guest Reviewers Helen Smyth and Benoit Saumur improved an earlier version of the manuscript.
ESS Contribution no. 20130459.

REFERENCES

Bédard, J.H., Naslund, H.R., Nabelek, P., Winpenny, A.,Hryciuk, M., Macdonald, W., Hayes, B., Steigerwaldt, K., Hadlari, T., Rainbird, R., Dewing, K., and Girard, E., 2012. Fault-mediated melt ascent in a Neoproterozoic continental flood basalt province, the Franklin sills, Victoria Island, Canada; Geological Society of America Bulletin, v. 124, p. 723–736. doi: 10.1130 /B30450.1

Elberling, B., and Langdahl, B.R. 1998. Natural heavy-metal release by sulphide oxidation in the High Arctic; Canadian Geotechnical Journal., v. 35, p. 895–901.

Embry, A., 2011. Chapter 36: Petroleum prospectivity of the Triassic–Jurassic succession of Sverdrup Basin, Canadian Arctic Archipelago; Geological Society of London, Memoirs, v. 35, p. 545-558. doi:10.1144/M35.36

Ernst, R. E., 2014. Large Igneous Provinces; Cambridge University Press, 653 p.

Friske, P.W.B., Day, S.J.A., McCurdy, M.W., 2002. Regional stream sediment and water geochemical data, Victoria Island, Northwest Territories and Nunavut; Geological Survey of Canada, Open File 4290; 1 CD-ROM. doi:10.4095/213483

Harris, J.R., Williamson, M.-C., Percival, J.B., Behnia, P., and MacLeod, R.F., 2015. Detecting and mapping gossans using remotely-sensed data, *in* Environmental and Economic Significance of Gossans, (ed.) Williamson, M.-C.; Geological Survey of Canada, Open File 7718, p. 3-13.

Harrison, J.C. and Jackson, M.P.A, 2011. Bedrock geology, Strand Fiord-Expedition Fiord, western Axel Heiberg Island, northern Nunavut (parts of NTS 59E, F, G, and H); Geological Survey of Canada, Map 2157A, 2 sheets, scale 1:125 000.

Harrison, J.C., and Jackson, M.P.A, 2014. Tectonostratigraphy and allochtonous salt tectonics of Axel Heiberg Island, central Sverdrup Basin, Arctic Canada; Geological Survey of Canada, Bulletin 607, 124 p.

Hulbert, L.J., Rainbird, R.H., Jefferson, C.W. and Friske, P., 2005. Map of mafic and ultramafic bodies related to the Franklin Magmatic Event, Minto Inlier, Victoria Island, NWT; Geological Survey of Canada, Open File 4928, scale 1:500 000.

Jowitt, S.M., Williamson, M.-C., and Ernst, R.E., 2014. Geochemistry of the 130 to 80 Ma Canadian High Arctic Large Igneous Province (HALIP) event and implications for Ni-Cu-PGE prospectivity; Economic Geology, v. 109, no. 2, p. 281-307. doi:10.2113/econgeo.109.2.281

Kingsbury, C.G., Williamson, M.-C., Day, S.J.A, and McNeil, R.J., 2013. The 2013 Isachsen Expedition to Axel Heiberg Island, Nunavut, Canada: A field report; Geological Survey of Canada, Open File 7539, 6 p. + poster. doi:10.4095/293842

McCurdy, M.W., Rainbird, R.H., and McNeil, R.J., 2013. Exploring for Lead and Zinc using indicator minerals with stream silt and water geochemistry in the Canadian Arctic Islands: An example from Victoria Island, Northwest Territories, *in* New Frontiers for Exploration in Glaciated Terrain, (eds.) R.C. Paulen and M.B. McClenaghan; Geological Survey of Canada, Open File 7374, p. 65-74.

McNeil, R.J., Day, S.J.A., and Williamson, M.-C., 2015. Stream sediment and water geochemical study, Axel Heiberg Island, Nunavut, Canada, *in* Environmental and Economic Significance of Gossans, (ed.) M.-C. Williamson; Geological Survey of Canada, Open File 7718, p. 85-96.

McNeil, R.J., Day, S.J.A, and Williamson, M.-C., in prep. Geochemical, mineralogical and indicator mineral data for stream silt sediment, heavy mineral concentrates and water, South Fiord area, Axel Heiberg Island, Nunavut (part of NTS 59G); Geological Survey of Canada, Open File 7779.

Percival, J.B., Williamson, M.-C., McNeil, R.J., and Harris, J.R., 2015. Morphology of gossans in the Canadian Arctic Islands, *in* Environmental and Economic Significance of Gossans, (ed.) M.-C. Williamson; Geological Survey of Canada, Open File 7718, p. 58-73.

Peterson, R.C., Williamson, M.-C., and Rainbird, R.H., 2014. Gossan Hill, Victoria Island, Northwest Territories: An analogue for mine waste reactions within permafrost and implication for the subsurface of Mars; Earth and Planetary Science Letters, v. 400, p. 88–93.

Thorsteinsson, R., and Tozer, E.T., 1962. Banks, Victoria and Stefansson Islands, Arctic Archipelago; Geological Survey of Canada, Memoir, v. 330, 85 p.

Williamson, M.-C., Percival, J.B., Harris, J., Peterson, R.C., Froome, J., Bédard, J., McNeil, R.J., Day, S.J., Kingsbury, C.G., Grunsky, E., McCurdy, M., Shepherd, J., Hillary, B., and Buller, G., 2014. Environmental and economic impact of oxide-sulphide gossans, Northwest Territories and Nunavut; Geological Survey of Canada, Open File 7486, 10 p. + poster. doi:10.4095/293922

Williamson, M.-C., Smyth, H.R., Peterson, R.C., Lavoie, D., 2011. Comparative geological studies of volcanic terrain on Mars: Examples from the Isachsen Formation, Axel Heiberg Island, Canadian High Arctic; *In* Garry, W.B., and Bleacher, J.E. (eds.), Analogs for Planetary Exploration; Geological Society of America, Special Paper 483, p. 249-261. doi 10.1130/2011.2483(16)

Williamson, M.-C., 2013a. Arctic Gossans Activity Science Definition Team Meeting – Part 1 (powerpoint).

Williamson, M.-C., 2013b. Arctic Gossans Activity Science Definition Team Meeting – Part 2 (powerpoint).

Williamson, M.-C., Percival, J.B., Rainbird, R.H., and Bédard, J.H., in prep. Mineralogical and geochemical data for reactive gossans in permafrost, Victoria Island, Northwest Territories; Geological Survey of Canada, Open File 7798.

Williamson, M.-C., Percival, J.B., McNeil, R.J., and Day, S.J.A., in prep. Mineralogical and geochemical data for reactive gossans in permafrost, Axel Heiberg, Nunavut; Geological Survey of Canada, Open File 7797.

STREAM SEDIMENT AND WATER GEOCHEMICAL STUDY, AXEL HEIBERG ISLAND, NUNAVUT, CANADA

Rick J. McNeil, Stephen J.A. Day and Marie-Claude Williamson
Geological Survey of Canada, 601 Booth Street, Ottawa, Ontario, K1A 0E8
(email: Rick.McNeil@nrcan.gc.ca)

INTRODUCTION

In July 2013, a pilot reconnaissance drainage study was carried out in the South Fiord area of western Axel Heiberg Island, in the Canadian Arctic Archipelago (Figure 1). The survey was part of a three-year study focused on the environmental impact of reactive gossans in permafrost (Kingsbury et al., 2013; Williamson et al., 2015). This portion of the project had two objectives: (1) to identify a geochemical signature related to the presence of gossans in the downstream environment and (2) to evaluate the economic potential of the area.

For the surveys, 21 sites were sampled for waters, stream silts and bulk sediments for heavy mineral concentrates (HMC) (Figure 2). Although limited in scope, the pilot study yielded the first stream sediment data for the northernmost part of Nunavut. Preliminary results suggest that the study area is prospective, potentially for Ni-Cu PGE mineralization and also for other types of economic deposits. Sediment and water geochemical data and mineralogical data for this reconnaissance study are presented in McNeil et al. (in press).

LOCAL GEOLOGY

Western Axel Heiberg Island is located within the Sverdrup Basin and is host to a dense cluster of evaporite diapirs in the Expedition and Strand Fiords area (Harrison and Jackson, 2014). Evaporite structures originating from the Mississippian to Middle Pennsylvanian Otto Fiord Formation are composed primarily of anhydrite and gypsum. They intrude the entire stratigraphic section occurring in the area, which consists of, from oldest to youngest, the Lower Cretaceous Isachsen Formation sedimentary-volcanic succession, Upper Cretaceous Strand Fiord Formation basalt, and some minor exposures of the Aptian-Albian Christopher Formation shales (Davies and Nassichuk, 1991; Figure 1). The diapirs (Figure 3) host many gossans believed to be formed by fluids circulating through local conduits in brecciated basaltic rafts within the diapirs, thereby resulting in the precipitation of sulphide mounds (Percival et al., 2015).

SAMPLING METHODS

Figure 4 illustrates the sampling equipment and protocols. A total of 21 sites were sampled where four sites have water only, seven sites have water and silt and ten sites have water, silt and a HMC sample (Figure 2). A set of three water samples, filtered-acidified (FA), unfiltered-acidified (UA) and filtered-unacidified (FU) were collected from the actively flowing part of the stream where the FA and FU are filtered on-site (Figure 4A). The FA and UA are preserved by acidifying with nitric acid. Stream sediment samples of silt and/or fine grained clastic material from the stream channel (Figure 4B) were collected by hand from several points in the active channel while moving upstream, typically over a distance of 5 to 15 m. Bulk stream sediment samples were collected for their heavy mineral content from high-energy environments such as the head of active gravel bars. Roughly 12–15 kg of $\leq$ 2mm stream sediment was wet-sieved on site (Figure 4C). Figure 4D shows the equipment used and the collected samples at each site.

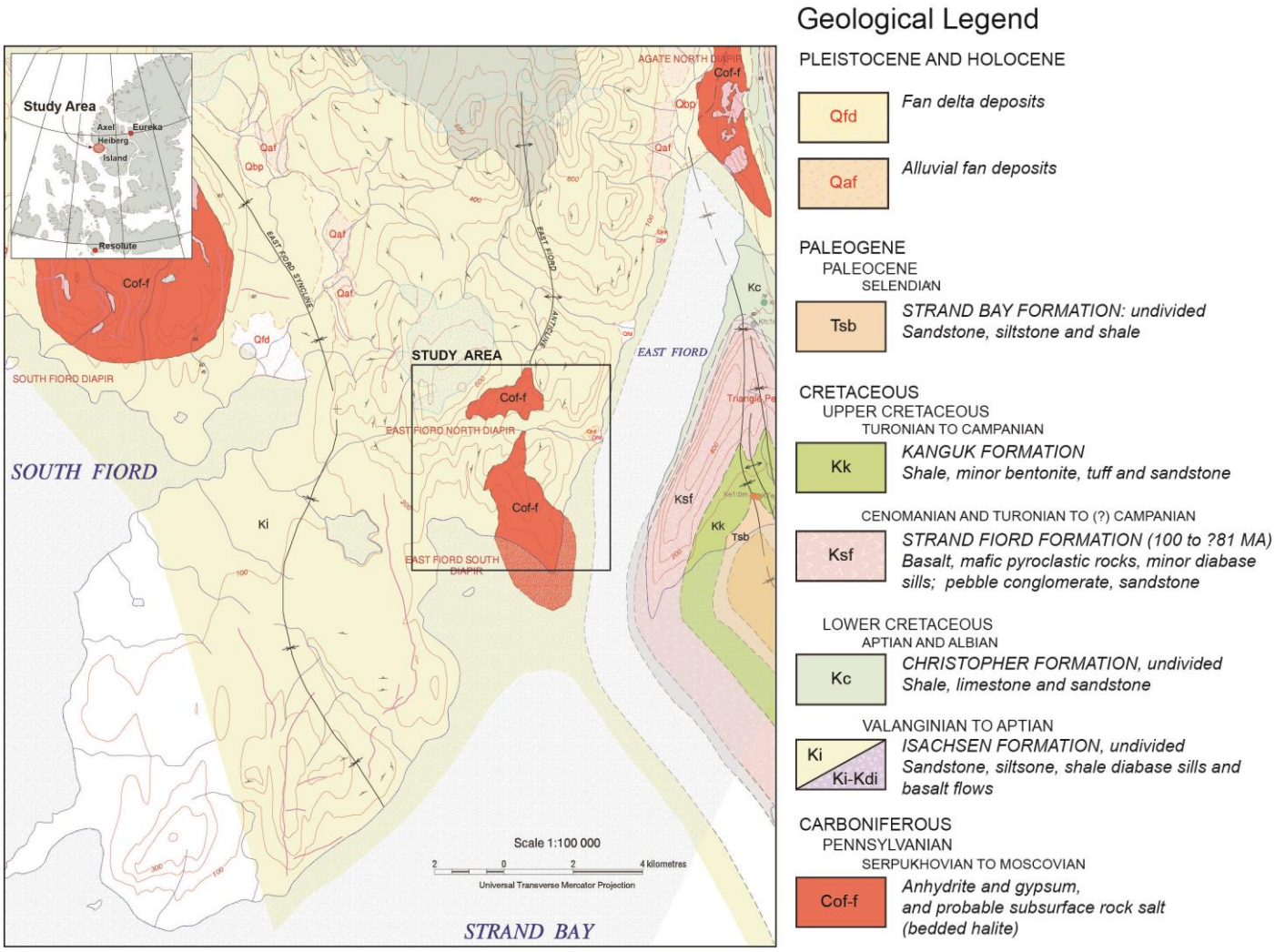

Figure 1. Bedrock geology of the northwestern shore of Expedition Fiord area modified from Harrison and Jackson (2011). The map shows the probable offshore extension of lithological units in the eastern part of the study area, including salt domes.

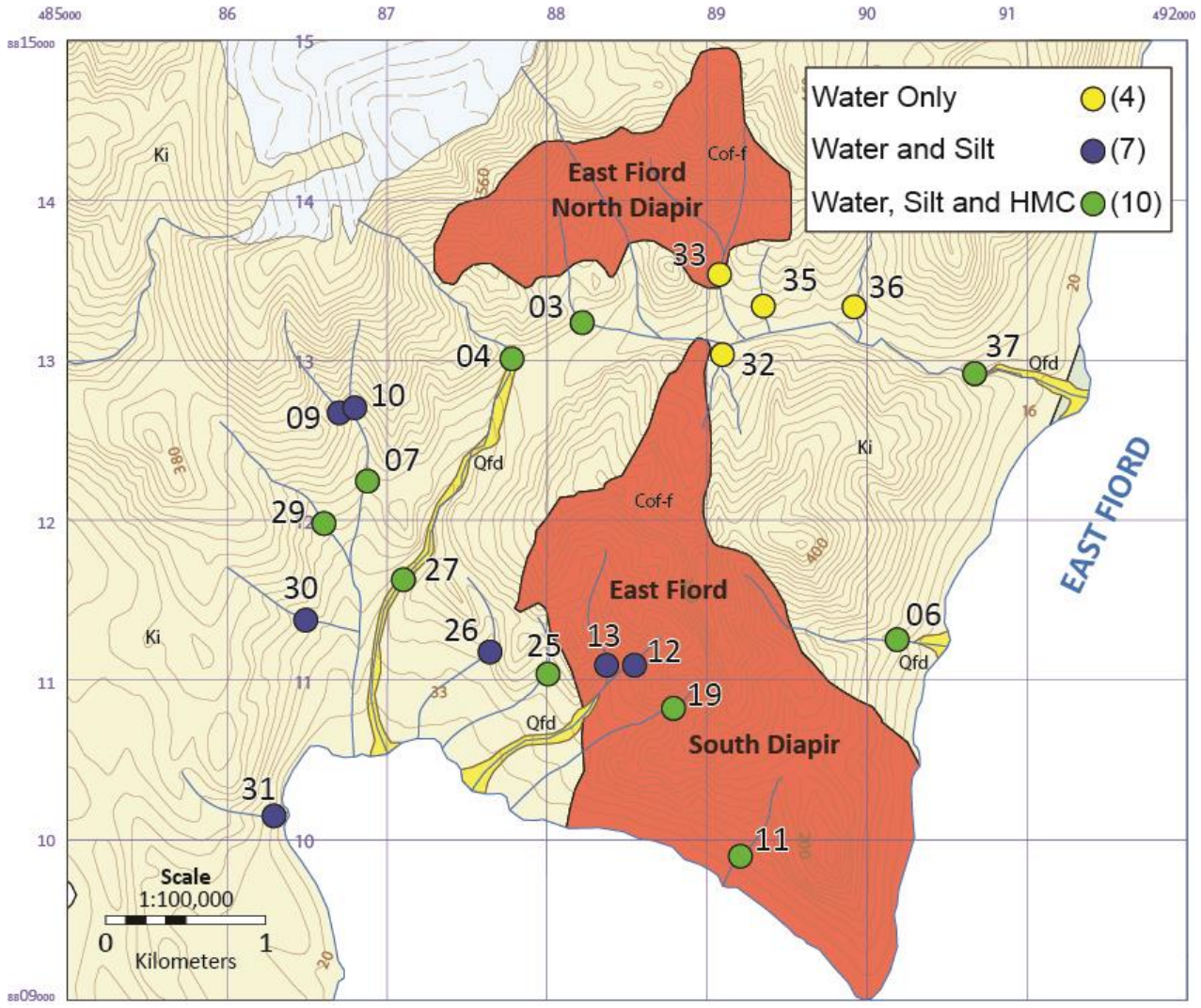

Figure 2: Location of stream sediment and water survey sites keyed to the sample types analysed.

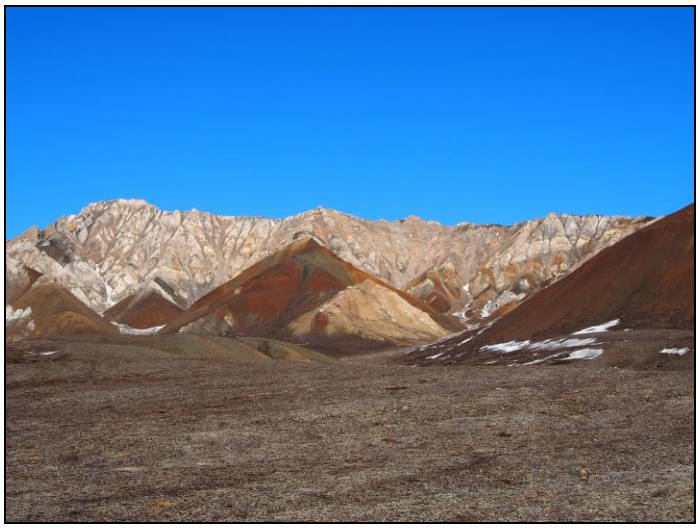

Figure 3. View of East Fiord South diapir looking NNE towards site 19. Photo taken at sea level with a field of view of approximately 2 km. Elevation of the salt diapir is 380 metres above sea level.

Figure 4. Sampling equipment and protocols: (A) Filtering water sample with 0.45 µm filter into 60 ml HDPE bottle. (B) Approximately 2 kg of wet silt and clay is collected from lower energy part of streams into a spun-bonded polyester cloth bag. (C) Approximately 12-15 kg bulk sediment for heavy minerals is collected by wet-sieving with a 2 mm mesh sieve in higher energy part of streams into large plastic bags. (D) Field equipment used and samples collected at a typical stream site.

Figure 5: Iron oxide precipitate on stream bed at site 35, formed from ground water seep through shale. The field of view is approximately 4 metres.

ANALYTICAL METHODS

Water samples were analyzed at the Inorganic Geochemistry Research Laboratory, Geological Survey of Canada, Ottawa. Analysis was performed on the FA and UA samples by ICP-MS for trace-elements and ICP-ES for the relatively soluble elements. FU samples were analyzed for alkalinity by titration, dissolved organic carbon by combustion and anions by titration. Physico-chemical water measurements for temperature, pH, conductivity, dissolved oxygen and Eh were recorded in-situ at each site. Sediment samples from the <177 μm fraction were analysed at ACME Analytical Laboratories in Vancouver by the complementary techniques of ICP-MS and ICP-ES; the latter being used for the more abundant major elements (e.g. Ca, Mg, Na, K and Fe) whereas the more sensitive ICP-MS technique was used for trace element determinations. Two different digestion procedures were used prior to analysis: (1) ICP-MS/ES (modified aqua-regia dissolution - "partial") using a 0.25 gram split; and (2) ICP-MS/ES (4-acid dissolution - "near

total") using a 0.5 gram split. Carbon and loss-on-ignition (LOI) were determined at the Sedimentology Laboratory, Geological Survey of Canada, Ottawa, following analytical methods described in Girard et al. (2004).

Bulk sediment samples were processed at Overburden Drilling Management Limited, Ottawa. The 12 to 15 kg bulk samples are processed through a riffle table and a methylene iodide heavy liquid with a specific gravity of 3.2 in order to recover gold grains, isolate the magnetic fraction and separate the four non-magnetic size fractions. The non-magnetic fractions are used for mineralogical identification of magmatic massive sulphide indicator minerals (MMSIM), kimberlite indicator minerals (KIM) and also for a representative 100 mineral grain count. Heavy mineral concentrate methods are described in Falck et al. (2014).

RESULTS

Stream water geochemical survey

Overall, the water geochemistry shows low values with little variation at the sampled sites. The low values probably result from the dilution of waters in short-lived streams during the spring thaw runoff as well as from the shortage of groundwater due to the presence of continuous permafrost. Therefore, subtle variations in water geochemistry are considered to be significant. Water pH values are neutral to slightly alkaline, ranging from 6.97 to 7.77 (McNeil et al., in press) and are probably strongly influenced by the presence of dissolved gypsum and anhydrite. However, subtle elemental variations in water chemistry does allow for the differentiation and identification of the local bedrock geology. The water data highlights the differences between evaporitic diapirs and the basalt, sandstone and shale units mapped as undivided Isachsen Formation (Harrison and Jackson, 2011).

Streams that are adjacent to the evaporite domes are geochemically distinct due to elevated salt concentrations (Na, K, Cl, F, Ca and SO_4), leading to high values of specific conductance (643-1950 µS/cm). Boron, Sr, Th and Li concentrations are also elevated in stream waters draining from the domes. Uranium concentrations ranging from 2.1 to 3.8 ppb (McNeil et al., in press) are comparable to those reported by Jonasson and Dunsmore (1979) based on stream sampling in the vicinity of evaporite domes on Ellef Ringnes Island.

Surrounding the domes, the Strand Fiord basalt and the Isachsen Formation (Figure 1) dominate. Regional water samples collected on the periphery of the domes are characterized by moderately elevated base metal concentrations (Co, Cu, Ni and Zn). Remarkably, site 35 located south of East Fiord North Diapir revealed the presence of a groundwater seep that surfaced through shale (Figure 5). Results for this site show highly anomalous base metal and rare earth element concentrations (McNeil et al., in press) but a direct source was not discovered.

Stream sediment geochemical survey

Stream silt sediment data show a similar geochemical pattern to that of the water data, with the highest metal concentrations located at the periphery of the diapirs. The variations between sites are less distinct than in water. The sediments collected at site 35 also show anomalous values in base metal and rare earth element concentrations.

Heavy mineral concentrates

Bulk sampling for HMCs in streams is a proven method to evaluate mineral potential of an area. Heavy mineral concentrates are typically composed of key indicator minerals that indicate the presence of a specific type of mineralization, alteration or lithology (McClenaghan, 2005). The survey revealed that sulphides such as chalcopyrite, sphalerite and galena are present at all sites and are highest at sites near the perimeter of the East Fiord South and North diapirs, Chalcopyrite grain counts range from 29 grains at site 04 to 452 and 553 grains at sites 06 and 11, respectively. Sphalerite grains are present at all sites ranging from 4 grains at sites 07 and 11 to 565 grains at site 06. Galena was

recovered at most sites ranging from 1 grain to 40 grains at site 06.

Figure 6 shows a selection of indicator minerals recovered from the heavy mineral concentrates. Preserved crystal faces indicate that grains are weakly physically eroded, suggesting that they have been transported only short distances from their source, and have not been subjected to long-term oxidation.

Minerals such as cinnabar, red rutile, pyrite and barite show a strong spatial link to the presence of the diapirs. Clinopyroxene and ilmenite reflect the presence of the mafic Strand Fiord basalts, which are mostly present west of the study area. In those samples, clinopyroxene ranges from 62 to 83% of the HMC sample composition. Ilmenite follows a similar distribution ranging from 4% to 19% of the HMC fraction in sample 07.

Figure 7 is a histogram that compares the chalcopyrite grain counts obtained during this study with those from stream sediment surveys carried out in the Mackenzie Mountains, Northwest Territories (Falck et al., 2012). In both cases, voluminous mafic igneous rocks intrude predominantly clastic sedimentary successions in a remnant large igneous province: the HALIP (e.g., Jowitt et al., 2014) and Gunbarrel LIP (e.g., Sandeman et al., 2014). The data sets are normalized to 100 grams of non-magnetic heavy minerals. The number of chalcopyrite grains recovered during our study is remarkably high, ranking above the 98th percentile with respect to the 189 Mackenzie Mountains samples.

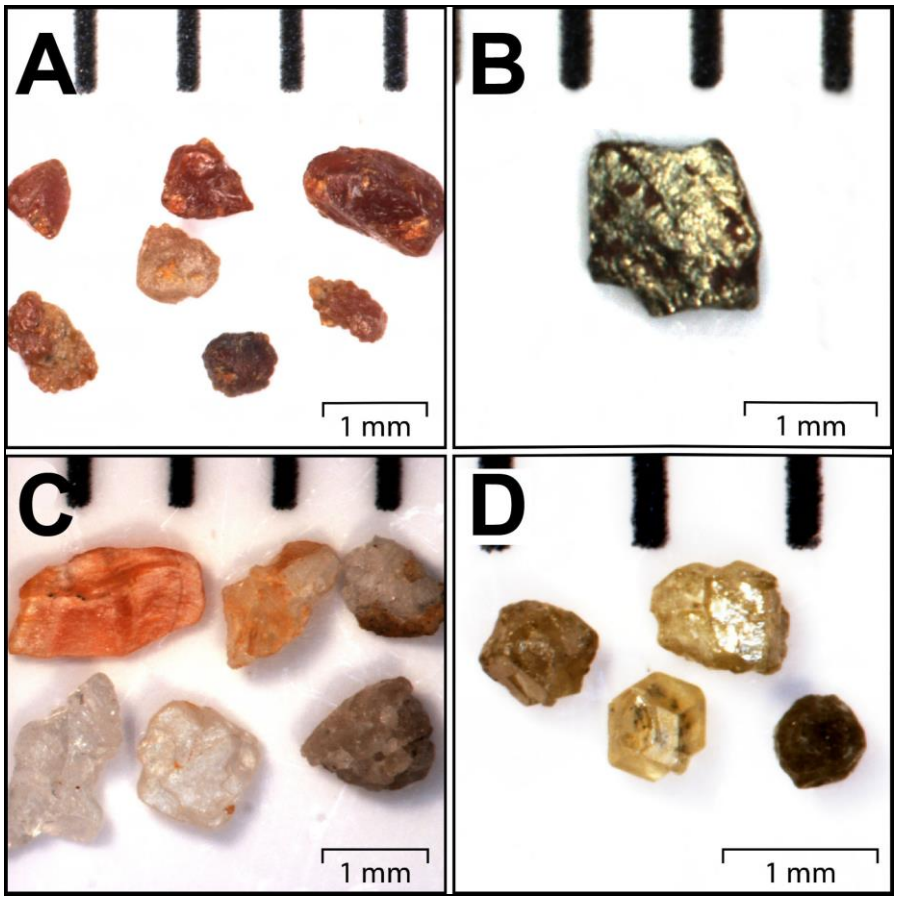

Figure 6: Examples of indicator minerals recovered from the heavy mineral concentrates. (A) Honey sphalerite in the 0.5-1.0 mm fraction from sample 06. (B) Chalcopyrite in the 1.0-2.0 mm fraction from sample 06. (C) Barite in the 1.0-2.0 mm fraction from sample 06. (D) Andradite in the 0.5-1.0 mm from sample 37.

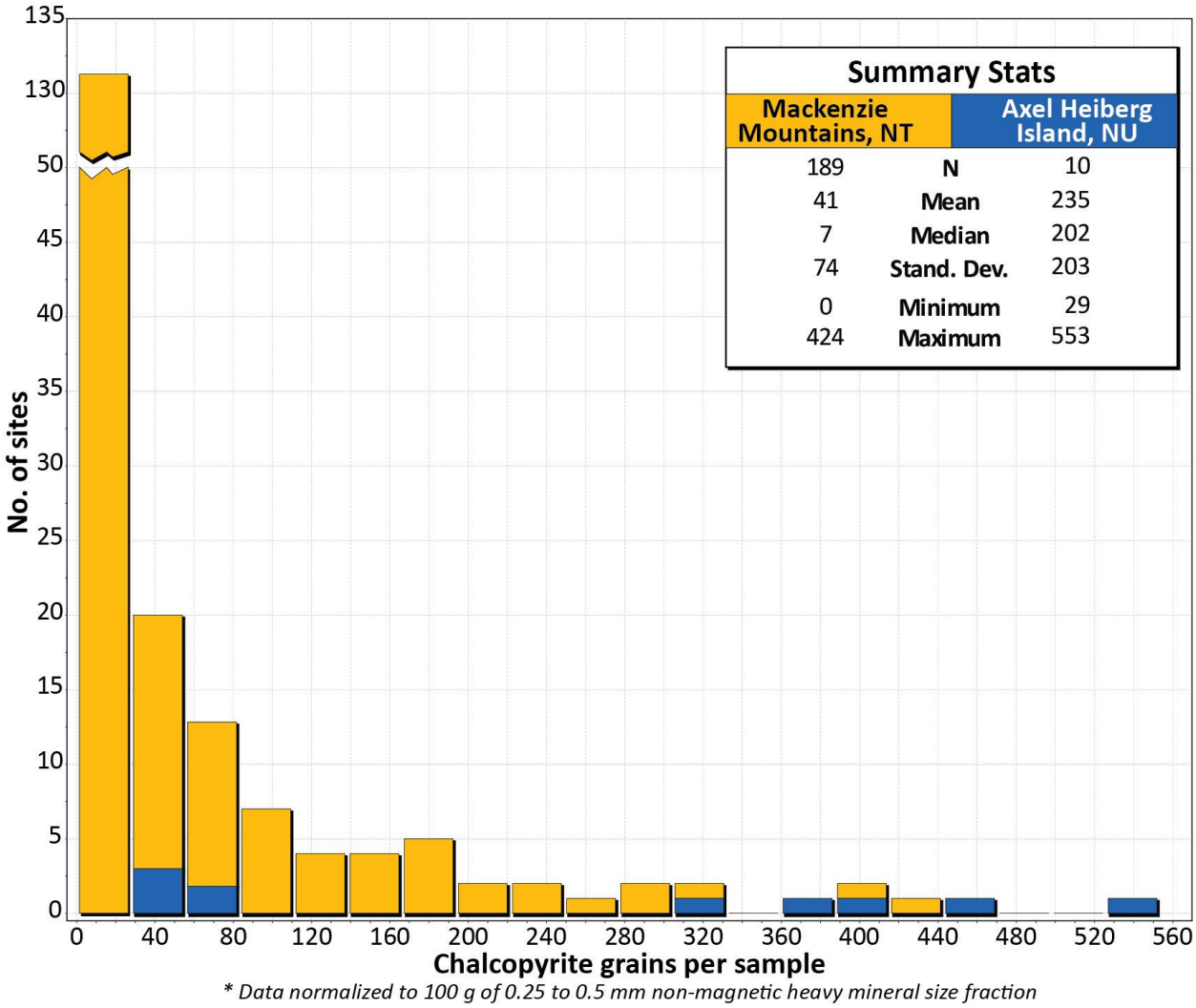

Figure 7: Histogram comparing the abundance of chalcopyrite grains recovered in the heavy mineral concentrates of samples from this study and from stream sediment surveys in the Mackenzie Mountains, Northwest Territories (Falck et al., 2012). In both study areas, the local bedrock consists of mafic igneous rocks intruding predominantly clastic sedimentary successions in a remnant large igneous province.

DISCUSSION

The first geochemical survey of stream silts and waters in the South Fiord area of western Axel Heiberg Island outlines the local lithologies very well, specifically differentiating the diapirs from the volcanic-sedimentary succession. When compared to the mineralogy of the HMCs, there is a weak correlation with the silt and water geochemistry. Despite the remarkably large number of chalcopyrite, sphalerite and galena grains recovered from the bulk samples, the mineralogy of the heavy mineral fraction does not show a clear correlation with anomalous Cu, Zn and Pb values in the silt and waters (see Figure 8 for distribution of zinc as sphalerite grains, zinc in sediment and waters). These differences may be attributed to the fact that at high latitudes, streams only flow for a short period of time in the summer over perennial permafrost where the main source of water is meltwater. The short-lived, torrential nature of meltwater flow combined with alkaline pH values, suggest little chemical dissolution of minerals, thereby inhibiting the transport of

metals in solution. The metals may only be mobilized a short distance before rapid

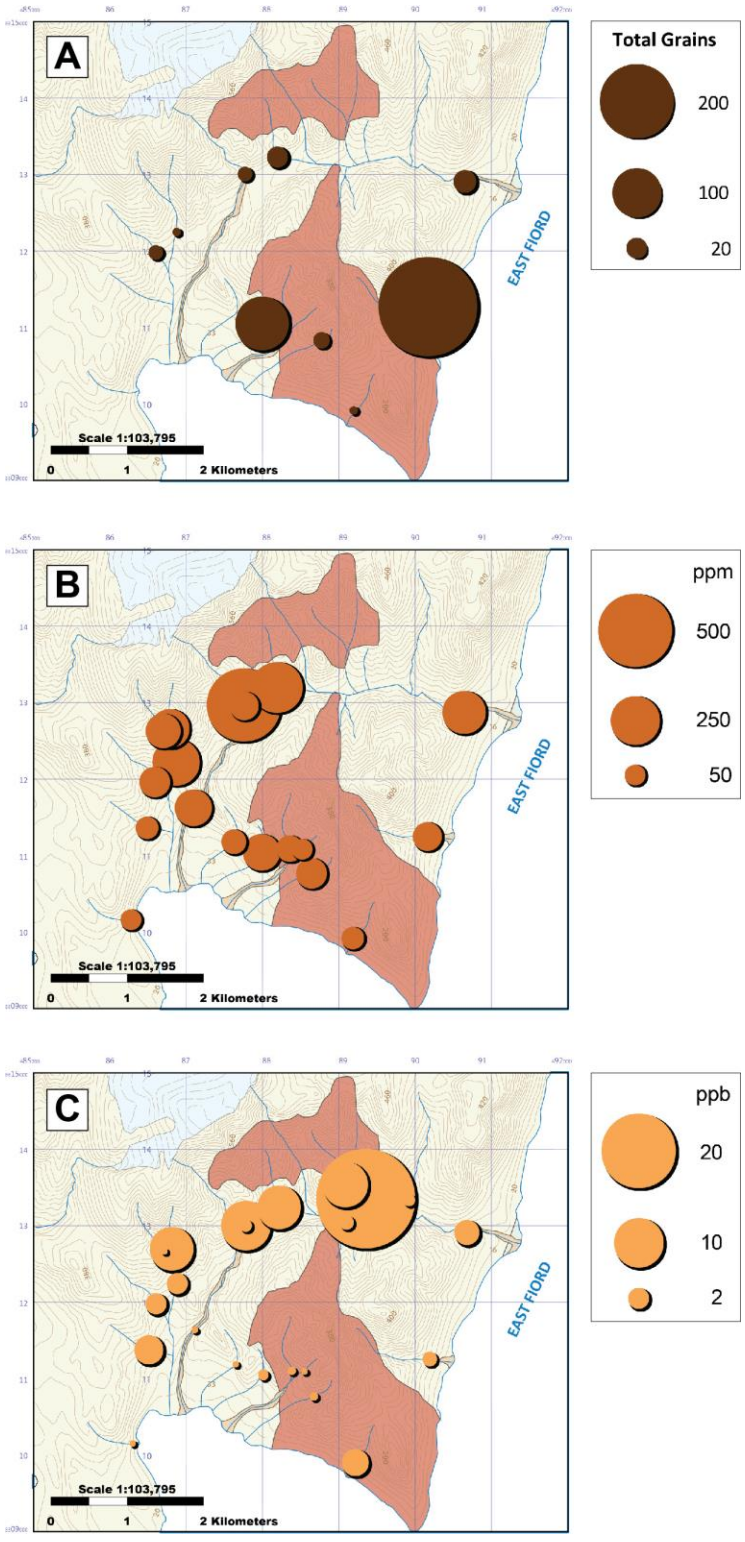

Figure 8: Maps showing the distribution of zinc in streams. (A) distribution of sphalerite grains (normalized to 100 grams of heavy mineral concentrate), (B) distribution of zinc in ppm by ICP-MS / aqua-regia in the stream silt (<0.177 mm fraction) samples and (C) distribution of zinc in stream waters.

precipitation out of solution as carbonate, oxide and hydroxide minerals.

This same discrepancy is observed in silt samples. The finer fractions of sediment are washed away downstream within the fast flowing water, leaving behind coarser sediment. Mechanical breakdown of grains is the main erosion process in northern latitudes and it appears the more resistant grains are not breaking down smaller than the analyzed grain size of < 0.177 mm. This analyzed size fraction appears to be too fine to capture the sulphide minerals in the stream. To correct this bias, a grain size analysis will be undertaken to define the most effective size fraction to analyze and capture the mineralogical anomalies in the sediment and water geochemistry. The grain size study will include five size fractions ranging from < 0.063 mm to >0.5 mm.

METALLOGENESIS

Allochtonous evaporite beds and diapirs can focus metalliferous basinal fluids and lead to sulphide mineralization. In the case of rift basins, the heat to drive the circulation of hypersaline brines could be supplied by hot basaltic magma erupted as lava flows at volcanic centres and/or intruded in the sedimentary succession as sills and dykes. The model for salt-allochton controlled base-metal (sedex) accumulation proposed by Warren (2000) could explain the presence of key indicator minerals such as chalcopyrite, sphalerite, and barite in the heavy mineral fraction recovered from stream sediments. Several features of the model can be observed in the Strand Fiord-Expedition Fiord area, for example: (1) the presence of a volcanic-sedimentary succession, (2) salt diapirs and canopies, and (3) complex faulting at the periphery of evaporite structures (Williamson et al., 2011; Harrison and Jackson, 2014). A compelling aspect of the model is the potential for both regional (deep) and local (shallow) faults to act as conduits for mineral-rich fluids to generate base metal deposits in proximity to evaporite diapirs.

CONCLUSIONS

A pilot reconnaissance drainage study – the first for this region of Nunavut – was carried out in the South Fiord area of western Axel Heiberg Island using GSC's established National Geochemical Reconnaissance regional survey methods (Friske and Hornbrook, 1991). This methodology has been a successful tool at southern latitudes to evaluate the mineral potential of an area as well as establishing environmental and geochemical baseline for environmental assessment (McCurdy et al., 2013). Preliminary results suggest that the short-lived flowing alkaline water in streams, mainly from meltwater, causes metals to become depleted in water samples. Abundant sulphide minerals recovered in the heavy mineral concentrates are a clear indication of their presence in local bedrock, however a comparable result is not found in silt samples.

The distribution of heavy mineral suites in stream sediment shows a good correspondence with the underlying bedrock lithologies which can be used as a valuable mapping tool and to characterize the prospectivity of the area for Ni-Cu-PGE mineralization and other deposit types.
The drainage geochemistry and mineralogical data presented here is a result of a reconnaissance study at northern latitudes. Additional work is required to better understand the effects of the arctic environment on stream geochemistry as a tool in characterizing the mineral potential of an area. Nevertheless, the large number of chalcopyrite grains and other sulphides recovered from HMCs definitely highlight the prospectivity of the South Fiord area for Ni-Cu PGE mineralization and most likely for other types of deposits. The gossans present in this study area tended to be small

when compared to the more spatially dominant sedimentary and igneous lithologies within the catchment basins. The acidic gossaneous material (Williamson et al., 2015) is rapidly neutralized by the buffering capacity of the slightly alkaline ground and surface waters which are influenced by the surrounding anhydrite salt diapirs and carbonaceous shales. The result therefore being that the geochemical signature of these gossans does not appear to be recognizable even at a short distance downstream. Gossans identified near sites 7 and 29 are not directly affected by the presence of diapirs and are recognizable in stream water by slightly lower pH values.

ACKNOWLEDGEMENTS

The Arctic Gossans activity was funded by the Environmental Geoscience Program of the Earth Sciences Sector-Geological Survey of Canada, Department of Natural Resources Canada. Field studies were carried out in collaboration with the GeoMapping for Energy and Minerals (GEM 1) and Polar Continental Shelf Programs. Special thanks to Cole Kingsbury from the Department of Earth Sciences at Carleton University for assistance in the field. Critical reviews by Helen Smyth, Jeanne Percival and Benoit Saumur improved an earlier version of the manuscript. ESS Contribution no. 20140284.

REFERENCES

Davies, G.R., and Nassichuk, W.W., 1991. Carboniferous and Permian history of the Sverdrup Basin, Arctic Islands, *in* Geology of the Innuitian Orogen and Arctic Platform of Canada and Greenland, (ed.) H.P. Trettin; Geological Survey of Canada, Geology of Canada, v.3, p. 344-368.

Falck, H., Day, S.J.A., Pierce, K.L., Rentmeister, K., Ozyer, C.A., and Watson, D.M., 2012. A compilation of heavy mineral concentrates: Results from stream sediment samples collected 2007-2010, Mackenzie Mountains, NWT; Northwest Territories Geoscience Office, NWT Open Report 2012-001. Digitial files.

Falck, H., Day, S., Pierce, K.L., and Cairns, S., 2014. Geochemical, mineralogical and indicator mineral data for stream silt sediment, heavy mineral concentrates and waters, Cranswick River area Northwest Territories, (part of NTS 106F); Northwest Territories Geoscience Office, NWT Open Report 2014-012.

Friske, P.W.B., and Hornbrook, E.H.W., 1991. Canada's National Geochemical Reconnaissance programme; Institution of Mining and Metallurgy, Transactions, Section B; Applied Earth Sciences, v.100, p. B47-B56.

Girard, I., Klassen, R.A., and Laframboise, R.R., 2004. Sedimentology Laboratory Manual, Terrain Sciences Division; Geological Survey of Canada, Open File 4823, 134 pp., 1 CD-ROM, doi:10.4095/216141.

Jackson, M.P.A. and Harrison, J.C., 2006. An allochtonous salt canopy on Axel Heiberg Island, Sverdrup Basin, Arctic Canada; Geology, v. 34, no. 12, p. 1045-1048, doi:10.1130/G22798A.1.

Harrison, J.C. and Jackson, M.P.A, 2010. Bedrock geology, Strand Fiord-Expedition Fiord, western Axel Heiberg Island, northern Nunavut (parts of NTS 59E, F, G, and H); Geological Survey of Canada, Map 2157A, 2 sheets, scale 1:125 000.

Harrison, J.C. and Jackson, M.P.A, 2014. Tectonostratigraphy and allochtonous salt tectonics of Axel Heiberg Island, central Sverdrup Basin, Arctic Canada; Geological Survey of Canada, Bulletin 607, 124 pp.

Jonasson, I.R., and Dunsmore, H.E., 1979. Low grade uranium mineralization in carbonate rocks from some salt domes in the Queen Elizabeth Islands, District of Franklin, *in* Current Research, Part A; Geological Survey of Canada, Paper 79 1-A, p. 61-70.

Jowitt, S.M., Williamson, M.-C., and Ernst, R.E., 2014. Geochemistry of the 130 to 80 Ma Canadian High Arctic Large Igneous Province (HALIP) event and implications for Ni-Cu-PGE prospectivity; Economic Geology, v. 109, no. 2, p. 281-307. doi:10.2113/econgeo.109.2.281

Kingsbury, C.G., Williamson, M.-C., Day, S.J.A., and McNeil, R.J., 2013. The 2013 Isachsen Expedition to Axel Heiberg Island, Nunavut, Canada: A field report, Geological Survey of Canada, Open File 7539, 6 p. + poster. doi:10.4095/293842

McCurdy, M.W., Rainbird, R.H., and McNeil, R.J., 2013. Exploring for Lead and Zinc using indicator minerals with stream silt and water geochemistry in the Canadian Arctic Islands: An example from Victoria Island, Northwest Territories, *in* New Frontiers for Exploration in Glaciated Terrain, (eds.) R.C. Paulen and M.B. McClenaghan; Geological Survey of Canada, Open File 7374, p. 65-74.

McClenaghan, M.B., 2005. Indicator mineral methods in mineral exploration; Geochemistry: Exploration, Environment, Analysis, v. 5, p. 233-245.

McNeil, R.J., Day, S.J.A., Williamson, M.-C., in press. Geochemical, mineralogical and indicator mineral data for stream silt sediment, heavy mineral concentrates and waters, South Fiord area Axel Heiberg Island, Nunavut, (part of NTS 59G); Geological Survey of Canada Open File 7779.

Percival, J.B., Williamson, M.-C., McNeil, R.J., and Harris, J.R. 2015. Morphology of gossans in the Canadian Arctic Islands, *in* Environmental and Economic Significance of Gossans, (ed.) M.-C. Williamson; Geological Survey of Canada, Open File 7718, p. 58-73.

Sandeman, H.A., Ootes, L., Cousens, B., and Kilian, T., 2014. Petrogenesis of Gunbarrel magmatic rocks: Homogeneous continental tholeiites associated with extension and rifting of Neoproterozoic Laurentia; Precambrian Research, v. 252, p. 166-179.

Warren, J.K., 2000. Evaporites, brines and base metals: low-temperature ore emplacement controlled by evaporite diagenesis; Australian Journal of Earth Sciences, v. 47, p. 179-208.

Williamson, M.-C., Smyth, H.R., Peterson, R.C., and Lavoie, D., 2011. Comparative geological studies of volcanic terrain on Mars: Examples from the Isachsen Formation, Axel Heiberg Island, Canadian High Arctic; Geological Society of America, Special Paper 483, p. 249-261.

Williamson, M.-C., McNeil, R.J., Day, S.J.A., McCurdy, M.W., Rainbird, R.H., and Grunsky, E.C., 2015. Environmental impact of gossans revealed by orientation surveys for base metals in the Canadian Arctic Islands, *in* Environmental and Economic Significance of Gossans, (ed.) M.-C Williamson; Geological Survey of Canada, Open File 7718, p. 74-84.